2013

IDENTIFICATION OF HUMAN PGC-1α-b ISOFORMS USING A NOVEL PGC-1α-b SPECIFIC ANTIBODY

Shannon Hedrick
Virginia Commonwealth University

IDENTIFICATION OF HUMAN PGC-1α-b ISOFORMS USING A NOVEL PGC-1α-b SPECIFIC ANTIBODY

A thesis submitted in partial fulfillment of the requirements for the degree of Master of Science at Virginia Commonwealth University

by

SHANNON HEDRICK

Bachelor of Science, University of Richmond, 2011

Advisors:

James Bennett, Ph.D.

Associate Professor

Department of Physiology and Biophysics

Shirley Taylor, Ph.D.

Associate Professor

Department of Microbiology and Immunology

Virginia Commonwealth University

Richmond, VA

December, 2012

ACKNOWLEDGEMENTS

I would like to acknowledge everyone who has helped me through my graduate school journey. First, I would like to thank Dr. James Bennett and Dr. Shirley Taylor for allowing me to work in their laboratories and providing me with the opportunity to earn my Master's Degree. I have learned much about academia and life from both of them. I would especially like to thank them for being so kind and understanding regarding my medical issues over the last few months. Dr. Taylor has always been there to listen and talk through any questions or concerns I have had, and I am very grateful for her kindness and support.

I would also like to thank the third member of my committee, Dr. John Bigbee, who since the beginning of my graduate studies, was always available to offer guidance. I would also like to acknowledge Dr. Christie, my first advisor and head of the Molecular Biology and Genetics program, who worked closely with Dr. Taylor to ensure my success. Two members of the microbiology office, Ms. Martha VanMeter and Ms. Nancy Fogg, have been very patient with me and were always available to answer any questions I had. I am very grateful to them for working with me and easing my stress.

I would like to thank all the members – past and present – of the Taylor and Moran laboratories: William Buchwald, Prashant Thakkar, Tim Lochmann, Elliot Burton, John Strang, Chen Yang, Chuck Lyons, Catherine Bell, Stuti Agarwal, and Joyce Balinang. They have been extremely helpful in showing me the ropes, troubleshooting experiment issues, and providing moral support and good conversation. I am very happy to know and be friends with such wonderful and intelligent people.

Last but not least, I would like to thank my family. I especially need to thank my husband, Eric Oberholtzer, for always being there for me and being my anchor of support throughout my graduate studies. He stayed up countless nights while I studied, and drove me late at night and on weekends to and from lab. Without him, I never could have accomplished such a feat. My mother and father-in-law, Cathy and Britt Oberholtzer, have kindly opened their hearts and home to me and I will be forever grateful for their love and support. My parents, John and Susan Hedrick, my grandparents, Rosemary and Alvin Hedrick, Lois and Joseph Colletti, and my Aunt Joan Hedrick have all been pillars of support for me, and have been completely understanding of my busy schedule and provided me with unconditional love and support. They are the ones who have always made me treasure education and were the fuel for my hard work and dedication.

LIST OF TABLES

LIST OF FIGURES

ABBREVIATIONS

AD	Alzheimer's Disease
AICAR	5-Aminoimidazole-4-carboxamide ribonucleotide
Akt	Protein kinase B
ALS	Amyotrophic lateral sclerosis
AMPK	AMP activated protein kinase
Ap-2	adipocyte protein-2
ATF2	activating transcription factor 2
ATP	adenosine triphosphate
BAT	brown adipose tissue
CA1	Cornu Ammonis area 1
CaMK	Ca2+-calmodulin dependent kinase
cAMP	cyclic adenosine monophosphate
CaN	calcineurin
CBP	CREB binding protein
cDNA	complementary DNA
CDS	coding sequence
chIP	chromatin immunoprecipitation
CIDEA	cell death-inducing DFFA-like effector a

CNS	central nervous system
COX	cytochrome C oxidase
CpG	cytosine guanine dinucleotide
CRE	cAMP response element
CREB	cAMP response element binding protein
CRM1	chromosome region maintenance 1 (exportin1)
CT	carboxy terminus
CytC	cytochrome C
DNA	deoxyribonucleic acid
DNMT3b	DNA methyltransferase 3 beta
Drp1	dynamin related protein I
eNOS	endothelial NO synthetase
ERR	estrogen-related receptor
Ers	estrogen receptors
FADH2	Flavin adenine dinucleotide, reduced
FKHR	forkhead in rhabdomysarcoma
FOXO1	forkhead box protein O1
GABP	guanine adenine binding protein
GCN5	general control nonderepressible 5
Glut4	glucose transporter type 4
GPX1	glutathione peroxidase 1
GR	glucocorticoid receptor
H3	histone 3
H3K4Me3	histone 3 trimethylated on lysine 4
H4	histone 4

HCF	host cell factor
HD	Huntington's disease
HEK293	human embryonic kidney 293 cells
HEPG2	hepatocellular carcinoma, human
HIF1	hypoxia inducing factor-1
HNF4alpha	Hepatocyte nuclear factor 4 alpha
ICC	immunocytochemistry
IHC	immunohistochemistry
IL-1alpha	interleukin 1 alpha
IL-6	interleukin-6
IM	muscle immobilization
IRS	insulin response sequences
KA	kainic acid
kDa	kilodalton
KO	knock out
L-PGC-1α	Liver PGC-1α
MAPK	mitogen activating protein kinase
MCAD	medium chain acyl-coenzyme A dehydrogenase
MEF2-C	Myocyte enhancing factor 2 c
Mfn1	mitofusin 1
Mfn2	mitofusin 2
MKK6	MAPK kinase 6
mPTP	mitochondrial permeability transition pore
MPTP	1-methyl-4-phenyl-1, 2, 3, 6- tetrahydropyridine
MRF4	myogenic regulatory factor 4

mRNA	messenger RNA
mtDNA	mitochondrial DNA
mTOR	mammalian target of rapamycin
mtTFA	mitochondrial transcription factor A
myb	myeloblastosis binding protein
MyoD	myogenic regulatory factor D
NAD+	nicotinamide adenine dinucleotide, oxidized
NADH	nicotinamide adenine dinucleotide, reduced
NMJ	neuro-muscular junction
NO	nitric oxide
NOS	nitric oxide synthase
NRF	nuclear respiratory factor
NT	amino terminus
NT-PGC-1α	Novel truncated PGC-1α
Opa1	optic atrophy 1
p53	tumor protein 53
PARIS	Parkin-interacting substrate
PD	Parkinson's Disease
PDGFbeta	platelet derived growth factor beta
PGC-1	Peroxisome proliferator-activated receptor gamma coactivator 1
PGC-1b	Peroxisome proliferator-activated receptor gamma coactivator 1 beta
PGC-1α	Peroxisome proliferator-activated receptor gamma coactivator 1alpha
PGC-1α-b 3T1	PGC-1α isoform b exon 3 truncation 1
PINK1	PTEN-induced putative kinase 1

POLG	polymerase gamma
PPAR	peroxisome proliferator activated receptor
PPARγ	peroxisome proliferator-activated receptor γ
PRC	PGC related coactivator
PRMT1	protein arginine methyltransferase-1
qRT-PCR	quantitative reverse transcription PCR
RIP140	nuclear receptor interacting protein 140
RLM RACE	RNA ligand mediated Rapid amplification of cDNA ends
RM	restoration of muscle movement
RMM	Ribonucleic acid binding motif
RNS	reactive nitrogen species
ROS	Reactive oxygen species
RS	arginine-serine rich
RT-PCR	reverse transcription polymerase chain reaction
RXRalpha	retinoid X receptor alpha
siRNA	small-interfering RNA
SIRT1	Sirtuin 1
SIRT3	NAD-dependent deacetylase sirtuin-3 (mitochondrial)
SOD2	superoxide dismutase 2 (mitochondrial)
SRC-1	steroid receptor coactivator-1
SREBP-1c	sterol regulatory element-binding protein 1
TC / TF	transcriptional coactivator / transcription factor
TFAM	mitochondrial transcription factor A
Tg	transgenic
TIM	translocase of the mitochondrial inner membrane

TNFalpha	tumor necrosis factor alpha
TOM	translocase of the mitochondrial outer membrane
TORC	transducer of regulated CREB-binding protein
TR	thyroid receptor
TSS	transcription start site
UCP	uncoupling protein
USF1	Upstream stimulatory factor 1
VDAC	voltage dependent anion channel
WAT	white adipose tissue
WCL	whole cell lysate
WT	wild type
YY1	Yin Yang 1
ZNF746	zinc finger protein 746

ABSTRACT

Identification of Human PGC-1α-b Isoforms Using a Novel PGC-1α-b Specific Antibody

Shannon E. Hedrick, B.S.

A thesis submitted in partial fulfillment of the requirements for the degree of Master of Science at Virginia Commonwealth University

Virginia Commonwealth University, 2013

Major Advisors:

James P. Bennett, Ph.D.

Associate Professor, Department of Physiology and Biophysics

Shirley Taylor, Ph.D.

Associate Professor, Department of Microbiology and Immunology

Peroxisome proliferator-activated receptor gamma coactivator 1-alpha (PGC-1 α) is known as the master regulator of mitochondrial biogenesis. PGC-1α holds this role by acting as a transcriptional coactivator for an array of transcription factors and nuclear hormone receptors, such as NRF-1/2 and ERRα/γ, whose downstream targets function in mitochondrial biogenesis and oxidative phosphorylation. PGC-1α is regulated both at the transcriptional and post-translational level in several signaling pathways, including p38 MAPK and AMPK. This regulation affects which transcription factor binding events can occur in a given tissue, and thus affects regulation of PGC-1α target genes. PGC-1α is downregulated in many neurodegenerative disorders as well as in muscular dystrophies, diabetes, and aging. Therefore, PGC-1α is prized as a potential therapeutic target to create novel treatments for these various diseases.

However, details governing the spatio-temporal regulation of PGC-1α are not completely understood, and overexpression of PGC-1α throughout the body or even in certain tissues or subsets of cells have had detrimental effects in animal and cell models. Therefore, it is necessary to gain knowledge of how to modulate PGC-1α in a tissue-specific manner utilizing these different levels of regulation in order to develop novel therapies. In order to further understand all the functions that have been attributed to PGC-1α, the PGC-1α isoforms need to be accounted for and understood in human tissues. Several murine isoforms have been published, as well as several human brain and muscle isoforms. However, most of these isoforms have only been validated as mature transcripts, and it is not known whether they produce functional protein. Our lab has identified the isoform b transcript in human brain tissue via 5' RACE and have developed an isoform b specific antibody. This project aimed to characterize the isoform b transcripts and also to validate and optimize this antibody for immunoblotting conditions for detection of further PGC-1α-b isoform protein variants in human tissues. Preliminary studies in our lab have shown that in postmortem frontal cortex from age-matched PD and healthy patients, isoform a transcript levels were 10-15 times more abundant than that of isoform b. These differences in regulation could be partially attributed to the isoform b promoter region being heavily methylated, as shown in this thesis through bisulphite cloning and sequencing as well as 454 bisulphite sequence analysis. The high degree of methylation, correlated with the low level of isoform b transcript in brain and it is not known whether this transcript would be translated into protein in this tissue. In order to probe for isoform b protein expression using human cell lines and tissues, however, it was necessary to create a recombinant protein in order to have a positive control with which to optimize our novel antibody. In our previous 5' RACE studies, an alternatively spliced PGC-1α-b transcript was found which coded for an early stop codon. This truncated isoform was called PGC-1α-b-3T1, and mature transcript was found in both human skeletal muscle and brain. For this project, PGC-1a-b-3T1 was cloned from human skeletal muscle into a bacterial expression vector to create a recombinant GST fusion protein. This protein was

used to validate and optimize our PGC-1α-b specific antibody as well as to determine sensitivity and specificity. The purified recombinant protein contained 3 bands of lower molecular weight that were detected via western blot with both GST and the PGC-1α-b specific antibody. These bands were trypsin cleaved and subjected to mass spectrometry analysis, which verified that all bands detected by the PGC-1a-b specific antibody contained the epitope sequence, and thus binding was specific. This protein was then used to determine western blotting conditions and sensitivity, which is 10 ng using a 1:100 dilution of the antibody. This antibody was then used to probe SH-SY5Y WCL, a human neuroblastoma cell line. Peptide competition assay confirmed 5 PGC-1α-b specific proteins in these lysates. The sizes of these proteins matched to several murine PGC-1α-b isoforms as well as putative PGC-1α-b versions of PGC-1a-a isoforms. These findings provided the putative identities of several endogenous functional human PGC-1α-b isoforms. Mammalian overexpression vectors of these isoforms are still in development. By using this antibody and these expression vectors to further characterize these isoforms, including determining tissue specificity, more knowledge of PGC-1α will be gained. This information could then be used to develop novel, tissue specific treatments for pharmacological intervention of diseases characterized by PGC-1α misregulation.

TABLE OF CONTENTS

Chapter 1: Introduction

I. Overview of Mitochondrial Biogenesis

Mitochondrial biogenesis is the process by which new mitochondria are made in the cell. An increase in mitochondrial mass can either be a normal response to increase ATP production as needed, such as during exercise, formation of new cells, and fasting, or it can be stimulated as a rescue response to cellular stress, such as cold exposure, increased concentration of reactive oxygen species (ROS), or oxidative stress. Thus mitochondrial biogenesis is upregulated in healthy oxidative as well as abnormal states of metabolism. Considering that the mitochondrial genome only encodes 13 proteins, there are thousands of nuclear-encoded mitochondrial genes that must be transcribed, translated, and imported into mitochondria for it to carry out its functions and undergo biogenesis.

The major processes of mitochondrial biogenesis include transcription of nuclear-encoded mitochondrial genes, importation of nuclear-encoded mitochondrial proteins, mitochondrial DNA replication and transcription, mitochondrial protein production and assembly, and ultimately mitochondrial fission and fusion (Fig. 1-1). The nuclear respiratory factors (NRF-1, NRF-2) and other nuclear receptors (PPARs, ERRs) are responsible for the regulation of many nuclear-encoded mitochondrial genes required for mitochondrial biogenesis (Wu et al., 1999). The translocases of the mitochondrial outer and inner membrane, TOM and TIM respectively, are primarily responsible for importation of these proteins into the mitochondrion (Kutik et al., 2007). For the mitochondrial encoded genes, TFAM (mitochondrial transcription

factor A) plays a major role their replication and transcription (Garstka, 2003)). Mitochondria can be thought of as a network rather than individual organelles, and thus the process of creating additional mitochondrial material to expand this network (mitochondrial biogenesis) is truly dynamic. This process is governed by mitochondrial fission and fusion, the breaking apart and joining of old and new mitochondrial material (Mozdy and Shaw, 2003). The mitofusins (Mfn1, Mfn2) are the proteins primarily responsible for mitochondrial fusion along with Opa1, whereas the dynamin-related proteins Drp1 and Fis1 are those involved in fission (Chen et al., 2003; Meeusen et al., 2006; Mozdy et al., 2000; Otsuga, 1998). Old and dysfunctional mitochondrial mass can be recycled via the process of mitophagy, completing the cycle of mitochondrial biogenesis (Lemasters, 2005).

Managing these processes requires much coordination between the nucleus and mitochondria to have correct levels and localization of necessary proteins at the correct times. The major family of proteins involved in coordinating all the events of mitochondrial biogenesis and metabolism are the PGC-1 (peroxisome proliferator-activated receptor γ coactivator-1) family of coactivators, including PGC-1α, PGC-1β, and PRC (PGC related coactivator) (Andersson and Scarpulla, 2001; Lin et al., 2002a; Puigserver et al., 1998) . PGC-1α, the most studied of this family, is known as the master regulator of mitochondrial biogenesis, which coordinates signaling input received during metabolic stress with transcriptional regulation for mitochondrial function and biogenesis (Wu et al., 1999).

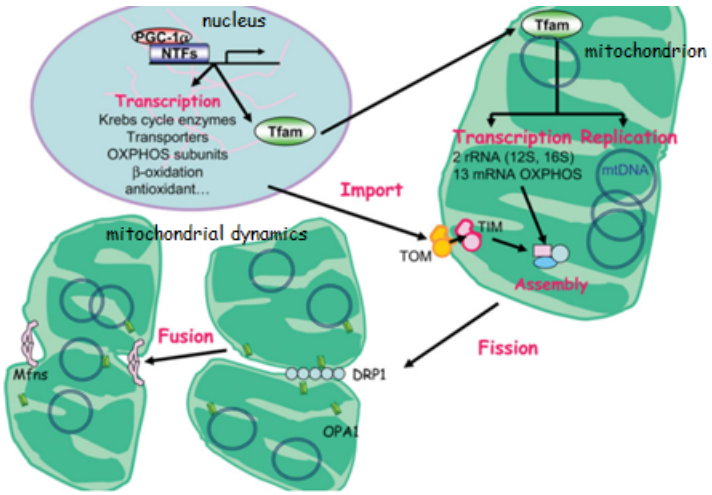

Fig. 1-1: Overview of the major events of mitochondrial biogenesis (Adapted from (Ventura-Clapier et al., 2008)**.** The major events include (1) transcription of nuclear encoded mitochondrial proteins, governed by PGC-1α / NRF-1/2 binding interaction to upregulate genes involved in mitochondrial processes, which includes TFAM (2) Import of those proteins into the mitochondrion into their respective mitochondrial compartment by TOM and TIM (3) Transcription of mitochondrial-encoded mitochondrial proteins and replication of mtDNA by the imported TFAM – as well as polγ, polRM, among others – and assembly of those proteins (4) Mitochondrial dynamics of fission and fusion governed by Fis1 and Drp1 and Mfn1/2 and OPA1, respectively.

II. PGC-1α as the master regulator of mitochondrial biogenesis

1. A history of PGC-1α and its family

A few decades ago while investigating adaptive thermogenesis, Puigserver and colleagues found that in mice PPARγ (peroxisome proliferator-activated receptor γ) activated uncoupling proteins (UCPs) only in brown adipose tissue (BAT) versus white adipose tissue (WAT). Using a mouse BAT cDNA library, they aimed to find the co-factor which was causing this activation. Over time, they were able to clone the novel protein responsible which they deemed PGC-1 (Puigserver et al., 1998). Renamed PGC-1α, it is a member of the PGC-1 family of transcriptional coactivators and was the first member of this family discovered.

Since then, two other members of the PGC family of coactivators have been identified. PGC-1β was found by its high degree of sequence homology to PGC-1α (Lin et al., 2002a). PRC does not share sequence homology with PGC-1α, but does bind PPARγ and also retains similar functional domains (Andersson and Scarpulla, 2001). In fact, these three family members share several important functional domains located at the N and C termini. These domains include an N-terminal transcriptional activation domain and C-terminal RNA processing motifs (RMM – RNA binding motif, RS - serine-arginine rich). This family differs from most coactivators in that the proteins themselves do not contain any enzymatic functions for chromatin remodeling and do not have homology to any other transcriptional coactivator families (Lin et al., 2002a). They can, however, recruit proteins with chromatin remodeling abilities through the NT activation domains, ultimately making the promoters of target genes accessible for transcriptional regulation. These recruited chromatin remodelers include CBP (CREB – cAMP response element binding protein - binding protein) and SRC-1 (steroid receptor coactivator-1), which both have histone acetyltransferase activity (Puigserver et al., 1998). The PGC-1 family also cannot bind DNA directly, but interact with DNA-binding partners to form transcriptional coactivator / transcription factor (TC/TF) binding pairs. Some of the common

transcription factors that interact with PGC-1 family coactivators are the NRFs (nuclear respiratory factors), TRs (thyroid receptors), PPARs (peroxisome proliferator-activated receptors), and the ERRs (estrogen related receptors) (Puigserver et al., 1998; Schreiber et al., 2004; Vega et al., 2000; Wu et al., 1999).

Considering that the PGC-1 family shares so many transcription factor binding partners, it is not surprising that some of their functions overlap. However, common binding partners do not necessarily mean that the interaction will have the same downstream effect. Strength of binding will differ based upon structural hindrances due to amino acid sequence variability in the region surrounding the LXXLL transcription factor binding motif, amount of ligand present, as well as post-translational modifications (Lin et al., 2002a; McInerney et al., 1998; Nolte et al., 1998; Westin et al., 1998). These factors can vary in different tissues among the common binding sites and can all affect the robustness of the transcriptional regulation and subsequent downstream interactions. This results in each member having some degree of overlapping but not entirely compensating functions for one another. For example, although each contributes to mitochondrial regulation and function, it is hypothesized that PGC-1α plays the most all-encompassing role of the three in mitochondrial processes based upon its upstream position in modulating nuclear encoded mitochondrial effectors, thus it is known as the master regulator of mitochondrial biogenesis (Lin et al., 2002a; Wu et al., 1999). Also, PGC-1β specifically induces genes involved in ROS removal (St-Pierre et al., 2006). Differences in transcriptional regulation of the three family members affect where and when they can be expressed and exert their functions. For example, PRC is constitutively expressed equally among all tissue types, whereas PGC-1α and β are enriched in mitochondrially abundant tissue types; however, PGC-1α is the only member of the family which can be induced by metabolic stress such as exercise, fasting, or cold (Meirhaeghe et al., 2003; St-Pierre et al., 2003). PGC-1β and PRC have not been studied extensively, unlike PGC-1α, and studies are still underway to determine all their

functional similarities and differences to PGC-1α.

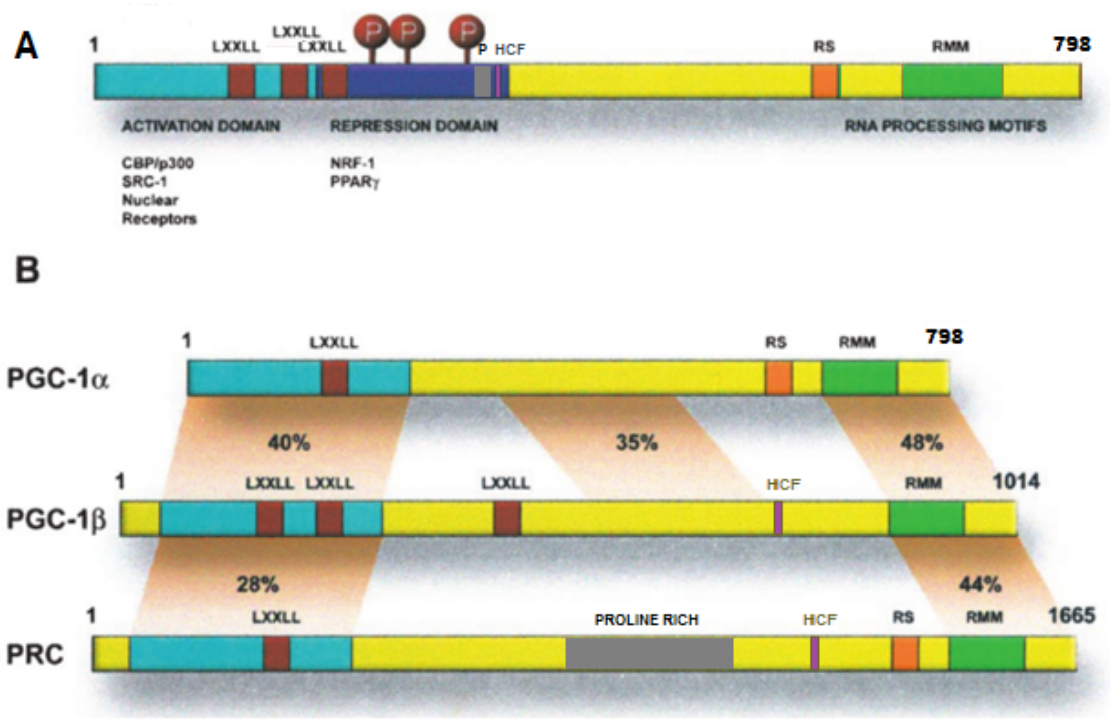

Fig. 1- 2: Conservation of functional domains in the PGC-1 family of transcriptional coactivators (Adapted from Puigserver, 2003)**.** (A) PGC-1α major functional domains include the activation, repression, and RNA processing motifs. LXXLL is a binding motif that typically allows binding to nuclear hormone receptor transcription factors, which grant PGC-1α its transcriptional coactivator ability. P = proline rich domain; HCF = host cell factor binding domain; RS = arginine / serine rich domain; RMM = RNA modeling motif. Phosphorylation sites (P balloons) are for p38 MAPK. (B) Conservation of domains in part A across the 3 members of the PGC-1 family of coactivators.

2. PGC-1α functional domains

There are several important functional domains of the PGC-1α protein. These include the NT activation domain, followed by a repression domain, a proline rich domain, and a host-cell factor binding domain, ultimately ending in an RS domain and an RMM domain (see Fig. 1-2). Moving from the N-terminus to the C-terminus, I will describe the features of each of these domains in more detail, including which areas can be targeted by post-translational modifications and how they contribute to PGC-1α regulation and function.

The activation domain (amino acids 1-200) contains many acidic amino acids. These allow it to interact with several potent transcription factors that contain chromatin remodeling activity, which PGC-1α itself lacks. These include SRC-1, CBP/p300, and GCN5. One of the most important features of this functional domain is the LXXLL transcription factor binding motif. This motif grants PGC-1α its abilities as a transcriptional coactivator (see Fig. 1-2). There are three total LXXLL sites in PGC-1α. One lies within the activation domain, the remaining two within the repression domain, and are used to bind nuclear hormone receptors in the presence of ligand. These receptors include ER, PPARα, RXRα, GR, and SRC-1 (Delerive et al., 2002; Knutti et al., 2000; Puigserver, 1999; Tcherepanova et al., 2000; Vega et al., 2000). HNF4a is the only transcription factor binding partner of PGC-1α which can bind this motif in the absence of ligand (Yoon et al., 2001). PGC-1α also has a series of transcription factor binding partners which do not interact with PGC-1α via its LXXLL binding motifs. These include PPARγ and NRF-1, which bind amino acids 200-400 of the repression domain (Puigserver et al., 1998; Wu et al., 1999), and MEF2-C, which binds at amino acids 400-500 (Michael et al., 2001).

The repression domain, amino acids 200-403, was originally observed to have a repressive effect on the transcriptional activity of PGC-1α (Puigserver, 1999). A repressor protein, the p160 myb binding protein (p160MYB) was later shown to bind this regulatory domain, and was responsible for the repressive effect (Fan et al., 2004). When p38 MAPK is

activated via stress, it can phosphorylate PGC-1α in 3 different locations within this repression domain: T262, S265, and T298 (Puigserver et al., 2001). This phosphorylation increases the stability of PGC-1α and leads to an increase in transcriptional activity of PGC-1α target genes (Knutti et al., 2001). The repression domain also contains one of the nuclear localization signals for PGC-1α, located at amino acids 326-333, allowing it to translocate to the nucleus upon de-repression as well (Monsalve et al., 2000).

The proline-rich domain follows the repression domain. While the function of this domain for PGC-1α has not been elucidated, proline-rich domains are commonly found in signaling proteins which contain multiple functional domains. Once bound to a transcription factor, for example, they typically function to guide the protein to assemble into complexes, with transcriptional complexes being a common target (Kay et al., 2000). Therefore, this proline-rich region is most likely involved in recruitment of PGC-1α to its transcription factor and chromatin remodeling binding partners gathered at the target gene's promoter.

The host cell factor (HCF) binding domain has been proposed to serve as a docking site for the host cell factor protein (Vogel and Kristie, 2000). HCF contains binding sites in several known PGC-1α transcription factor binding partners, such as NRF-2α and β. PGC-1α interaction with NRF-2 is necessary for its activation of some target promoters (Handschin et al., 2007a) (Lin et al., 2002). However, the two proteins do not appear to interact directly, either in vivo or in vitro; HCF is therefore a likely candidate to promote the interaction between these factors for transcriptional activation (Lin et al., 2002a).

The C-terminal region of PGC-1α carries the RS and RMM domains. These two types of domains have been known to be involved in RNA processing, an uncommon feature of a transcriptional coactivator. These domains are specifically responsible for complexing with phosphorylated RNA polymerase II and elongation factors, providing a link between transcription and RNA processing (Monsalve et al., 2000; Yuryev et al., 1996). PGC-1α has also

been shown to be able to complex with several different splicing factors, and thus also has the potential to be involved in RNA splicing events, although most likely only to RNA derived from transcription target genes. There are also two nuclear localization signals located within the CT region (amino acids 627-633, 651-667). Interestingly, IHC for PGC-1α shows a “speckled” distribution of signal in the nucleus, a pattern that is typical of splicing proteins. This non-homogenous intra-nuclear localization was shown to be dependent upon the RMM and RS domains (Monsalve et al., 2000). Thus, PGC-1α has the potential to both activate the transcription of its target genes and subsequently process the resulting transcript, although direct evidence for this latter activity is still circumstantial.

Several post-translational modifications control PGC-1α activity (Table 1-1). PGC-1α can be phosphorylated by p38 MAPK (Knutti et al., 2001; Puigserver et al., 2001). This phosphorylation is related to cytokine effects on PGC-1α and its effectors. AMPK can also directly phosphorylate PGC-1α, allowing PGC-1α to co-activate its own transcription (Jäger et al., 2007). When PGC-1α is deacetylated by NAD+ dependent SIRT1 deacetylase, PGC-1α can then bind to its transcription factors responsible for activation of fatty acid oxidation during fasting conditions, such as the orphan nuclear hormone receptors ERRα and ERRγ (Gerhart-Hines et al., 2007). Arginine methylation across the length of PGC-1α by PRMT1 (protein arginine methyltransferase-1) can also activate PGC-1α (see Table 1-1). If any of these arginines are mutated, PGC-1α ability to regulate its target genes is negatively affected (Teyssier et al., 2005).

Although PGC-1α interacts with transcription factors that affect the downstream regulation of several target genes within a pathway, only some of those genes are induced by an interaction of that transcription factor with PGC-1α. This shows that there is promoter specificity for PGC-1α coactivational binding. For example, PPARγ can directly bind UCP-1 and Ap-2 (adipocyte protein-2) promoters and is a binding partner for PGC-1α. Upon coactivation

with excess PGC-1α, UCP-1 mRNA is upregulated, but the Ap-2 gene was not activated (Puigserver et al., 1998; Tontonoz et al., 1993). Thus, PGC-1α as a transcriptional coactivator not only increases a transcription factor's transcriptional activity, but also confers specificity to certain target genes. Also, chromatin immunoprecipitation studies on the ERs (estrogen receptors) indicates that the nuclear hormone receptors will bind different coactivators at different promoters. Therefore, promoters can lend specificity to certain transcriptional activator / coactivator pairs, and thus lead to the induction of different target genes (Shang et al., 2000). PGC-1α can have different binding partners due to interactions outside of the promoter region as well. This can occur by nuclear factors drawing it to enhancer or repressor regions in a target gene. For example, there are nuclear hormone receptors bound at the UCP1 (uncoupling protein 1) enhancer with which PGC-1α can interact depending on the presence of ligand. If ligand is present, PGC-1α can interact with the RAR (retinoid A receptor) or TR (thyroid receptor); without ligand, PGC-1α can interact with PPARγ (Puigserver et al., 1998). This leads to induction of different UCP-1 downstream targets, depending on the transcription factor pair that activated it.

Table 1-1. Post-translational modifications of PGC-1a

Post-translational modification	Responsible protein	Location (aa)	Functional Domain	Reference
Phosphorylation	AKT	S570	RNA processing	Li et al., 2007
	AMPK	T177, S538	Activation, RNA processing	Jäger et al., 2007
	P38 MAPK	T262, S265, T298	Repression	Puigserver et al., 2001
Acetylation	GCN5	K77, K144, K183, K253, K270, K277, K320, K346, K412, K441, K450, K757, K778	Activation, repression, ligand-independent binding, proline rich, RNA processing	Lerin et al., 2006
Deacetylation	SIRT1			Rodgers et al., 2005
Methylation	PRMT1	R665, R667, R669	RNA processing	Teyssier et al., 2005

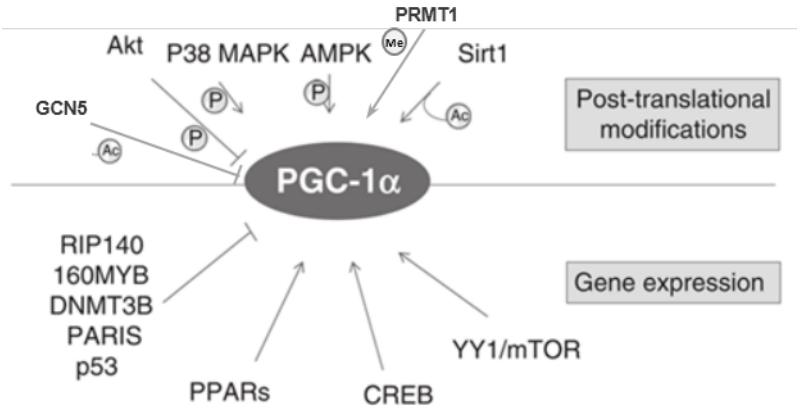

Fig. 1-3: Transcriptional regulation and post-translational modifications of PGC-1α (Adapted from Wenz, 2013). The upper portion of the diagram indicates proteins which post-translationally modify PGC-1α. Pointed arrowheads represent a modification that leads to activation of PGC-1a, whereas flatheads indicate modifications that lead to inhibition of PGC-1α activity. Ac = acetylation; P = phosphorylation; Me = methylation. The lower portion of this diagram indicates proteins which affect gene expression, either by binding to or modifying the PGC-1α promoter. Pointed arrowheads represent of interactions that lead to upregulation of PGC-1a, whereas flatheads indicate interactions that lead to repression of PGC-1α expression.

3. Environment, stress, and diet: upstream PGC-1α regulation.

Several metabotropic receptor signaling pathway proteins are responsible for activating PGC-1α. These interactions can occur through a number of different interactions with various PGC-1α functional domains. All of these signaling proteins are initially stimulated by changes in concentrations of hormones, energy intermediates, or free radicals. These include glucagon, AMP, ROS, and NOS, among others. There are several routes through which PGC-1α can be regulated either at the level of post-translational modifications or gene expression (see Fig. 1-3, table 1-1). The enzymes responsible for post-translational modifications which result in alteration of PGC-1α activity include SIRT1, Akt, AMPK, and p38 MAPK (Table 1-1). At the level of gene expression, there are both negative and positive regulators of PGC-1α mRNA. The positive regulators include the PPARs, CREB, and mTOR/YY1. The negative regulators include RIP140, 160myb, PARIS, DNMT3b, and p53. The details of these interactions and their regulatory roles on PGC1a levels and activity are under intense investigation.

3a. Post-translational modifiers and regulators of PGC-1α activity:

SIRT1: SIRT1 is a deacetylase of histones H3 and H4 and activates PGC-1α through this activity (Lagouge et al., 2006). Excess pyruvate in the diet (or lactate in the case of endurance exercise) leads to an increase in NAD+ concentrations. This provides substrate for SIRT1, which removes the acetyl group added to PGC-1α via GCN5 (Cantó and Auwerx, 2009). This diet-dependent modification specifically upregulates PGC-1α activity in liver (Nemoto et al., 2004; Rodgers et al., 2005). In addition, oxidative stress and SIRT1 deacetylation activate FOXO1 and FKHR (forkhead in rhabdomysarcoma) to bind to the PGC-1α promoter at its insulin response elements to promote its transcription (Daitoku et al., 2003; Frescas et al., 2005).

Akt and AMPK: FOXO3 and Akt work to prevent nuclear translocation of FOXO1 and FKHR, respectively, and thus repress PGC-1α activation and mitochondrial biogenesis (Daitoku et al.,

2003; Frescas et al., 2005). AMPK pathways serve in opposition to Akt pathways in that AMPK is activated in anabolic states (hypoxia, fasting, prolonged exercise) to promote catabolism, whereas Akt is activated in catabolic states to promote anabolism (Birnbaum, 2005). Exercise results in increased AMP, which activates AMPK, resulting in PGC-1α phosphorylation and mitochondrial biogenesis (Chabi et al., 2005). While short bouts of hypoxia stimulate AMPK and thus PGC-1α via NO synthesis, HIF-1 inhibits the AMPK pathway, suppressing mitochondrial biogenesis (Gutsaeva et al., 2008; Mason et al., 2007).

p38 MAPK: β-adrenergic receptors innervated by the sympathetic nervous system are the first to regulate PGC-1α transcription in response to hypothermia and changes in diet (Puigserver et al., 1998). In response to oxidative stress or inflammation, these receptors along with cytokine cell surface receptors such as IL-1α, β, and TNFα, can directly phosphorylate p38 MAPK. This phosphorylation activates the PKA and p38 MAPK pathways via signaling cascades. PKA will eventually phosphorylate CREB, which can directly bind to the PGC-1α promoter to activate PGC-1α gene expression (Puigserver et al., 2001). Once p38 MAPK is activated, it can also phosphorylate PGC-1α directly. This causes a conformational change in the PGC-1α repression domain, thus destabilizing the repressive factor 160myb, which releases PGC-1α, making it active. Therefore, p38 MAPK phosphorylation ultimately activates and stabilizes PGC-1α, allowing it to translocate to the nucleus. Following exercise, p38 MAPK is stimulated in skeletal muscle. This stimulation results in the activation of transcription factors MEF2 and ATF2. ATF2 upregulates PGC-1α expression and MEF2 functions as a TF binding partner for PGC-1α enabling activation of target genes. p38 MAPK can also directly phosphorylate PGC-1α in response to inflammation in muscle via cytokine signaling (Cao et al., 2004; Puigserver et al., 2001).

3b. Positive regulators of PGC-1α expression

CREB (and MEF2): Exercise activates calcineurin (CaN) and Ca2+-calmodulin dependent kinase (CaMK) via contractile activity that increases the concentration of intracellular calcium. This rise in intracellular calcium causes CaMK to activate CREB in adipose tissue and muscle. CREB can then translocate to the nucleus to activate PGC-1α transcript expression in these tissues. TORC (transducer of regulated CREB-binding protein) can act as an enhancer for this interaction (Akimoto et al., 2004a, 2004b; Wu et al., 2006). CREB works to stimulate PGC-1α production in the nucleus via signal transduction of TORC1 and TORC2. TORCs respond to increases in calcium and cAMP in the cytosol and translocate to the nucleus to bind and activate CREB. In the nucleus, CREB then upregulates PGC-1α (Herzig et al., 2001; Wu et al., 2006). In liver, CREB activates PGC-1α in response to glucagon, and in brown adipose tissue, CREB induces PGC-1α expression in response to cold temperature (Herzig et al., 2001; Puigserver et al., 1998). CaN functions and is activated similarly to CaMK. It can also indirectly activate PGC-1α in skeletal muscle, via activation of MEF2 (myocyte enhancer factor-2). MEF2, via interaction with its coactivator PGC-1α, is able to bind to the PGC-1α promoter and activate it; in this scenario, PGC-1α co-activates itself. (Handschin et al., 2003).

PPARs: PPARs are able to detect dietary changes via their endogenous ligands such as fatty acids and eicosanoids. Via this ligand dependent binding, PPARs can associate with and activate PGC-1α and thus mitochondrial biogenesis (Gervois et al., 2000). Fasting causes the expression of eNOS (endothelial NO synthetase), which causes NO production. NO stimulates mTOR and the FOXO transcription factors, which are regulators of PGC-1α. This ultimately activates PGC-1α and mitochondrial biogenesis (López-Lluch et al., 2006; Nisoli et al., 2005).

YY1/mTOR: It is possible for PGC-1α to self-regulate its gene expression via yin-yang 1 (YY1) as well. Through chIP assays, including overexpression and siRNA knockdown in cultured myotubes, it was determined that YY1 is a target of mammalian target of rapamycin (mTOR)

and PGC-1α. mTOR directly modulates the physical interaction of PGC-1α with YY1 and thereby modulates mitochondrial activity. mTOR is under the control of p53 and AMPK. Once stimulated via the AMPK signaling cascade, mTOR can complex with PGC-1α and YY1 (Cunningham et al., 2007; Schieke et al., 2006). Decrease in mTOR activity by p53 likely inhibits YY1-PGC-1α function resulting in decreased expression of mitochondrial genes.

3c. Negative regulators of PGC-1α

RIP140: During adipogenesis, ERRα can also function to inhibit expression of PGC-1α via its ability to stimulate RIP140 (a nuclear corepressor). This represses both fatty acid oxidation and mitochondrial biogenesis. PGC-1α can also directly interact with RIP140 to repress ERRα and NRF-1 expression of CIDEA, a gene involved in apoptosis and metabolism. These interactions show negative feedback loops centering on PGC-1α in control of metabolism (Hallberg et al., 2008; Nichol et al., 2006).

PARIS: PARIS (ZNF746) is a zinc finger protein that was found to be a substrate for parkin, a protein in which mutations were found to be associated with PD. PARIS can repress the expression of PGC-1α and thus its target gene, NRF-1 by binding to IRS (insulin response) sequences in the PGC-1α promoter (Shin et al., 2012). Under normal circumstances, parkin regulates PARIS expression by binding to and ubiquitinating it. When parkin is dysfunctional, as in Parkinson's disease, PARIS is no longer capable of being sequestered and degraded through parkin interaction, thus PGC-1α repression occurs in an uncontrolled and detrimental manner.

p53: Shortening of telomeres occurs as a result of aging. This shortening activates the telomere- p53 pathway, which results in p53 binding and repression of PGC-1α and β transcription (Sahin et al., 2013).

DNMT3b: The PGC-1α promoter can be methylated by DNMT3b to repress its expression (Barrès et al., 2009). This was found to occur when levels of palmitate, a free fatty acid, were high, inducing the non-CpG methylation of the PGC-1α promoter. This resulted in decreased

PGC-1α as well as mtDNA levels.

4. PGC-1α binding partners and downstream signaling

Once PGC-1α has been activated or derepressed by the several pathways described, it can carry out its function as a transcriptional coactivator and form complexes with its transcription factor binding partners at the promoters of its target genes. The main families of binding partners PGC-1α interacts with include the NRFs, ERRs, and the PPARs. These families of binding partners mainly function in mitochondrial biogenesis, but all other functions have a main theme of oxidative metabolism (see Fig. 1-4). These include fatty acid oxidation, peroxisome function, glucose sensing and utilization, as well as free radical detoxification. Other functions that operate outside of oxidative metabolism include osteogenesis, neuromuscular junction stabilization, adipocyte cell fate, and myotube cell fate.

NRFs: PGC-1α activates the expression of subunits of the respiratory chain and TFAM through the induction of NRFs and the coactivation of NRF-1-mediated transcription. TFAM subsequently translocates into the mitochondrion and directly increases the transcription and replication of mtDNA necessary for mitochondrial biogenesis (Evans and Scarpulla, 1990; Virbasius et al., 1993; Wu et al., 1999). The NRF-1/ PGC-1α transcription factor / coactivator pair (TF/TC) can also target VHL (von Hippel-Lindau tumor suppressor), a negative regulator of HIF-1. HIF-1 can function to suppress AMPK signaling pathways, which would cause a decrease in overall PGC-1α expression; however, the activation of VHL would prevent this decrease in non-disease states (Hervouet et al., 2005). PGC-1α also interacts with NRF-2α. This TF/TC pair targets and thus induces β-ATP synthase in addition to the nuclear-encoded mitochondrial cytochrome C genes (Mootha et al., 2004). These interactions show that the NRF/PGC-1α binding pair is crucial for mitochondrial biogenesis and preservation of normal mitochondrial function. Our lab discovered the mitochondrial DNMT1 isoform, which is transported into the mitochondrion via a mitochondrial leader sequence. Once in the

mitochondrion, mtDNMT1 can methylate mitochondrial DNA (Shock et al., 2011). Our lab also found that mtDNMT1 is a target of the PGC-1α / NRF1 TC/TF binding pair. This was shown via immunoblot where mitochondrial levels of DNMT1 increased after cotransfection of PGC-1α and NRF1 (Shock et al., 2011). These findings show that PGC-1α plays an indirect role in the methylation and subsequent epigenetic regulation of mitochondrial DNA.

ERRs: The ERRs are orphan nuclear hormone receptors. When bound to PGC-1α, ERRα and ERRγ can target genes involved in the scavenging, production, and transport of ATP and its precursors across the mitochondrial membranes as well as intracellular fuel sensing (Dufour et al., 2007). ERRα controls MCAD (medium chain acyl-coenzyme A dehydrogenase) to promote β-oxidation of fatty acids and thus also provide reducing equivalents NADH and FADH2 for the respiratory chain. This TC/TF pair also controls several genes important for mitochondrial biogenesis. PGC-1α also utilizes ERRα to create a positive feedback loop. This is possible because the ERRα promoter can bind NRF2 and itself to activate its own transcription. ERRα can subsequently bind PGC-1α to upregulate NRF-1 (Mootha et al., 2004; Schreiber et al., 2003). ERRγ is similarly activated by PGC-1α, except its target genes lie in areas of glucose sensing as well as fatty acid oxidation during fasting conditions (Gerhart-Hines et al., 2007).

PPARs: Both PPARα and PPARγ function as binding partners for PGC-1α. PGC-1α / transcription factor pairs function to target a series of tissue specific promoters to mediate different controls of metabolism. In adipose tissue, PGC-1α is activated in response to environmental cold via β-adrenergic receptors functioning in response to the temperature change triggered by the sympathetic nervous system. Once PGC-1α is activated in this tissue, it coactivates PPARγ and TH (thyroid hormone receptor) on the UCP1 enhancer. This interaction ultimately leads to BAT-mediated adaptive thermogenesis in mammals (Fan et al., 2004; Puigserver et al., 1998). PGC-1α stimulates genes of fatty acid oxidation in cardiac cells as well as in adipocytes via its binding interaction with PPARα (Barger et al., 2000). PPARα regulates

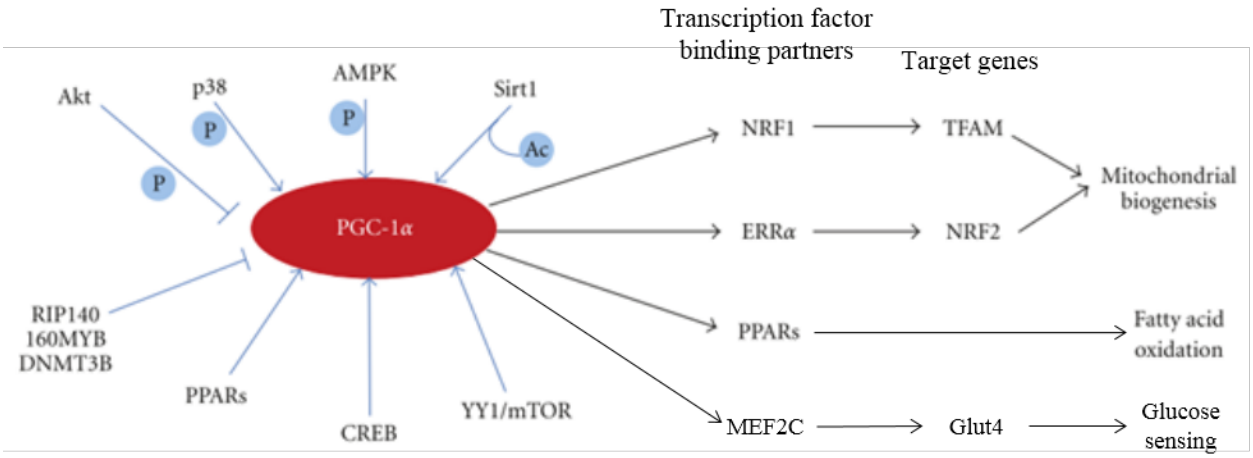

Fig. 1-4: PGC-1α binding partner interaction and downstream regulation (Adapted from Wenz, 2011). The left side of this diagram follows the same logic as in Fig. 1-3. (moving from left to right) After PGC-1α is regulated at the transcript or protein level, PGC-1α-protein can interact with its transcription factor binding partners through their respective domains (see Fig. 1-2). PGC-1α can now indirectly bind to the target gene of the pair and up or downregulate expression. These target genes are involved in an array of processes including mitochondrial biogenesis and oxidative phosphorylation.

carnitine O-palmitoyltransferase-1 in this β oxidation process (Vega et al., 2000). This provides reducing equivalents NADH and FADH2 for the respiratory chain, contributing to mitochondrial function and biogenesis.

Other targets functioning in oxidative metabolism:

PGC-1α induces the gene expression of Glut4 (insulin sensitive glucose uptake transporter), increasing glucose uptake; this connection is mediated through PGC-1α binding to the transcription factor MEF2C (myocyte enhancer factor-2C) (Michael et al., 2001). YY1 is an initiator element-binding factor which can be activated via interactions with mTOR and PGC-1α as previously detailed. It can both enhance and suppress certain cytochrome oxidase subunit genes important in mitochondrial biogenesis (Seelan and Grossman, 1997). Thyroid hormone response elements in the PGC-1α promoter can bind thyroid hormone and thus coactivate and upregulate thyroid hormone receptor (TR) (Weitzel and Iwen, 2011). PGC-1α also controls peroxisome biogenesis. This is interesting to note, because mitochondria and peroxisomes work together to carry out oxidative metabolism, with peroxisomes providing partially broken down fatty acids for complete breakdown to their energy equivalents via β-fatty acid oxidation by mitochondria (Bagattin et al., 2010). PGC-1α may also localize to the mitochondria to directly coordinate the induction of mitochondrial genes via interactions with TFAM (Aquilano et al., 2010; Safdar et al., 2011). PGC-1α also co-activates expression of mammalian homolog of tribble3 (TRB-3), an Akt pathway inhibitor (Koo et al., 2004)(O'Hagan et al., 2009). This is interesting since Akt phosphorylation can repress PGC-1α. PGC-1α target genes also include genes regulated by HIF-1α (O'Hagan et al., 2009). When there is sufficient oxygen, PGC-1α is able to induce HIF-1α responsive genes by stabilizing HIF-1α. It has been recently shown that this may be a tissue specific interaction, in that PGC-1α is required to regulate the response of adipocytes (Pino et al., 2012) as well as endothelial and neuronal cells under hypoxic conditions (Zhao et al., 2012).

PGC-1α has several targets that function in antioxidant production and ROS detoxification. One of these targets is SIRT3 (Kong et al., 2010). Once induced, SIRT3 localizes to the mitochondria to aid in mitochondrial biogenesis by regulating metabolic enzymes and ROS detoxification (Verdin et al., 2010). SIRT3 can also target the mitochondrial permeability transition pore (mPTP, referred to in this work as VDAC). Once activated, it regulates cyclophilin D and prevents the pore from opening. This pore plays a role in apoptosis and mitophagy, thus SIRT3 provides an additional downstream function for mitochondrial stability. SOD2 (superoxide dismutase) and GPX1 (glutathione peroxidase), also activated by PGC-1α, assist in the removal of superoxide and hydrogen peroxide (St-Pierre et al., 2003, 2006; Valle et al., 2005). The FOXO transcription factors function as binding partners for PGC1α, particularly FOXO3. FOXO3 target genes require coactivation by PGC-1α to be induced. These include ROS detoxifying proteins (Olmos et al., 2009).

Targets functioning outside of oxidative metabolism:

In complex with NRF-2α (GABP), PGC-1α can upregulate genes involved in neuromuscular junction function (Handschin et al., 2007b). PGC-1α can also control VEGF expression and thus contributes to muscle angiogenesis (Chinsomboon et al., 2009). Through interaction with ERRα as well as coactivation of the vitamin D receptor, PGC-1α may play an important role in bone formation and maintenance (Savkur et al., 2005; Zirngibl et al., 2008).

Overall, PGC-1α binding interactions regulate the transcription of its downstream target genes. This transcriptional regulation is key to producing the proteins necessary to govern all aspects of mitochondrial biogenesis. This role of master regulator which PGC-1α holds is truly demonstrated in its ROS management activity. Since PGC-1α activity can result in increased mitochondrial mass, PGC-1α indirectly induces naturally increased levels of ROS. This increase could be detrimental to the cell, but PGC-1α is able to upregulate genes involved in antioxidant production and ROS detoxification, compensating for its own potential negative effects. Therefore proper PGC-1α function in mitochondrial biogenesis and ROS management is crucial

to the maintenance of cell health.

III. PGC-1α: animal and cell models

Over the past 15 years, animal and cell models have been developed as tools to elucidate the overarching processes controlled by PGC-1α. Many of these models also gave insight into the genes up or downregulated by the overexpression or absence of PGC-1α and thus the pathways controlled by PGC-1α. Immunoprecipitation using tissue from transgenic mice as well as cell lines overexpressing PGC-1α also allowed identification of binding partners. Although the pathways involved and binding partners have already been described here, I will provide an overview of the findings of PGC-1α animal and cell models that are available and point out how these studies gave insight into potential roles of PGC-1α in mitochondrial dysfunction and disease.

1. Knock out and silencing studies

PGC-1α null mice, created using a Cre-Lox system with a ZP3 promoter, resulted in directing homologous recombination removing exons 3-5 of the PGC-1α gene to oocytes, thus driving the deleted allele into the germline. Breeding of mice heterozygous for the null allele resulted in homozygous PGC-1α null mice. Under normal conditions germline PGC-1α knockout mice are viable and appear to function normally; however, under stress they cannot maintain body temperature and are unable to maintain energy production or cardiac output (Arany et al., 2005; Leone et al., 2005; Lin et al., 2004). As a result, these mice are very sensitive to cold exposure, becoming hypothermic to the point of death in a short period (Leone et al., 2005; Lin et al., 2004). This is a direct consequence of the requirement for PGC-1α in adaptive thermogenesis in brown fat via targeting of UCP1 through activation of TR and PPARγ. PGC-1α KO animals also showed deficits in converting from fed to fasted state, resulting in hypoglycemia and hepatic steatosis (Koo et al., 2004; Leone et al., 2005). Since PGC-1α is responsible for

mediating all metabolic changes in the liver during fasting, including gluconeogenesis and fatty acid β oxidation, this result would also be expected (Yoon et al., 2001).

In addition to metabolic stress related changes, behavioral and cell morphological changes were also observed in these mice. The behavioral changes include increased anxiety and hyperactivity, which causes the mice to be very lean and have difficulty gaining weight. The brains of knockout mice showed distinct morphological changes, including vacuolizations localized mainly to the dorsolateral striatum but also seen sporadically throughout the brain (i.e. cortex, thalamus, basal ganglia, and hippocampus), accompanied by reactive glia and neurodegeneration (Leone et al., 2005; Lin et al., 2004). Another feature of the brains of these PGC-1α global knockout mice is that the neurons in the substantia nigra and the CA1 of the hippocampus are more susceptible to chemically induced neurodegeneration, such as from MPTP and KA (St. Pierre et al., 2006). As another potential cause for these abnormalities and the inability to maintain homeostatic functions under stress, real-time RT-PCR of these mice revealed vast decreases in levels of mitochondrial genes (Lin et al., 2004).

Conditional knockouts of PGC-1α have been accomplished using tissue specific Cre recombinase. The KOs generated were specific to mouse forebrain and mouse skeletal muscle. By deleting PGC-1α in CaMKIIα expressing neurons, Ma and colleagues were able to investigate the role of PGC-1α in the forebrain (Ma et al., 2010). These mice had many similar characteristics to the global PGC-1α knockout mice, except they were able to maintain certain functions that operated outside of the CNS, such as habituation to cold and fasting (brown adipose tissue and liver, respectively). Similarly to the global KO mice, the forebrain KO mice retained neurodegeneration in the striatum as well as resistance to obesity due to increased metabolic rate. Therefore, the majority of the function of PGC-1α in these neurons was attributed to maintaining neuronal stability and energy balance.

In skeletal muscle-specific PGC-1α KO mice, cytokine TNF-α levels of transcript and protein were increased following acute endurance exercise (Handschin et al., 2007c). A reduction in levels of antioxidant genes was also observed in these muscle-specific knockouts (Valle et al., 2005). These included reduced mRNA levels of SOD1, SOD2, and GPx1 with reductions in SOD2 protein levels as well (Geng et al., 2010; Leick et al., 2010). This provides evidence that one of the roles of PGC-1α is to prevent inflammation in response to metabolic stress. PGC-1α knockdown models have been developed as well, which have similar phenotypes to the PGC-1α KO models. PGC-1α knockdowns in mice are characterized by a reduced capacity for exercise, inability to maintain glucose and insulin levels, inflammation, and muscle fiber damage during exercise (Handschin et al., 2007b, 2007c). A knockdown model specific to human pancreatic islets was also created. siRNA knockdown of PGC-1α expression in human pancreatic islets resulted in a reduction in insulin secretion (Ling et al., 2008). This provides evidence that PGC-1α aids in normal pancreatic function and glucose sensing, and therefore its dysregulation may play a significant role in diabetes.

2. Overexpression studies

From studies involving overexpression of PGC-1α, there is proof of spatial regulation, i.e. tissue-specific effects, as well as temporal regulation, i.e. age-specific effects. This spatio-temporal regulation could potentially be controlled via epigenetics. Overexpression of PGC-1α can be harmful in the incorrect space and time, having similar effects to PGC-1α KO mice. For example, overexpression of PGC-1α in mice causes cardiac myopathy (Barger et al., 2000). When PGC-1α was overexpressed in the rat nigrostriatal tract, neuron degeneration was observed in dopaminergic cells of the substantia nigra pars compacta (SNp) (Ciron et al., 2012), a result that was similar to that obtained with tissue-specific KO mice. Therefore too much or too little PGC-1α can be equally detrimental.

Overexpression can be beneficial, however, in the correct space and time. During development, elevated levels of PGC-1α are natural. In older mice transgenically overexpressing PGC-1α, PGC-1α inhibits FoxO3 activity to upregulate genes involved in denervation and muscle atrophy, resulting in a decrease in muscle wasting as a response to aging (Sandri et al., 2006; Wenz et al., 2009). When overexpression is targeted to specific tissues for short periods PGC-1α effects are also beneficial. For example, overexpression of PGC-1α in the skeletal muscle of transgenic mice promotes the conversion to slow, oxidative type I and IIA muscle fibers. This is accompanied by the induction of oxidative phosphorylation and fatty acid oxidation genes along with increased mitochondrial mass (Lin et al., 2002b). In studies of mice ectopically expressing PGC-1α in muscle (MCK-PGC-1α transgenics), it was seen that mitochondria isolated from muscle of these mice vs. wild-type mice had a higher capacity for respiration and also preferred different substrates (lipids vs. carbohydrates) for that respiration (Hoeks et al., 2012; St-Pierre et al., 2003). This shows that new mitochondria created from PGC-1α induction have different properties than those not influenced by activation of PGC-1α. The converse is also true in PGC-1α deficient mice (Zechner et al., 2010). These changes could be due to differences in levels of protein necessary for respiration in these animals, such as increases in citrate synthase and β-hydroxyacyl CoA dehydrogenase (Hoeks et al., 2012). This phenomenon is referred to as organelle remodeling.

The mitochondria of the MCK-PGC-1α Tg mice, despite having higher levels of mitochondrial ROS production than their WT counterparts, show decreases in oxidative damage over time. This is due to subsequent PGC-1α upregulation of detoxifying enzymes that clear the ROS, which outweighs the extra being produced. This is further supported by increased levels of circulating ROS and oxidative damage in muscle from PGC-1α null mice. This increase in the amount of ROS produced initially compared to WT in the Tg mice is believed to be due to PGC-1α transcription modulation to increase the amount of complex I and complex III expressed in

the new mitochondria (Austin et al., 2011; St-Pierre et al., 2006; Valle et al., 2005; Wenz et al., 2009). In cultured cells, overexpression of PGC-1α increases protein levels of COXIV and Cytochrome C, and increases mtDNA copy number (Wu et al., 1999). Other beneficial effects of PGC-1α overexpression include up-regulation of SOD2 protein content, decreased inflammatory cytokine production, and decreased protein degradation due to denervation as observed in mouse skeletal muscle (Sandri et al., 2006; Wenz et al., 2009). These tissue-specific effects together with the fact that PGC-1α is highly expressed during development and then decreases shows that there are both spatial and temporal changes in PGC-1α regulation over an organism's lifetime. These changes could potentially be modulated via epigenetics and epigenetics based therapeutics. If overexpression could be targeted to certain tissues where an overabundance of PGC-1α is beneficial, its therapeutic effects could be harnessed.

IV. PGC-1α: Potential therapeutic interventions

If PGC-1α would be targeted therapeutically, it could not be done so directly. As demonstrated in animal and cell models, too little or overly excessive levels of PGC-1α can be harmful. Therefore directly targeting PGC-1α in order to drastically increase or decrease overall body levels would be similarly detrimental. Rather, drugs targeted to transcriptional regulation, protein modifications, or binding partner interactions of PGC-1α should be developed. Ideally, tissue-specific interactions in these three areas would be targeted to modulate levels of PGC-1α in a disease relevant manner. If drastic changes in protein levels were necessary to ameliorate dysfunction, administering tissue-specific PGC-1α targeting therapies would prevent detrimental effects in other tissues. The major classes of diseases with which PGC-1α has been associated include aging and muscle dysfunction, diabetes, and neurodegenerative diseases. I will

describe below the connections that PGC-1α has to several diseases and what therapeutic strategies are currently being considered that revolve around these connections.

Aging and Muscle Dysfunction:

Prolonged inactivity can result in muscle wasting, as seen in aging and muscle dysfunction diseases. This inactivity (IM) results in a natural loss of PGC-1α in skeletal muscle (Shin et al., 2012). Even when muscle movement is restored (RM), in cases of return to mobilization after rehabilitation, the body responds with increased ROS, cytokine, and oxidative stress levels, presumably due to the lag phase of PGC-1α attempting to return to normal levels (Kang and Ji, 2013). This response actually slows rebuilding of the muscle and functional rehabilitation. In a recent study in mice, it was found that local overexpression of PGC-1α after IM followed by RM lowered the initial inflammatory response naturally incited by RM while increasing mitochondrial biogenesis and oxidative phosphorylation (Kang and Ji, 2013).

Studies have shown that both endurance and resistance training can improve the aging phenotypes of human skeletal muscle. Exercise induces PGC-1α levels (Feng et al., 2013; Matiello et al., 2010; Suwa et al., 2008). Interestingly, older adults who regularly performed resistance type exercise had transcriptomes that were more similar to young adults than to less active people of their same age group, including elevated PGC-1α levels (Handschin and Spiegelman, 2008). It was shown in old mice as well that not only continuous participation in exercise training could result in this pro-PGC-1α young muscle phenotype, but even short periods of training can restore PGC-1α levels and increase mitochondrial biogenesis, and thus mtDNA content and ATP production in older mice (Kang and Ji, 2013).

Mutant POLG mice (polymerase γ, the only polymerase that transcribes mtDNA), exhibit early aging phenotypes including decreases in mitochondrial number and function. When these

mice also transgenically overexpress PGC-1α, mitochondrial activity increases, improving cardiac and muscular function, including decreases in sarcopenia (Dillon et al., 2012) This shows that PGC-1α can function to reduce or delay the mitochondrial dysfunction that contributes to aging. In mice, transgenic elevation of PGC-1α in muscle reduces muscle fiber atrophy induced by statins, as well as in models of Duchenne muscular dystrophy and mitochondrial myopathy (Hanai et al., 2007; Handschin et al., 2007b; Sandri et al., 2006). This is presumably due to overexpression of PGC-1α inducing an exercised phenotype, which is potentially due to its role in the control of neuromuscular junction genes as well as muscle fiber type switching. Together, these studies show that exercising regularly can improve muscle function and prevent muscle wasting associated with aging as well as muscle dysfunction diseases via increases in PGC-1α and mitochondrial biogenesis.

Diabetes and Obesity:

PGC-1α expression has been shown to be reduced in WAT (white adipose tissue) of morbidly obese and diabetic patients (Semple et al., 2004; Yang et al., 2003)(Patti et al., 2003). It was also found that early signs of insulin resistance included reduced levels of PGC-1α, NRF1, and mtDNA (Patti et al., 2003). This was determined to be due to hypermethylation of PGC-1α potentially achieved through environmental changes, such as a buildup of fatty acids in the diet (Barrés et al., 2009). Although demethylases do exist, there are no ways as of yet to target them to particular promoters. Therefore activating PGC-1α has been the only therapeutic strategy in relation to the connection of PGC-1α to diabetes that has been used in the treatment of this disease. Fibrates and thiazoledinediones are currently in use (PPAR activators; (Wilson-fritch et al., 2004)). Also, with the various important roles in metabolism for PGC-1α, including glucose sensing, it could be a pharmacological target for developing new drugs to treat diabetes or obesity.

NEURODEGENERATIVE DISEASES

Some evidence has shown that reactive oxygen species (ROS) may play a protective role in metabolism by stimulating mitochondrial biogenesis. In fact, levels of ROS and reactive nitrogen species (RNS) produced during exercise activate the specific PGC-1α pathway that stimulates antioxidant production. This system is likely disrupted in neurodegenerative diseases, resulting in detrimental effects (Gomez-Cabrera et al., 2008; St-Pierre et al., 2006).

Huntington's Disease (HD)

In HD patient brain, there is a reduction in PGC-1α mRNA and protein levels (Cui et al., 2006; Taherzadeh-Fard et al., 2009; Weydt et al., 2006), which is also apparent in a transgenic mouse model of HD (Cui et al., 2006). The transgene introduced in mouse contains the 5' end of human mutant Huntington gene, through exon 1. Within this portion of the transgene, transcript encoding for CAG repeats, aka the polyglutamine tract, is expanded compared to normal Huntington protein. This region is variable from animal to animal of the same species, with a normal protein containing about 30 glutamine repeats. Once this variable region expands (through unknown means) over generations to >115 glutamine repeats, this protein exhibits a toxic gain of function, resulting in Huntington's Disease. This expanded number of glutamine repeats from ~27 to 115-150 in the transgene induces an HD phenotype, resulting in HD model mice (Mangiarini et al., 1996), PGC-1α KO mice as well as these HD transgenic mice exhibit the same behavioral and neuro-morphological abnormalities that are seen in Huntington's Disease patients, including choireform movements, tremor, epileptic seizures, and spongiform striatum (Cui et al., 2006; Lin et al., 2004; Weydt et al., 2006). In HD mice, exogenous restoration of PGC-1α expression via lentiviral vectors maintained the morphological integrity of the striatum (Cui et al., 2006). PGC-1α overexpression in these HD mice rescues neurons from altered morphology, degeneration and apoptosis, as well as mitochondrial dysfunction (Cui et al.,

2006). Therefore, maintenance of proper PGC-1α levels is important to neuron function and viability, specifically those neurons residing in the most highly affected area of both the PGC-1α KO mice and Huntington's patients: the striatum. Although the mechanics are unknown, the disease etiology is believed to be caused partially by PGC-1α repression by the mutant form of Huntington protein. This PGC-1α downregulation seen in these studies results in alteration of its downstream functions, particularly the maintenance of mitochondrial processes. Mitochondrial fragmentation is also observed in the striatal neurons of these HD mice, which is a sign of a pre-apoptotic cell (Kaddour-djebbar et al., 2010; Wang et al., 2009).This mitochondrial dysfunction may or may not be directly due to loss of PGC-1α, but it does present a likely possibility. PGC-1α ultimately regulates transcription of proteins necessary for mitochondrial dynamics, including Drp1 which is integral to the mitochondrial fragmentation process that can lead cells into an apoptotic state (Kaddour-Djebbar et al., 2010). Considering this connection as well as evidence in PGC-1α KO models of the importance of PGC-1α to maintaining the integrity of neurons in the striatum points to PGC-1α repression being a leading cause of HD, and more specifically, its role in the mitochondrial dynamics aspect of mitochondrial biogenesis.

Parkinson's Disease

Several studies have linked PGC-1α to Parkinson's Disease pathogenesis. A gene set enrichment analysis of 17 independent microarray datasets of human PD samples found that 425 PGC-1α regulated genes were down-regulated in this disease (Zheng et al., 2010). These genes were all found to be affected in substantia nigra homogenates as well as laser captured substantia nigra dopaminergic neurons gathered post-mortem from asymptomatic PD (incidental Lewy bodies) as well as symptomatic late stage PD patients. Their analysis indicated that the processes of mitochondrial electron transport, glucose utilization, and glucose sensing – all linked by PGC-1α – are misregulated early on in Parkinson's Disease pathology (Zheng et al., 2010).

Another link between PGC-1α and Parkinson's Disease is PARIS (ZNF746). PARIS is a zinc finger protein which can act as a substrate for parkin, a protein known to be associated with PD when mutated. PARIS can repress the expression of PGC-1α and thus its target gene, NRF-1. When parkin is conditionally knocked-out in mice, loss of dopaminergic neurons is observed. This neuron-specific neurodegeneration increases upon higher expression of PARIS. Cell loss was rescued by the addition of either parkin or PGC-1α (Shin et al., 2011). This exhibits the neuroprotective effects of PGC-1α, which was also observed in cell culture models of PD (Wareski et al., 2009; Zheng et al., 2010). The PARIS/PGC-1α interaction provides insight into PD pathology. PARIS interacts with PGC-1α at IRSs (insulin response sites) which regulate transcripts associated with insulin responsiveness and energy metabolism (Mounier and Posner, 2006). This relationship may connect mitochondrial dysfunction and improper glucose utilization to PD. A potential treatment that has emerged to target PGC-1α in PD is resveratrol. Resveratrol is a SirtI activator, which is involved in activating PGC-1α control of glucose sensing genes. By using it to activate PGC-1α in degenerating dopaminergic neurons, resveratrol rescued the cells, as did overexpression of PGC-1α (Mudò et al., 2012). Therefore, resveratrol has neuroprotective effects on dopaminergic neurons due to its downstream activation of PGC-1α, and thus is a potential therapy for attenuating the neurodegenerative effects of PD.

Alzheimer's and ALS

PGC-1α control of glucose utilization seems to play a role not only in PD, but also in AD pathogenesis (Qin et al., 2009). In neurons of an AD mouse model, these investigators showed a dose-dependent relationship between high glucose and β-amyloid plaque formation. This dose-dependent relationship also applied to PGC-1α expression: the higher the glucose concentration, the lower the PGC-1α. This provided a direct relationship between glucose utilization and AD pathology, linked together by PGC-1α. Upon exogenous addition of PGC-1α under these same hyperglycemic conditions, β-amyloid plaque formation was stopped. The root

of this process was found to be that hyperglycemic PGC-1α suppression in PD derepressed the FOXO3a transcription factor, thus contributing to β-amyloidogenic cutting by α-secretase (Qin et al., 2009).

PGC-1α is underexpressed in AD patients and mouse models. In cell models of AD, when PGC-1α is overexpressed, the phenotype returns to that of a non-disease state (Qin et al., 2009; Sheng et al., 2012). This shift occurs in mouse models of ALS as well upon expression of PGC-1α (Da Cruz et al., 2012; Liang et al., 2011; Zhao et al., 2012).

Similarly to its effects on dopaminergic neurons in PD, resveratrol offers neuroprotection to hippocampal neurons in a mouse model of AD through indirect activation of PGC-1α via Sirt1 (Kim et al., 2007). Reseveratrol is therefore a potential future therapy for AD, by its link to PGC-1α. Some drugs inadvertently targeting PGC-1α are already available and may be beneficial in diseases for which the drugs were not initially developed. These include fibrates and thiazoledinediones (PPAR activators), resveratrol (Sirt1 activator), as well as metformin and AICAR (AMPK activators).

V. Emerging PGC-1α isoforms

As of this year, there have been a total of 19 published PGC-1α isoforms (see table 1-2, Fig. 1-5). This number includes the canonical isoform, henceforth PGC-1α-a, of which all the information laid out in this introduction up until this point has been based upon. Although 19 exist, they can be broken into a few different categories based upon the promoter utilized to form the transcript. This list includes 4 PGC-1α-a variants (Puigserver et al., 1998; Soyal et al., 2012; Zhang et al., 2009), 3 PGC-1α-b variants (Miura et al., 2008; Ruas et al., 2012), 2 PGC-1α-c variants (Miura et al., 2008; Ruas et al., 2012), 1 NT-truncated (Felder et al., 2011), and 9 NT-extended (Choi et al., 2013; Soyal et al., 2012).

PGC-1α-a variants: Thus far, other than the canonical form of PGC-1α, there have been 3 other variants reported. These include NT-PGC-1α (Zhang et al., 2009), PGC-1α ex1-3ext and PGC-1α ex1-8a (Soyal et al., 2012). While PGC-1α ex1-3ext and 8a are the most recent isoform a variants to be identified, little is known about them. These two novel isoform a splice variants were found in human brain tissue via 5' RLM RACE (Soyal et al., 2012). Sequencing revealed that both isoforms involve exon extension via alternative splicing, producing in frame early stop codons for the resultant predicted protein. Specific roles for these two PGC-1α-a variants have not been identified.

Much more is known about NT-PGC-1a, with several studies published on its regulation and localization in different tissues since its original identification in mice (Chang et al., 2010; Shen et al., 2012; Zhang et al., 2009). NT-PGC-1α was first reported by Zhang and colleagues in 2009.Its transcript utilized the same promoter as the canonical isoform, but alternative 3' splicing between exons 6 and 7 resulted in a frameshift, introducing a stop codon in the 31 bp splicing insert 3 bases after the retained canonical sequence. This resulted in a 270 amino acid truncated form of PGC-1α-a, which they named NT-PGC-1α (Novel Truncated). This truncated version retains the activation domain and half of the repression domain (see Fig. 1-2). These remaining domains retain 2 out of 3 LXXLL motifs, 2 out of 3 p38 MAPK phosphorylation sites, 1 AMPK phosphorylation site, and 5 acetylation / deacetylation sites (see table 1-1). It is missing all other post-translational modification sites, NLSs, and RNA processing domains. Despite this truncation, they found that endogenous levels of this transcript were present at higher levels than PGC-1α-a by 1.5 fold. They also found readily detectable levels of NT-PGC-1α protein in several tissues (adipose - BAT and WAT, liver, brain, heart, spleen, skeletal muscle, and kidney) from mice, rats, and humans. Protein levels of NT-PGC-1α were highest in brain, but also detected in mouse BAT, brain, kidney and human heart between 35-38 kDa (predicted 30 kDa; PGC-1α-a predicted: 93 kDa, observed: 113 kDa). They also found that, as expected since

no NLSs were retained, NT-PGC-1α localized to the cytoplasm in mouse adipocytes; however, a small proportion of the exogenous NT-PGC-1α (~10%) is localized to the nucleus. This percentage increased to 20% upon activation by cAMP but not p38MAPK. Activation of PKA by cAMP also increased transcriptional activity of PPARγ, PPARα, and recruitment of NT-PGC-1α to associated transcriptional complexes. In a follow-up study (Chang et al., 2010), it was found that NT-PGC-1α was regulated by PKA and its interaction with CRM1, a nuclear exportin. This exportin also interacts with PGC-1α-a, however, the multiple NLSs present override the CRM1 induced export from the nucleus to the cytoplasm. PKA functions to inhibit CRM1 by phosphorylating NT-PGC-1α at 3 amino acids leading to a retainment of NT-PGC-1α in the nucleus, raising its effective concentration. Inhibition of CRM1 resulted in slow increase in effective nuclear concentration, therefore nuclear export of NT-PGC-1α must also be taking place by CRM1 independent mechanisms as well. Lastly, Shen and colleagues wanted to identify the subcellular localization of NT-PGC-1α. Using NT-FLAG NT-PGC-1α in skeletal muscle fibers, they found that NT-PGC-1α is localized to the myoplasm.

Similar proteins to NT-PGC-1α and PGC-1α ex1-3ext have been predicted, with only a few amino acids different at the N-terminus (Ruas et al., 2012; Lochmann, T. and Hedrick, S., unpublished findings). The reason that there would be two extremely similar versions of these isoforms is not yet known, and would be a mystery that this project can contribute to solving.

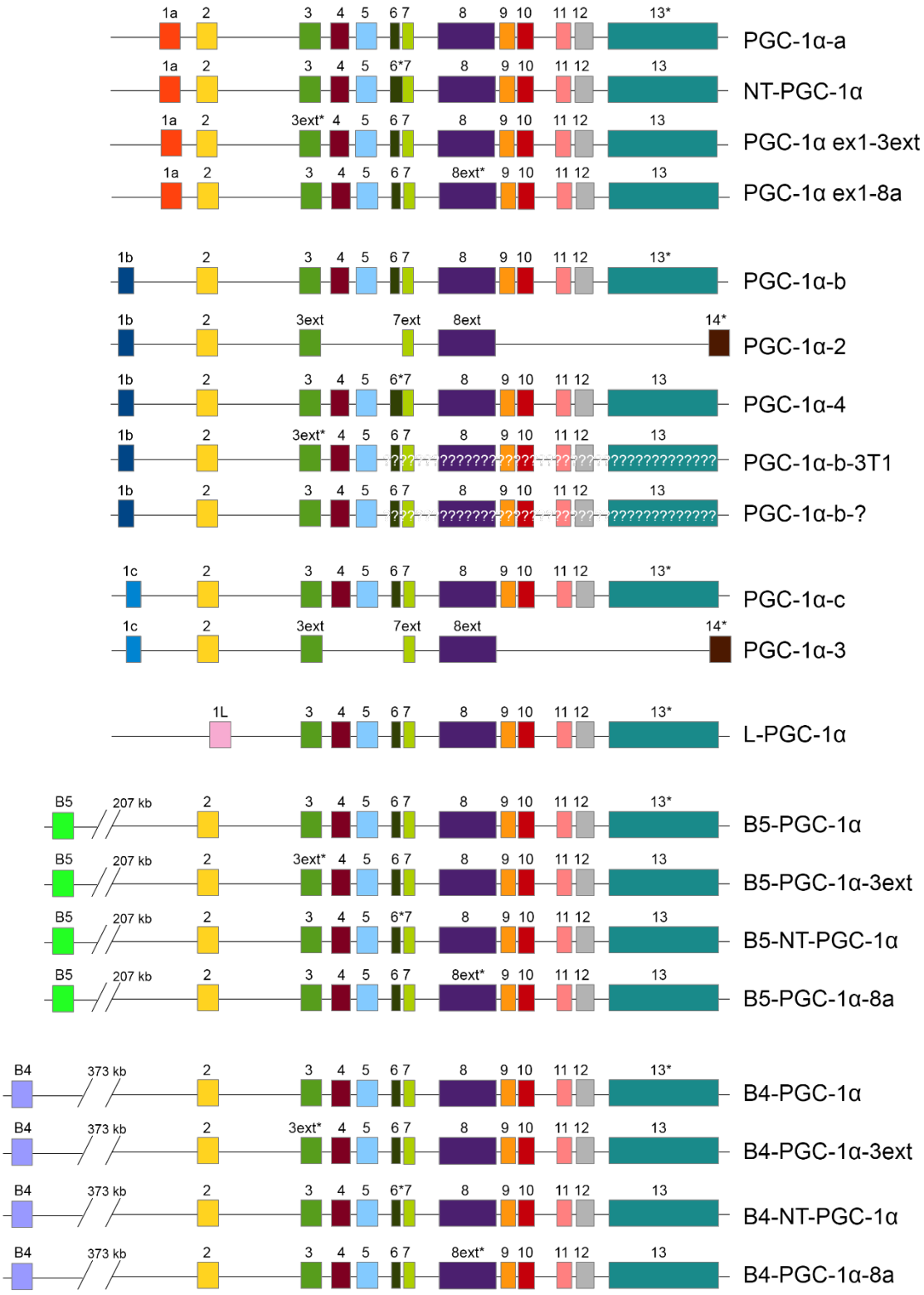

Fig. 1-5: PGC-1α isoforms. Exon maps of all PGC-1α isoforms to date. Boxes represent exons. Like colors represent the same exon, Lines represent introns. See **Table 1-2** for more detailed information about each isoform.

Table 1-2. PGC-1α isoforms

PGC-1a isoform category	Isoform name	Human? (Y or N)	Tissues	Predicted MW	Migrating MW	Primary Reference
a variants	PGC-1α-a	Y	All*	91 kDa	90-115 kDa	Puigserver et al., 1998
	NT-PGC-1α	Y	heart, brain, kidney, BAT	30 kDa	35-38 kDa	Zhang et al., 2009
	PGC-1a ex1-3ext	Y	brain	16 kDa	TBD	Soyal et al., 2012
	PGC-1a ex1-8a	Y	brain	33 kDa	TBD	Soyal et al., 2012
b variants	PGC-1α-b	Y	SM, heart, brain	92 kDa	TBD	Muira et al., 2008
	PGC-1α-2	N	brain, BAT, kidney, heart, SM	42 kDa	50 kDa	Ruas et al., 2012
	PGC-1α-4	N	brain, BAT, kidney, heart, SM	29 kDa	~40 kDa	Ruas et al., 2012
	PGC-1α-b-3T1	Y	HSM, brain	15 kDa	17 kDa*	Current thesis data
	PGC-1α-b?	Y	HSM, brain	TBD	TBD (90 kDa)	Current thesis data
c variants	PGC-1α-c	N	SM, heart, brain	92 kDa	TBD	Miura et al., 2008
	PGC-1α-3	N	brain, BAT, kidney, heart, SM	41 kDa	50 kDa	Ruas et al., 2012
NT-truncated	L-PGC-1α	Y	liver	74 kDa	77 kDa	Felder et al., 2012
NT-extended	B5-PGC-1α	Y	brain	92 kDa	TBD	Soyal et al., 2012
	B5-PGC-1α-3ext	Y	brain	17 kDa	TBD	Soyal et al., 2012

*All refers to all tissues mentioned in this table.

**Putative migration size

PGC-1α-b variants: Three isoform b variants are known. In the literature these are known as PGC-1α-b, PGC-1α-2, and PGC-1α4 (Miura et al., 2008; Ruas et al., 2012). PGC-1α-b was the first identified novel isoform of PGC-1α, present in mouse skeletal muscle, BAT, and liver by Miura and colleagues in 2008. They found a full-length transcript, compared with that of PGC-1α-a that was under the control of an upstream promoter. This promoter utilizes an alternative exon 1, which they denoted as exon 1b. Alternative splicing allowed exon 1b to be spliced to canonical exon 2, and thus the remainder of the transcript is identical to that of PGC-1α. The CDS – ending in exon 13 – only differs from PGC-1α-a by 12 amino acids at the NT, as it is coded by the only differing region in the transcript: exon 1b. It was found that although mRNA content was only 10% of that of PGC-1α-a, this isoform was greatly upregulated in skeletal muscle in response to endurance exercise, while PGC-1α-a remained unchanged (Miura et al., 2008). This was thought to be caused by β-2 adrenergic receptor activation, because clenbuterol treatment of inactive mice caused similar fold increases on isoform b expression only in skeletal muscle, while leaving canonical levels unaffected. Transcript levels of isoform b also changed in BAT in response to cold exposure while canonical PGC-1α-a remains the same. In liver, however, fasting produced changes in canonical PGC-1α, but not isoform b transcript expression. Exogenous overexpression of PGC-1α-b in both HEK293 cells and mice resulted in the upregulation of nuclear encoded mitochondrial genes necessary for mitochondrial biogenesis and fatty acid oxidation (mtTFA, COX2, COX4, ERRα, MCAD) which increased upon coexpression of PPARs (Miura et al., 2008). These initial isoform b findings showed that this isoform was functional as a transcriptional coactivator both in vitro and in vivo, though by forced overexpression. This isoform has low basal levels under normal physiological conditions (varying from 1 to 10% of total PGC-1α mRNA detected in various mouse tissues). Under stress, however, this isoform's level increased dramatically (28-350 fold) in a tissue-specific manner, accounting for a majority of total PGC-1α increase under these conditions

(Miura et al., 2008). This was one of the first insights to being able to control PGC-1α levels in a spatio-temporal manner for translational applications.

In response to this publication, several studies have been done regarding the transcriptional regulation of this isoform in both mice and humans, more specifically in skeletal muscle. Yoshioka and colleagues were the first to identify PGC-1α-b transcript in human skeletal muscle (Yoshioka et al., 2009). They described a functional E-box as well as a putative CRE site in the promoter region of the isoform b transcript in human skeletal muscle. They demonstrated in vitro that both of these sites are able to directly bind MyoD / MRF4 and CREB, respectively, resulting in promoter activation and increase in mRNA levels of PGC-1α-b. They also showed that the recruitment of CREB to the CRE site occurs in several ways via calcium induced signaling in response to exercise to induce PGC-1α-b expression. These include CamKIV and CnA, which activate CREB directly via serine phosphorylation or indirectly via activation and nuclear import of CREB coactivator TORC, respectively. Alternatively, exercise induced cAMP or p38 MAPK signaling can also recruit CREB. Forskolin, which increases cAMP levels, causes PKA activation which can phosphorylate and thus activate CREB. Considering β-2 adrenergic receptor stimulation upon catecholamine release upon exercise would also increase cAMP release, this model works nicely with the clenbuterol activation of this isoform shown by Miura and colleagues in mice. They also showed that MKK6, an activator of p38 MAPK signaling, can also lead to CREB phosphorylation and activation (Yoshioka et al., 2009). P38 MAPK and CnA involvement in PGC-1α-b activation has come into question; however, Norrbom and colleagues suggested that there is a role for AMPK instead, in that isoform b is stimulated via AICAR and norepinephrine (Norrbom et al., 2011). This finding also aligns with the model of β-2 adrenergic receptor activation in response to exercise (Miura et al., 2008). These findings reveal several ways to target PGC-1α in a tissue-specific manner.

Two new PGC-1α isoforms were found by Ruas and colleagues recently (Ruas et al., 2012). These are somewhat similar to some previously described isoforms found in mice and humans. These isoforms are called PGC-1α-2 and PGC-1α-4. PGC-1α-2 is an isoform b (PGC-1α-b: Miura et al., 2008) variant. It begins at the same exon 1b (called exon 1''' in Ruas paper) and instead of extending down to exon 13 with the same splicing as canonical PGC-1α, contains partial sequence conservation due to alternative splicing of only exons 3, 7, and 8 (excluding all other exons downstream of exon 3 from canonical PGC-1α). This alternative splicing does not result in the formation of an early stop codon, however, and ends in a newly described exon 14. This would results in a predicted protein of 379 amino acids (41.9 kDa). From gene expression array studies, it was determined that this isoform affected 110 genes, some differing from canonical PGC-1α. No functional studies have been reported on this isoform as of yet.

The second isoform they described, PGC-1α-4, is very similar to NT-PGC-1α. It contains the same splicing variation between exons 6 and 7, resulting in the formation of an early stop codon, but instead of the primary exon being exon 1a, it is exon 1b; therefore making this an isoform b variant under the control of the same alternate promoter (Ruas et al., 2012). This results in a predicted protein of 266 amino acids (29.1 kDa). In a gene expression array, PGC-1α-4 held 98 out of 519 genes affected in common with PGC-1α-a. It did not seem to affect several classic target genes of PGC-1α-a, including several genes involved with oxidative phosphorylation. These include CytC, CoxVb, Glut4, PDGFb, and MCAD. Despite this difference in regulation, presumably due to being under the control of an alternate promoter region as well as having vastly different C-termini, this isoform was found to be similar to PGC-1α-a in most ways. It retained transcriptional coactivator function, however, no longer could coactivate ERRα or ERRγ, which could explain changes in classic target genes. It also was not upregulated in skeletal muscle (in vivo human and murine biopsied muscle) in response to

endurance exercise, unlike PGC-1α-a. PGC-1α-4 was upregulated in response to resistance exercise, however. Also differing from PGC-1α-a, PGC-1α-4 upregulation in response to resistance training also results in increased IGF1 levels and decreased myostatin levels. IGF1 is an activator for muscle fiber hypertrophy and myostatin is a negative regulator of muscle size and strength (Ruas et al., 2012). These differences in function are the first described for a PGC-1α isoform. This information provides more evidence for the therapeutic potential of PGC-1α. For this particular isoform alone, there is the possibility for future translational developments to improve muscle-wasting in various diseases, including muscular dystrophies, neurodegenerative disorders, aging, and cancer cachexia. For this reason, determining the functional and tissue differences among the remaining PGC-1α isoforms is extremely important.

PGC-1α-c variants: PGC-1α-c is very similar to PGC-1α-b, with a few known exceptions to date. Both utilize the same alternative exon 1b and promoter, splicing to exon 2 and continuing the splicing of canonical PGC-1α down to exon 13. PGC-1α-c, though, is spliced to exon 2 using a different slice donor in exon 1b than PGC-1α-b, resulting in a slightly shorter CDS (Miura et al., 2008). In response to exercise, similar to PGC-1α-b, PGC-1α -c expression was induced 41 fold in skeletal muscle. Unlike PGC-1α-b, however, PGC-1α-c was not induced in response to cold exposure in BAT. Neither were induced in fasting conditions in the liver; only PGC-1α-a (Miura et al., 2008). Only noted in mice thus far, and although the TSS is conserved in humans, the mRNA transcript for isoform c was not found in human skeletal muscle in 5' RLM-RACE experiments in our laboratory (Lochmann, T. unpublished observation). Considering these isoforms share the same promoter, it is unclear how they could be targeted differently. For example, isoform b but not isoform c is upregulated in BAT of mice in response to cold exposure. The alternative promoter which produces isoform b and c transcripts contains a putative CRE site and E-box. These two features are common in muscle-specific COX genes, depending upon E-box consensus elements for their tissue-specific expression (Moreadith,

1995). This is interesting considering that both these isoforms are found to be upregulated in immediate response to short bouts of exercise in skeletal muscle of both mice and humans (Miura et al., 2008; Yoshioka et al., 2009; Norrbom et al., 2011). No further investigations into isoform c regulation or function have been published to date.

Ruas and colleagues found an isoform c transcript variant, occurring as the result of alternative splicing which they called PGC-1α-3. The TSS is shared with that of PGC-1α-c, and the rest of the transcript follows the same alternative splicing pattern as that of PGC-1α-2, another isoform variant they described in the same publication (Ruas et al., 2012). It would result in a protein of 370 amino acids (41.0 kDa). A gene expression array showed that its upregulation affects 69 genes, some of which differ from that of canonical PGC-1α. No further investigations into the regulation or function of this isoform c variant have been published to date.

Interestingly, even though isoform b and c transcripts increase together in response to stress in tissues tested, this increase did not fully account for the amount of total PGC-1α in qPCR studies. This also applies in human tissues tested in our lab (Lochmann, T.; Hedrick, S.; Thomas, R. unpublished observations). This leads us to believe that these are not the only PGC-1α isoforms that exist. Since the reverse primers used in the qRT-PCR experiments lie in exons 2 and 3, the remaining isoforms must have alternative splicing or novel exons and promoters upstream or downstream of these exons.

NT-truncated: The NT-truncated category describes the PGC-1α isoforms whose promoter lies downstream of that of canonical PGC-1α. One such isoform, called L-PGC-1α, was described in human liver (Felder et al., 2011). It was found via 5' RLM RACE of human liver and identified via amplicon sequencing. It is transcribed off a novel alternative PGC-1α promoter located within the reference intron following exon 2, which continues on to exon 3 with the reminder of the

transcript identical to canonical PGC-1α. This transcript is thought to be human specific, as it was not detected within a panel of other mammalian tissues. It is also not found in other human tissues investigated (kidney, brain, skeletal muscle). Thus, this is believed to be an isoform which evolved specifically for function in human liver.

The resultant 77 kDa protein, found endogenously translated in human liver and HEPG2 cells via immunoblot, is missing several functional domains compared to PGC-1α-a. These omissions include the SRC-1 and CREB-binding protein recruitment regions of the activation domain, the first LXXLL binding motif, an NES, and a GCN5 binding site. Lacking SRC-1 and CBP sites is especially interesting because these are necessary for recruiting and binding and PGC-1α chromatin remodeling partners. The inability for this isoform to indirectly dock and / or modify regions of chromatin and therefore make DNA available for changes in transcription could definitely lead to functional differences in comparison to its full-length counterpart. Similar to PGC-1α-a, L-PGC-1α was found to localize to the nucleus and is functional there, upregulating the same genes as PGC-1α-a in trans-activation studies (Felder et al., 2012). As aforementioned, SIRT1 can deacetylate PGC-1α which specifically decreases the ability for PGC-1α-a to upregulate genes involved in gluconeogenesis. The fact that L-PGC-1α lacks this site and its liver specificity suggests that it prevents constitutive gluconeogenesis from being shut down in humans.

NT-extended: The NT-extended category describes the remaining PGC-1α isoforms whose promoter lies upstream of that of canonical PGC-1α. Most of these isoforms were described in a publication by Soyal et al. in 2012, in which they found promoters 373 and 207 kb upstream of the promoter region for canonical PGC-1α in human brain tissue via 5' RLM RACE, and verified via long-range PCR followed by sequencing as well as northern blot. These resulted in several full length as well as alternatively spliced transcripts. These transcripts code for several potential brain-specific full-length and truncated proteins delineated in Table 1-2. Novel exons B4 and B5

continue to exon 2 producing two novel 803 and 786 amino acid human PGC-1α isoforms. These novel exons B4 and B5 can also be subjected to alternative splicing near exons 3, 7, and 8. These splicing events result in frameshifts and thus early stop codons, producing truncated forms of their full-length counterparts. These isoforms are delineated in Fig. 1-2.

In the studies by Soyal et al. (2012), although an immunoblot using an antibody to PGC-1α resulted in several bands in SH-SY5Y nuclear and cytosolic extracts, it was unclear whether any of the bands corresponded to the predicted proteins, as the predicted molecular weights did not align, and the size of three of the potential isoforms were very similar to the size of canonical PGC-1α (</= 1 kDa difference) which should have also been present in the nuclear extract (Soyal et al., 2012). In a recent publication, a protein was found in mitochondrial extracts of human brain and SY5Y cells that was ultimately unable to be sequenced to determine its identity (Choi et al., 2013). These investigators reported that they believed this transcript to be one of the NT-extended isoforms predicted to be a similar molecular weight. This could correspond to either B4 or B5 isoforms that are truncated in the coding sequence of exons 7a or 8a (Soyal et al., 2012). The true identity of the transcript resulting in this mitochondrial isoform is unknown. This 35 kDa PGC-1α isoform has been found to associate with PINK1 and VDAC in mitochondrial extracts of mouse hippocampal tissue as well as the human SH-SY5Y cell line. Its import was believed to be dependent upon VDAC binding shown by VDAC siRNA studies. Inside the mouse hippocampal mitochondrion, this 35 kDa form of PGC-1α was found to co-localize with PTEN-inducible kinase 1 (PINK-1). 35 kDa PGC-1α could potentially be phosphorylated by this kinase in order to carry out its signaling inside the mitochondrion. This is interesting considering that downregulation of either of these proteins is associated with both neurodegenerative disease – for PINK1, Parkinson's Disease in particular – and diabetes. This provides insight into a potential direct link of PGC-1α control to mitochondrial function and dysfunction.

Choi et al. also reported that their P-120 antibody detected several other bands which were not detected upon siRNA knockdown. These occurred in HEK WCLs at 100, 91, 45, 40, and 35 kDa. Other than the canonical form at 91 kDa, and the mitochondrial form at 35 kDa, these could be potential undescribed human isoforms transcribed from promoters previously mentioned in which transcripts have been detected but no protein described (isoform b, c, NT-extended promoters). Alternatively, these could be post-translationally modified versions of PGC-1α-a or its isoforms.

None of the functions of the NT-extended isoforms reported by Soyal et al. have been investigated. Clues to their potential roles have been noted, however. In the promoter region lies an Ebox, a potential binding site for transcription factors such as USF1 and SREBP-1c. E-boxes are glucose response elements that have the ability to bind to transcription factors in the basic helix-loop-helix-leucine zipper family. One of these such TFs is USF1 (upstream stimulatory factor), which is a mediator of glucose action and fatty acid synthesis. However, there is no evidence that changes in levels of glucose directly cause changes in transcriptional activity of USF1. SREBP-1c, however, has now been demonstrated as the TF that is directly downregulated and upregulated by increases in glucagon and insulin, respectively. SREBP-1c is thus responsible for the transcriptional regulation of glucose induced genes, such as those regulated by USF1 (Foretz et al., 1999). SREBP-1c can also bind to E-boxes and thus may work together with USF1 in glucose sensing and response as well as fatty acid production (Tontonoz et al., 1993). It is interesting that these E-boxes have been found both in the promoters of PGC-1α-b and the NT-extended brain-specific isoforms (Yoshioka et al., 2009; Soyal et al., 2012). These may contribute to the role of PGC-1α in glucose sensing, uptake, and fatty acid metabolism identified in neurons in genome-wide expression studies (GWES) of early asymptomatic Parkinson's Disease (Zheng et al., 2011). Also similar to isoform b, these NT-extended isoforms have the potential to be epigenetically regulated. Their promoter regions lie

within a large CpG island which was found in chIP studies to have a brain-specific neuron H3K4Me3 histone modification (Soyal et al., 2012). These regulation sites suggest a spatio-temporal regulation of these novel PGC-1α isoforms.

VI. Project overview

Since the first PGC-1α isoforms were identified in 2008 by Miura and colleagues in mice, several others have been published. For some, only a mature transcript have been identified. For others, the encoded protein has been detected via western blot deduced from predicted molecular mass. None have been positively confirmed to correspond to a particular transcript. Most of these isoforms have been identified in rodents, but some have also been described in human tissues. Some are similar in length to canonical PGC-1α, and some are truncated, missing important functional domains compared to canonical PGC-1α that could alter its comparative function. Most of these isoforms are also regulated in a tissue-specific manner. It is necessary to find and characterize all isoforms of PGC-1α to fully understand ways of modulating PGC-1α in a tissue-specific and thus pharmacologically targetable and disease-relevant manner.

Therefore, the goals of this project were to identify which PGC-1α-b variants exist in different human tissues and also which make viable proteins. This is the cornerstone to determining the functions of those proteins and discerning if those functions are unique to particular isoforms previously thought to be accomplished by canonical PGC-1α-a.

We have developed a PGC-1α isoform b specific primary antibody (Genscript). Its epitope lies in the coding sequence of exon1b, the only region that differs between full length isoform b and canonical PGC-1α. One of the aims of this project is to optimize and characterize this new antibody against a recombinant isoform b variant, which we are calling PGC-1α-b 3T1 (exon 3 truncation 1, Table 1-2), as well as endogenous PGC-1α-b present in whole cell lysates.

Once this antibody is characterized, it will open opportunities to probe for PGC-1α -b to determine which of its variants exist in different human tissues. If the tissue-specific effects of these isoforms – which have already been hinted to in isoform b transcript regulation studies – can be fully elucidated, this information can be harnessed to serve as a target for therapeutics, including pharmacological intervention.

CHAPTER 2

MATERIALS AND METHODS

Tissue samples

Genomic DNA and RNA from prefrontal cortex brain tissue samples from age-matched healthy and Parkinson's disease patients were obtained from the UVA brain bank (Charlottesville, VA), with DNA and RNA purified from snap frozen homogenized tissue samples from PFC using AllPrep DNA/RNA mini kit using manufacturer's instructions (Qiagen, Valencia, CA). Six patient samples were used total, blinded via patient number (3 healthy, 3 PD) until all results were analyzed: 122, 170, 174 (healthy control), 191, 203, 213 (PD).

qRT-PCR

RNA from patient brain samples were reverse transcribed (3.5 µg each) using Superscript III First-Strand cDNA synthesis kit (Invitrogen, Grand Island, NY) using manufacturer's instructions for random hexamer primed RNA. Primer sets were optimized using human skeletal muscle cDNA. Once melting temperatures were optimized, qPCR was performed using DNA Engine Plus real-time PCR system (Bio-Rad, Hercules, CA) with the FastStart Universal SYBR Green Master kit (Roche, Indianapolis, IN). DNA template (0.1 µg) and 0.2 µM primers were used in each reaction in a final volume of 20 µL. The amplification reaction program was set as a total of 40 cycles of denaturation at 94°C for 45 seconds, annealing at the appropriate temperature

(57^{O}C) for each target region for 45 seconds, and extension at 68°C for 45 seconds, with an initial denaturation at 94°C for 5 minutes and a final extension at 68°C for 10 minutes along with a melt curve analysis step extended to 98^{O}C. Data were analyzed by Opticon Monitor software. Relative RNA abundance was determined by normalizing to an average of two mitochondrial housekeeping genes, GAPDH and CYC9, which showed the least variance in this particular tissue type compared to an array of other housekeeping genes.

Table 2-1a: primer usage part A: cloning and TOPO clone and sequence bisulphite sequencing primers.

primer usage table					
primer set	Name	assay	Forward	Reverse	optimized Tm
hPGC-1α-a	RT1, RT2	qRT-PCR	GAC ATG TGC AAC CAG GAC TC	GTC ACT GCA CCA CTT GAG TC	57
hPGC-1α-b	RT3, RT2		ACA CAC ATG TTG GGG TTA TCA TC	GTC ACT GCA CCA CTT GAG TC	57
hPGC-1α total	RT4, RT5		GAC TCA AGT GGT GCA GTG AC	TCA TCC ACA GGG AGA CTG TC	57
hPGC-1α-b, fragment 1	B5, B6	BSFT TOPO-clone and sequence	GAT AGA AAT TAT AGG GAG AGT GTA TTA AGG	ACT AAT ATC ATA AAA TAA AAA AAC ACT CAC AAC	56
hPGC-1α-b, fragment 2	B7, B8		GGG TTT AGT ATA TTT TAG TTG ATT TTA GTT TTT AG	ACC CTA ATT CAA AAA CAC TAA ATA AAT ATA AC	56
hPGC-1α-b, fragment 3	B9, B10		GAG TTG AAA GTG TGA TTA TAT TTT TAT GTT TG	AAT ACC AAT CAT ATC CAA TTT AAA TCT AAA AAC	56
hPGC-1α-b 3T1 ATG2 (HSM) for Gateway subcloning	outer (hPGC1a isoB 3T fwd nested, hPGC1a isoAB 3T rev nested)	nested RT-PCR	GTTCATTTAGTAGTGACTCTGAGATG	GCAATAAGACTACACGAAGACG	55
	inner (clonPGC1a IsoB 3T1 ATG2 fwd, clonPGC1a IsoB 3T1 rev)		GGTACC AT CTCGAG ATGTTGGGGTTATCATCTATGGATTCAA	GGATCC CG AACAGTAGGAAGGGTTCTTACTAGAGAC	57
hPGC-1α-a (pDest26 CT FLAG, HEK293) transcription	isoA 3'end fw, FLAGrev	RT-PCR	GCTTCCACCAAGAGCAAGTA	TGTCGTCATCGTTCTTTGTAGTC	55
hPGC-1α-b 3T1 (pDest40, HEK293) transcription	isoB 3T1 3'end fw, V5 asn		GTGCAGTGACCAATCAGAAATAATA	TAGAATCGAGACCGAGGAGAG	55
hPGC-1α-b 3T1 (HSM) for pET41a subcloning	cF PGC1aB pET41a Bam, pET30a pGC1a isoB 3T1 rev		GAACTC GGATCC ACACACATGTGGGGGTTATC	GAAC CTCGAG AACAGTAGGAAGGGTTCTTACTAGAGAC	59
hPGC-1α-a pDEST 26 CT FLAG end CMV - CDS deletion	IsoA CDSd sense, anti	site-directed mutagenesis	GCACATGTCCCACGCCATAGCTCTGCTTATATAGAC	GTCTATATAAGCAGAGCTATGGCGTGGGACATGTGC	58
hPGC-1α-b 3T1 pDEST 40 end CMV - CDS deletion	IsoB ATG2d sense, anti		GAGGTCTATATAAGCAGAGCTATGTTGGGGTTATCATCTATG	CATAGATGATGGCCCCAACATAGCTCTGCTTATATAGACCTC	58

Table 2-1b Primer usage part B: PGC-1a-b 454 bisulphite sequencing primers

primer set	Name	assay	Forward	Reverse	optimized Tm
hPGC-1α-b, sample 122, fragment 1	S1.B.F1, R1	454 bisulphite sequencing	**CGTATCGCCTCCCTCGCGCCATCAGACGAGTGCGTGG**TTGGAAAGGGAATTATTTGTTTTA	**CTATGCGCCTTGCCAGCCCGCTCAGACGAGTGCGT**CCATAAATAATAACCCCAACATATATATCATTC	57
hPGC-1α-b, sample 122, fragment 2	S1.B.F2, R2		**CGTATCGCCTCCCTCGCGCCATCAGACGAGTGCGTGG**GTGAAATAATTTAGTAAAGTTTTGAGTAG	**CTATGCGCCTTGCCAGCCCGCTCAGACGAGTGCGT**TAAAACAAATAATTCCCTTTCCAACC	57
hPGC-1α-b, sample 122, fragment 3	S1.B.F3, R3		**CGTATCGCCTCCCTCGCGCCATCAGACGAGTGCGTGG**GAGTGGGGTTTTTTAAAATAGAT	**CTATGCGCCTTGCCAGCCCGCTCAGACGAGTGCGT**TACTCACAAAAAAACACCCCATAA	57
hPGC-1α-b, sample 170, fragment 1	S2.B.F1, R1		**CGTATCGCCTCCCTCGCGCCATCAGACGCTCGACAGG**TTGGAAAGGGAATTATTTGTTTTA	**CTATGCGCCTTGCCAGCCCGCTCAGACGCTCGACA**CCATAAATAATAACCCCAACATATATATCATTC	57
hPGC-1α-b, sample 170, fragment 2	S2.B.F2, R2		**CGTATCGCCTCCCTCGCGCCATCAGACGCTCGACAGG**GTGAAATAATTTAGTAAAGTTTTGAGTAG	**CTATGCGCCTTGCCAGCCCGCTCAGACGCTCGACA**TAAAACAAATAATTCCCTTTCCAACC	57
hPGC-1α-b, sample 170, fragment 3	S2.B.F3, R3		**CGTATCGCCTCCCTCGCGCCATCAGACGCTCGACAGG**GAGTGGGGTTTTTTAAAATAGAT	**CTATGCGCCTTGCCAGCCCGCTCAGACGCTCGACA**TACTCACAAAAAAACACCCCATAA	57
hPGC-1α-b, sample 174, fragment 1	S3.B.F1, R1		**CGTATCGCCTCCCTCGCGCCATCAGAGACGCACTCGG**TTGGAAAGGGAATTATTTGTTTTA	**CTATGCGCCTTGCCAGCCCGCTCAGAGACGCACTC**CCATAAATAATAACCCCAACATATATATCATTC	57
hPGC-1α-b, sample 174, fragment 2	S3.B.F2, R2		**CGTATCGCCTCCCTCGCGCCATCAGAGACGCACTCGG**GTGAAATAATTTAGTAAAGTTTTGAGTAG	**CTATGCGCCTTGCCAGCCCGCTCAGAGACGCACTC**TAAAACAAATAATTCCCTTTCCAACC	57
hPGC-1α-b, sample 174, fragment 3	S3.B.F3, R3		**CGTATCGCCTCCCTCGCGCCATCAGAGACGCACTCGG**GAGTGGGGTTTTTTAAAATAGAT	**CTATGCGCCTTGCCAGCCCGCTCAGAGACGCACTC**TACTCACAAAAAAACACCCCATAA	57
hPGC-1α-b, sample 203, fragment 1	S4.B.F1, R1		**CGTATCGCCTCCCTCGCGCCATCAGAGCACTGTAGGG**TTGGAAAGGGAATTATTTGTTTTA	**CTATGCGCCTTGCCAGCCCGCTCAGAGCACTGTAG**CCATAAATAATAACCCCAACATATATATCATTC	57
hPGC-1α-b, sample 203, fragment 2	S4.B.F2, R2		**CGTATCGCCTCCCTCGCGCCATCAGAGCACTGTAGGG**GTGAAATAATTTAGTAAAGTTTTGAGTAG	**CTATGCGCCTTGCCAGCCCGCTCAGAGCACTGTAG**TAAAACAAATAATTCCCTTTCCAACC	57
hPGC-1α-b, sample 203, fragment 3	S4.B.F3, R3		**CGTATCGCCTCCCTCGCGCCATCAGAGCACTGTAGGG**GAGTGGGGTTTTTTAAAATAGAT	**CTATGCGCCTTGCCAGCCCGCTCAGAGCACTGTAG**TACTCACAAAAAAACACCCCATAA	57
hPGC-1α-b, sample 213, fragment 1	S5.B.F1, R1		**CGTATCGCCTCCCTCGCGCCATCAGATCAGACACGGG**TTGGAAAGGGAATTATTTGTTTTA	**CTATGCGCCTTGCCAGCCCGCTCAGATCAGACACG**CCATAAATAATAACCCCAACATATATATCATTC	57
hPGC-1α-b, sample 213, fragment 2	S5.B.F2, R2		**CGTATCGCCTCCCTCGCGCCATCAGATCAGACACGGG**GTGAAATAATTTAGTAAAGTTTTGAGTAG	**CTATGCGCCTTGCCAGCCCGCTCAGATCAGACACG**TAAAACAAATAATTCCCTTTCCAACC	57
hPGC-1α-b, sample 213, fragment 3	S5.B.F3, R3		**CGTATCGCCTCCCTCGCGCCATCAGATCAGACACGGG**GAGTGGGGTTTTTTAAAATAGAT	**CTATGCGCCTTGCCAGCCCGCTCAGATCAGACACG**TACTCACAAAAAAACACCCCATAA	57
hPGC-1α-b, sample 191, fragment 1	S6.B.F1, R1		**CGTATCGCCTCCCTCGCGCCATCAGATATCGCGAGGG**TTGGAAAGGGAATTATTTGTTTTA	**CTATGCGCCTTGCCAGCCCGCTCAGATATCGCGAG**CCATAAATAATAACCCCAACATATATATCATTC	57
hPGC-1α-b, sample 191, fragment 2	S6.B.F2, R2		**CGTATCGCCTCCCTCGCGCCATCAGATATCGCGAGGG**GTGAAATAATTTAGTAAAGTTTTGAGTAG	**CTATGCGCCTTGCCAGCCCGCTCAGATATCGCGAG**TAAAACAAATAATTCCCTTTCCAACC	57
hPGC-1α-b, sample 191, fragment 3	S6.B.F3, R3		**CGTATCGCCTCCCTCGCGCCATCAGATATCGCGAGGGG**AGTGGGGTTTTTTAAAATAGAT	**CTATGCGCCTTGCCAGCCCGCTCAGATATCGCGAG**TACTCACAAAAAAACACCCCATAA	57

Table 2-1c Primer usage part C: PGC-1a-a 454 bisulphite sequencing primers, samples 1-3.

primer set	Name	assay	Forward	Reverse	optimized Tm
hPGC-1α-a, sample 122, fragment 1	S1.A.F1, R1	454 bisulphite sequencing	**CGTATCGCCTCCCTCGCGCCATCAGACGAGTGCGT**TTGT AGGGGATTTTGGTTATTATATGGTTAG	**CTATGCGCCTTGCCAGCCCGCTCAGACGAGTGCG**TAACCTC CCTTCCCCTATACAAC	56
hPGC-1α-a, sample 122, fragment 2	S1.A.F2, R2		**CGTATCGCCTCCCTCGCGCCATCAGACGAGTGCGT**ATTG AAGTAGAGGGTTGTTTTTGAGTG	**CTATGCGCCTTGCCAGCCCGCTCAGACGAGTGCG**TCTACAA TCCCCAATCACATAACAAAAC	56
hPGC-1α-a, sample 122, fragment 3	S1.A.F3, R3		**CGTATCGCCTCCCTCGCGCCATCAGACGAGTGCGT**GGAA TTGAATATTTTTGTTAATAGTGTGTTGG	**CTATGCGCCTTGCCAGCCCGCTCAGACGAGTGCG**TCCCATC CTTTCAACTTCCTTCT	56
hPGC-1α-a, sample 122, fragment 4	S1.A.F4, R4		**CGTATCGCCTCCCTCGCGCCATCAGACGAGTGCGT**GGAG ATTTTAGAATTAAAGAGTTTTTAGGGAA	**CTATGCGCCTTGCCAGCCCGCTCAGACGAGTGCG**TACTTCA AACATCATACTATAATTAAAACCAAC	56
hPGC-1α-a, sample 122, fragment 5	S1.A.F5, R5		**CGTATCGCCTCCCTCGCGCCATCAGACGAGTGCGT**GTTG GTATTTTTTATTGTTATGGGGGTAG	**CTATGCGCCTTGCCAGCCCGCTCAGACGAGTGCG**TTTCCCTA AAAACTCTTTAATTCTAAAATCTCC	56
hPGC-1α-a, sample 122, fragment 6	S1.A.F6, R6		**CGTATCGCCTCCCTCGCGCCATCAGACGAGTGCGT**GTTG GGTTATTTTAGATTGTTTTTTTTATAGA	**CTATGCGCCTTGCCAGCCCGCTCAGACGAGTGCG**TTTTCCCC CCTATATAAATTATAACCAAC	56
hPGC-1α-a, sample 122, fragment 7	S1.A.F7, R7		**CGTATCGCCTCCCTCGCGCCATCAGACGAGTGCGT**GTAG GATTGTGTGTGGAGTTG	**CTATGCGCCTTGCCAGCCCGCTCAGACGAGTGCG**TAAACTT AATCCTCCCCCTTACC	56
hPGC-1α-a, sample 170, fragment 1	S2.A.F1, R1		**CGTATCGCCTCCCTCGCGCCATCAGACGCTCGACA**TTGT AGGGGATTTTGGTTATTATATGGTTAG	**CTATGCGCCTTGCCAGCCCGCTCAGACGCTCGACA**AACCTC CCTTCCCCTATACAAC	56
hPGC-1α-a, sample 170, fragment 2	S2.A.F2, R2		**CGTATCGCCTCCCTCGCGCCATCAGACGCTCGACA**ATTG AAGTAGAGGGTTGTTTTTGAGTG	**CTATGCGCCTTGCCAGCCCGCTCAGACGCTCGACA**CTACAA TCCCCAATCACATAACAAAAC	56
hPGC-1α-a, sample 170, fragment 3	S2.A.F3, R3		**CGTATCGCCTCCCTCGCGCCATCAGACGCTCGACA**GGAA TTGAATATTTTTGTTAATAGTGTGTTGG	**CTATGCGCCTTGCCAGCCCGCTCAGACGCTCGACA**CCCATC CTTTCAACTTCCTTCT	56
hPGC-1α-a, sample 170, fragment 4	S2.A.F4, R4		**CGTATCGCCTCCCTCGCGCCATCAGACGCTCGACA**GGAG ATTTTAGAATTAAAGAGTTTTTAGGGAA	**CTATGCGCCTTGCCAGCCCGCTCAGACGCTCGACA**ACTTCA AACATCATACTATAATTAAAACCAAC	56
hPGC-1α-a, sample 170, fragment 5	S2.A.F5, R5		**CGTATCGCCTCCCTCGCGCCATCAGACGCTCGACA**GTTG GTATTTTTTATTGTTATGGGGGTAG	**CTATGCGCCTTGCCAGCCCGCTCAGACGCTCGACA**TTCCCTA AAAACTCTTTAATTCTAAAATCTCC	56
hPGC-1α-a, sample 170, fragment 6	S2.A.F6, R6		**CGTATCGCCTCCCTCGCGCCATCAGACGCTCGACA**GTTG GGTTATTTTAGATTGTTTTTTTTATAGA	**CTATGCGCCTTGCCAGCCCGCTCAGACGCTCGACA**TTTCCCC CCTATATAAATTATAACCAAC	56
hPGC-1α-a, sample 170, fragment 7	S2.A.F7, R7		**CGTATCGCCTCCCTCGCGCCATCAGACGCTCGACA**GTAG GATTGTGTGTGGAGTTG	**CTATGCGCCTTGCCAGCCCGCTCAGACGCTCGACA**AAACTT AATCCTCCCCCTTACC	56
hPGC-1α-a, sample 174, fragment 1	S3.A.F1, R1		**CGTATCGCCTCCCTCGCGCCATCAGAGACGCACTC**TTGT AGGGGATTTTGGTTATTATATGGTTAG	**CTATGCGCCTTGCCAGCCCGCTCAGAGACGCACTC**AACCTC CCTTCCCCTATACAAC	56
hPGC-1α-a, sample 174, fragment 2	S3.A.F2, R2		**CGTATCGCCTCCCTCGCGCCATCAGAGACGCACTC**ATTG AAGTAGAGGGTTGTTTTTGAGTG	**CTATGCGCCTTGCCAGCCCGCTCAGAGACGCACTC**CTACAA TCCCCAATCACATAACAAAAC	56
hPGC-1α-a, sample 174, fragment 3	S3.A.F3, R3		**CGTATCGCCTCCCTCGCGCCATCAGAGACGCACTC**GGAA TTGAATATTTTTGTTAATAGTGTGTTGG	**CTATGCGCCTTGCCAGCCCGCTCAGAGACGCACTC**CCCATC CTTTCAACTTCCTTCT	56
hPGC-1α-a, sample 174, fragment 4	S3.A.F4, R4		**CGTATCGCCTCCCTCGCGCCATCAGAGACGCACTC**GGAG ATTTTAGAATTAAAGAGTTTTTAGGGAA	**CTATGCGCCTTGCCAGCCCGCTCAGAGACGCACTC**ACTTCA AACATCATACTATAATTAAAACCAAC	56
hPGC-1α-a, sample 174, fragment 5	S3.A.F5, R5		**CGTATCGCCTCCCTCGCGCCATCAGAGACGCACTC**GTTG GTATTTTTTATTGTTATGGGGGTAG	**CTATGCGCCTTGCCAGCCCGCTCAGAGACGCACTC**TTCCCTA AAAACTCTTTAATTCTAAAATCTCC	56
hPGC-1α-a, sample 174, fragment 6	S3.A.F6, R6		**CGTATCGCCTCCCTCGCGCCATCAGAGACGCACTC**GTTG GGTTATTTTAGATTGTTTTTTTTATAGA	**CTATGCGCCTTGCCAGCCCGCTCAGAGACGCACTC**TTTCCCC CCTATATAAATTATAACCAAC	56
hPGC-1α-a, sample 174, fragment 7	S3.A.F7, R7		**CGTATCGCCTCCCTCGCGCCATCAGAGACGCACTC**GTAG GATTGTGTGTGGAGTTG	**CTATGCGCCTTGCCAGCCCGCTCAGAGACGCACTC**AAACTT AATCCTCCCCCTTACC	56

Table 2-1d Primer usage part D: PGC-1a-a 454 bisulphite sequencing primers, samples 1-3.

primer set	Name	assay	Forward	Reverse	optimized Tm
hPGC-1α-a, sample 203, fragment 1	S4.A.F1, R1	454 bisulphite sequencing	**CGTATCGCCTCCCTCGCGCCATCAGAGCACTGTAG**TTGTAGGGGATTTTGGTTATTATATGGTTAG	**CTATGCGCCTTGCCAGCCCGCTCAGAGCACTGTAG**AACCTCCCTTCCCCTATACAAC	56
hPGC-1α-a, sample 203, fragment 2	S4.A.F2, R2		**CGTATCGCCTCCCTCGCGCCATCAGAGCACTGTAG**ATTGAAGTAGAGGGTTGTTTTTGAGTG	**CTATGCGCCTTGCCAGCCCGCTCAGAGCACTGTAG**CTACAATCCCCAATCACATAACAAAAC	56
hPGC-1α-a, sample 203, fragment 3	S4.A.F3, R3		**CGTATCGCCTCCCTCGCGCCATCAGAGCACTGTAG**GGAATTGAATATTTTTGTTAATAGTGTGTTGG	**CTATGCGCCTTGCCAGCCCGCTCAGAGCACTGTAG**CCCATCCTTTCAACTTCCTTCT	56
hPGC-1α-a, sample 203, fragment 4	S4.A.F4, R4		**CGTATCGCCTCCCTCGCGCCATCAGAGCACTGTAG**GGAGATTTTAGAATTAAAGAGTTTTTAGGGAA	**CTATGCGCCTTGCCAGCCCGCTCAGAGCACTGTAG**ACTTCAAACATCATACTATAATTAAAACCAAC	56
hPGC-1α-a, sample 203, fragment 5	S4.A.F5, R5		**CGTATCGCCTCCCTCGCGCCATCAGAGCACTGTAG**GTTGGTATTTTTTATTGTTATGGGGGTAG	**CTATGCGCCTTGCCAGCCCGCTCAGAGCACTGTAG**TTCCCTAAAAACTCTTTAATTCTAAAATCTCC	56
hPGC-1α-a, sample 203, fragment 6	S4.A.F6, R6		**CGTATCGCCTCCCTCGCGCCATCAGAGCACTGTAG**GTTGGGTTATTTTAGATTGTTTTTTTTATAGA	**CTATGCGCCTTGCCAGCCCGCTCAGAGCACTGTAG**TTTCCCCCCTATATAAATTATAACCAAC	56
hPGC-1α-a, sample 203, fragment 7	S4.A.F7, R7		**CGTATCGCCTCCCTCGCGCCATCAGAGCACTGTAG**GTAGGATTGTGTGTGGAGTTG	**CTATGCGCCTTGCCAGCCCGCTCAGAGCACTGTAG**AAACTTAATCCTCCCCCTTACC	56
hPGC-1α-a, sample 213, fragment 1	S5.A.F1, R1		**CGTATCGCCTCCCTCGCGCCATCAGATCAGACACG**TTGTAGGGGATTTTGGTTATTATATGGTTAG	**CTATGCGCCTTGCCAGCCCGCTCAGATCAGACACG**AACCTCCCTTCCCCTATACAAC	56
hPGC-1α-a, sample 213, fragment 2	S5.A.F2, R2		**CGTATCGCCTCCCTCGCGCCATCAGATCAGACACG**ATTGAAGTAGAGGGTTGTTTTTGAGTG	**CTATGCGCCTTGCCAGCCCGCTCAGATCAGACACG**CTACAATCCCCAATCACATAACAAAAC	56
hPGC-1α-a, sample 213, fragment 3	S5.A.F3, R3		**CGTATCGCCTCCCTCGCGCCATCAGATCAGACACG**GGAATTGAATATTTTTGTTAATAGTGTGTTGG	**CTATGCGCCTTGCCAGCCCGCTCAGATCAGACACG**CCCATCCTTTCAACTTCCTTCT	56
hPGC-1α-a, sample 213, fragment 4	S5.A.F4, R4		**CGTATCGCCTCCCTCGCGCCATCAGATCAGACACG**GGAGATTTTAGAATTAAAGAGTTTTTAGGGAA	**CTATGCGCCTTGCCAGCCCGCTCAGATCAGACACG**ACTTCAAACATCATACTATAATTAAAACCAAC	56
hPGC-1α-a, sample 213, fragment 5	S5.A.F5, R5		**CGTATCGCCTCCCTCGCGCCATCAGATCAGACACG**GTTGGTATTTTTTATTGTTATGGGGGTAG	**CTATGCGCCTTGCCAGCCCGCTCAGATCAGACACG**TTCCCTAAAAACTCTTTAATTCTAAAATCTCC	56
hPGC-1α-a, sample 213, fragment 6	S5.A.F6, R6		**CGTATCGCCTCCCTCGCGCCATCAGATCAGACACG**GTTGGGTTATTTTAGATTGTTTTTTTTATAGA	**CTATGCGCCTTGCCAGCCCGCTCAGATCAGACACG**TTTCCCCCCTATATAAATTATAACCAAC	56
hPGC-1α-a, sample 213, fragment 7	S5.A.F7, R7		**CGTATCGCCTCCCTCGCGCCATCAGATCAGACACG**GTAGGATTGTGTGTGGAGTTG	**CTATGCGCCTTGCCAGCCCGCTCAGATCAGACACG**AAACTTAATCCTCCCCCTTACC	56
hPGC-1α-a, sample 191, fragment 1	S6.A.F1, R1		**CGTATCGCCTCCCTCGCGCCATCAGATATCGCGAG**TTGTAGGGGATTTTGGTTATTATATGGTTAG	**CTATGCGCCTTGCCAGCCCGCTCAGATATCGCGAG**AACCTCCCTTCCCCTATACAAC	56
hPGC-1α-a, sample 191, fragment 2	S6.A.F2, R2		**CGTATCGCCTCCCTCGCGCCATCAGATATCGCGAG**ATTGAAGTAGAGGGTTGTTTTTGAGTG	**CTATGCGCCTTGCCAGCCCGCTCAGATATCGCGAG**CTACAATCCCCAATCACATAACAAAAC	56
hPGC-1α-a, sample 191, fragment 3	S6.A.F3, R3		**CGTATCGCCTCCCTCGCGCCATCAGATATCGCGAG**GGAATTGAATATTTTTGTTAATAGTGTGTTGG	**CTATGCGCCTTGCCAGCCCGCTCAGATATCGCGAG**CCCATCCTTTCAACTTCCTTCT	56
hPGC-1α-a, sample 191, fragment 4	S6.A.F4, R4		**CGTATCGCCTCCCTCGCGCCATCAGATATCGCGAG**GGAGATTTTAGAATTAAAGAGTTTTTAGGGAA	**CTATGCGCCTTGCCAGCCCGCTCAGATATCGCGAG**ACTTCAAACATCATACTATAATTAAAACCAAC	56
hPGC-1α-a, sample 191, fragment 5	S6.A.F5, R5		**CGTATCGCCTCCCTCGCGCCATCAGATATCGCGAG**GTTGGTATTTTTTATTGTTATGGGGGTAG	**CTATGCGCCTTGCCAGCCCGCTCAGATATCGCGAG**TTCCCTAAAAACTCTTTAATTCTAAAATCTCC	56
hPGC-1α-a, sample 191, fragment 6	S6.A.F6, R6		**CGTATCGCCTCCCTCGCGCCATCAGATATCGCGAG**GTTGGGTTATTTTAGATTGTTTTTTTTATAGA	**CTATGCGCCTTGCCAGCCCGCTCAGATATCGCGAG**TTTCCCCCCTATATAAATTATAACCAAC	56
hPGC-1α-a, sample 191, fragment 7	S6.A.F7, R7		**CGTATCGCCTCCCTCGCGCCATCAGATATCGCGAG**GTAGGATTGTGTGTGGAGTTG	**CTATGCGCCTTGCCAGCCCGCTCAGATATCGCGAG**AAACTTAATCCTCCCCCTTACC	56

Bisulphite conversion – PCR amplification

Genomic DNA (500 ng) from patient prefrontal cortex samples were treated with bisulphite using the EZ Gold DNA methylation kit (Zymo Research, Orange, CA) and eluted in 30 µl of HPLC grade water. The bisulphite treated DNA was then amplified using 10 primer sets (7 for isoform A, 3 for isoform b) containing Cs converted to Ts. Each amplicon was 300-400bp in length across a 1 kb span of the upstream promoter region; these primers also contained sample specific multiplex identifiers (MIDs), synthesized by Eurofins MWG Operon (Huntsville, AL). These amplicons were generated with Invitrogen Platinum PCR Supermix – high fidelity polymerase (Grand Island, NY) (single reaction, 0.5 µL of bisulphite converted template (approximately 17.5 ng DNA) and 0.2 µM of forward and reverse primers using BioRad DNA Engine thermocycler. All PCR amplifications consisted of a total of 40 cycles of denaturation at 94°C for 45 seconds, annealing at the appropriate temperature for each target region for 45 seconds (see primer usage table), and extension at 68°C for 45 seconds, with an initial denaturation at 94°C for 5 minutes and a final extension at 68°C for 10 minutes. The amplicons were gel purified from a 3% Nu-Sieve agarose gel with 1xTBE, run at 80V for 1 hr. Bands were excised and DNA extracted using EZNA Gel Extraction Kit (Omega Bio-tek, Norcross, GA), following manufacturer's instructions except eluted twice with15uL elution buffer, with a 10min, RT incubation for each elution. All amplicons for isoform A and B, each with different MIDs for each sample (60 amplicons total) were combined in equimolar ratios and sent to Eurofins MWG operon for 454 high throughput bisulphite sequencing and subsequent sample separation via MIDs. Methylation levels (% protected Cs) were assessed at the single CpG dinucleotide level using multiple sequence alignment compared to unconverted DNA with an extended and improved version of BiQ Analyzer (Bock et al., 2005), the BiQ Analyzer-HT software (Lutsik et al. 2011). Percent conversion exceeded 99%.

Subcloning and Gateway Cloning

(1) PGC1a Mammalian expression vectors

HSM PGC-1a-b-3T1 to PCR 4 TOPO: PGC-1α-b-3T1 was amplified from human skeletal muscle total RNA (Ambion) using primers which added KpnI and NotI restriction sites on the 5' and 3' ends, respectively (see primer usage table; Fig. 3A). The amplicon was then purified using QiaQuick PCR purification kit (Qiagen, Valencia, CA), subsequently TOPO cloned using the PCR 4 TOPO – TA cloning kit (Invitrogen, Carlsbad, CA), and then transformed into TOP10 cells according to manufacturer's instructions (Life Technologies, Grand Island, NY). The transformation was plated onto 50 µg/mL Carbenicillin LB agar at RT for 30 hours. Colonies were then picked, diluted in 20 µL SOC, PCR screened with the same primers used for initial amplification, and simultaneously streaked onto a fresh 50 µg/mL Carbenicillin LB agar plate to obtain pure colonies. Pure colonies from several positive clones containing the correct size insert were grown in 5mL 2xYT cultures in 15-mL polypropylene snap-cap culture tubes for 6-8 hours under antibiotic selection, with 500 µL made into 10% glycerol stocks at O.D. 0.5-0.6, and spun down for 20 min. at 4°C between O.D. 1.0-1.5. DNA was purified from these cells using the EZNA Plasmid Mini Kit I (Omega Bio-tek, Norcross, GA) following manufacturer's instructions with the exception of the elution step, which was carried out twice using 15uL of elution buffer following a 10 minute incubation at RT. Mini-prepped DNA was then restriction digested with XhoI to ensure no rearrangement occurred during culture growth. Three correctly digested clones from each construct were then sequenced (Operon) to ensure no mutations were introduced during PCR using T7 and M13R standard primers. Clones containing correct, high quality sequence were then midi-prepped (Purelink HiPure Plasmid DNA purification Kit: Invitrogen, Carlsbad, CA), restriction digest verified (BamHI, EcoRI, XhoI FastDigest restriction enzymes: Thermo Scientific, Pittsburgh, PA), and subsequently quantified via densitometry

using Li-COR's DNA gel analysis software (LI-COR biosciences, Lincoln, NE) with the 1 kb and 100 bp mass ladders (New England Biolabs, Ipswich, MA).

PCR 4 TOPO to pENTR1a: 10 µg of PGC-1a-b-3T1 TOPO plasmid as well as the pENTR1a dual selection Gateway vector (Life Technologies, Grand Island, NY) were then restriction digested with fast digest enzymes (Thermo Scientific, Pittsburgh, PA) according to manufacturer's protocol using the restriction sites initially introduced for subcloning. The entire digest reaction was run on a 1% TAE agarose gel, and the correct bands corresponding to insert and empty vector were excised. The DNA was then gel extracted using EZNA Gel Extraction Kit (Omega Bio-tek, Norcross, GA). Ligation was carried out using Roche Rapid DNA Ligation Kit (Roche, Indianapolis, IN) with a 3:1 molar excess of insert to vector using 100 ng of vector DNA. 5 µL of the ligation reaction was used to transfect 100 µL of SURE2 competent cells, using manufacturer's instructions (Agilent, Santa Clara, CA), and 50 µL of the cell suspension was plated on LB agar with 50 µg / mL Carbenicillin for overnight incubation at 37^{o}C. Clones were screened by colony-PCR, mini-prepped and further validated by restriction digest and sequencing.

pENTR1a / pDONR201 to pDEST40 and pDEST 26 CT FLAG: Previously in our lab, PGC-1α-a in pENTR22.1 was obtained from DNASU plasmid repository and subcloned via BP gateway reaction into pDONR201 with BP clonase following manufacturer's instructions (Lochmann, T.). I then subcloned PGC-1α-a into pDEST26 CT FLAG (modified Life Technologies vector kindly provided by Dr. Rita Shiang) and PGC-1α-b-3T1 into pDEST40 via LR clonase reaction following manufacturer's instructions (Life Technologies, Grand Island, NY). 2 µL of the LR clonase reaction was then used for transformation into 50 µL of SURE2 cells. 50 µL of the transformation reaction was plated onto 50 µg / mL Carbenicillin LB agar for 37°C incubation overnight. Clones were screened once again as described above and midi-prepped. Both pDEST constructs were sequenced with T7 and BGHrev as well as interior forward and reverse

primers to cover the entire 2.5 kb isoform A construct (pGC1a IsoA inner Fw, Rv 5' – GCAAAAGCCACAAAGACGTCC – 3', 5' – CTACTGCCTGGAGACCTTGATC – 3').

(2) PGC1a-3T1 Bacterial expression vector

DNA was amplified from human skeletal muscle cDNA using primers which added on KpnI and NotI restriction sites to the 5' and 3' end of the amplicon, respectively (Table 2-1). The PCR product (4 reactions worth) was combined and subsequently cleaned of excess primers using the QiaQuick PCR Purification Kit per manufacturer's instructions (Qiagen, Valencia, CA) and reduced to a 30 µL total volume. 10 ug of this PCR product and the vector (pET41a) were then restriction digested with BamHI and XhoI Fast Digest enzymes per the manufacturer's protocol (Thermo Scientific, Pittsburgh, PA). Subsequent DNA gel, gel extraction, ligation, transformation, and colony / clone screening were carried out as stated in mammalian vector preparation portion of the methods. Exceptions include that the ligation reaction was transformed into DH5alpha subcloning efficiency competent cells (Life Technologies, Grand Island, NY) with 50 ug / mL Kanamycin selection, no midi-prepping was necessary for this construct, and that it was subsequently transformed into BL21(DE3) competent cells for bacterial expression of the recombinant protein. Recombinant GST/PGC-1α-b-3T1 fusion contains an NT GST and 6x His tag fused to PGC-1α isoform b 3T1, followed by a CT 6x His tag to aid in protein purification (see Fig. 3-3C for vector schematic; Fig. 2-2 for Plasmid and amino acids sequence).

Recombinant bacterial protein expression and purification

The colony used for this bacterial protein expression was restriction digest checked with the enzymes used to clone in the construct (KpnI and NotI) as well as one enzyme interior to the construct (NheI) prior to protein expression. Conditions for recombinant protein expression were

optimized to growing a single pure colony in 6 mL LB until an OD of 0.5 was reached. The cultures were then kept at 4°C, overnight and spun down at 8,000 rpm for 5 min. at 4°C, and the pellet gently resuspended in 2 mL of fresh LB. This was added to 48 mL of 50 ug / mL supplemented LB and incubated at 37°C until an OD of 6.0 was reached. At this point, a 3-2 mL aliquots were pelleted and frozen for later analysis of uninduced bacterial lysate and IPTG was added to a final concentration of 1 mM. The induced culture was incubated for 4 hours at 37°C, then the OD was taken and 2-1mL aliquots were pelleted and frozen for later analysis. Cells were then harvested at 4000 rpm for 30min. at 4°C. After the supernatant was removed, the pellet was frozen prior to lysis for higher protein yields. The pellet was resuspended in 2 mL BugBuster protein extraction reagent (Novagen; Merck KGaA, Darmstadt, Germany) plus 1x Roche “complete” protease inhibitor cocktail, following manufacturer's protocol. The lysed cells were then bath sonicated for 10 minutes on high setting, 30s on/off. The lysate was then batch purified using 0.5 mL resin bed volume of glutathione agarose according to manufacturer's instructions (Pierce, Rockford, IL). Elutions were collected as 5-0.5 mL fractions and stored at 4°C.

A

5’- TGTCCCCTATACTAGGTTATTGGAAAATTAAGGGCCTTGTGCAACCCACTCGACTTCTT

TTGGAATATCTTGAAGAAAAATATGAAGAGCATTTGTATGAGCGCGATGAAGGTGATAAATG
GCGAAACAAAAAGTTTGAATTGGGTTTGGAGTTTCCCAATCTTCCTTATTATATTGATGGTG
ATGTTAAATTAACACAGTCTATGGCCATCATACGTTATATAGCTGACAAGCACAACATGTTG
GGTGGTTGTCCAAAAGAGCGTGCAGAGATTTCAATGCTTGAAGGAGCGGTTTTGGATATTA
GATACGGTGTTTCGAGAATTGCATATAGTAAAGACTTTGAAACTCTCAAAGTTGATTTTCTTA
GCAAGCTACCTGAAATGCTGAAAATGTTCGAAGATCGTTTATGTCATAAAACATATTTAAAT
GGTGATCATGTAACCCATCCTGACTTCATGTTGTATGACGCTCTTGATGTTGTTTTATACAT
GGACCCAATGTGCCTGGATGCGTTCCCAAAATTAGTTTGTTTTAAAAAACGTATTGAAGCTA
TCCCACAAATTGATAAGTACTTGAAATCCAGCAAGTATATAGCATGGCCTTTGCAGGGCTG
GCAAGCCACGTTTGGTGGTGGCGACCATCCTCCAAAATCGGATggttcaactagtggttctggtcatcac
catcaccatcactccgcgggtctggtgccacgcggtagtactgcaattggtatgaaagaaaccgctgctgctaaattcgaacgccagc
acatggacagcccagatctgggtaccggtggtggctccggtgatgacgacgacaagagtcccatgggatatcggggatccACAC
ACATGTTGGGGTTATCATCTATGGATTCAATTTTGAAATGTGCTGCTCTGGTTGGTGAAGAC
CAGCCTCTTTGCCCAGATCTTCCTGAACTTGATCTTTCTGAACTAGATGTGAACGACTTGGA
TACAGACAGCTTTCTGGGTGGACTCAAGTGGTGCAGTGACCAATCAGAAATAATATCCAAT
CAGTACAACAATGAGCCTTCAAACATATTTGAGAAGATAGATGAAGAGAATGGGGCAAACT
TGCTAGCAGTCCTCACAGAGACACTAGACAGTCTCCCTGTGGATGAAGACGGATTGCCCT
CATTTGATGCGCTGACAGATGGAGACGTGACCACTGACAATGAGGCTAGTCCTTCCTCCAT
GCCTGACGGCACCCCTCCACCCCAGGAGGCAGAAGAGCCGTCTCTAGTAAGAACCCTTCC
TACTGTTctcgagcaccaccaccaccaccaccactaa – 3’

B

MSPILGYWKIKGLVQPTRLLLEYLEEKYEEHLYERDEGDKWRNKKFELGLEFPNLPYYIDGDVK
LTQSMAIIRYIADKHNMLGGCPKERAEISMLEGAVLDIRYGVSRIAYSKDFETLKVDFLSKLPEML
KMFEDRLCHKTYLNGDHVTHPDFMLYDALDVVLYMDPMCLDAFPKLVCFKKRIEAIPQIDKYLK
SSKYIAWPLQGWQATFGGGDHPPKSDGSTSGSGHHHHHHSAGLVPRGSTAIGMKETAAAKF
ERQHMDSPDLGTGGGSGDDDDKSPMGYRGSTHMLGLSSMDSILKCAALVGEDQPLCPDLPE
LDLSELDVNDLDTDSFLGGLKWCSDQSEIISNQYNNEPSNIFEKIDEENGANLLAVLTETLDSLP
VDEDGLPSFDALTDGDVTTDNEASPSSMPDGTPPPQEAEEPSLVRTLPTVLEHHHHHHHH*

Fig. 2-2: Coding region for recombinant GST/PGC-1a-b-3T1 fusion. (A) DNA sequence of the coding region for GST/PGC-1a-b-3T1 in pET41a. (B) Resultant amino acid sequence translated from part A. Red = pgc1a isoform b 3T1; Green = His tags; Blue = GST; Red = epitope.

Generation and validation of expression plasmids for PGC1a isoforms

Midi-prepped DNA (Purelink HiPure Plasmid DNA purification Kit: Invitrogen, Carlsbad, CA) was restriction digest verified (FastDigest restriction enzymes: Thermo Scientific, Pittsburgh, PA) and subsequently quantified for DNA concentration via densitometry using Li-COR's gel analysis software (LI-COR biosciences, Lincoln, NE) and comparison to the 1 kb and 100 bp mass ladders (New England Biolabs, Ipswich, MA). This endotoxin-free DNA was then transfected into HEK293 cells at 80% confluency in 6-well plates (~960,000 cells / well)(American Type Culture Collection, Manassas, VA) using Polyjet DNA *in vitro* Transfection Reagent, according to the manufacturer's protocol (SignaGen Laboratories, Rockville, MD) with the exception that a 3:2 polyjet (µL)/DNA (µg) ratio was used with 2ug of DNA per dish An expression vector encoding eGFP (pmaxGFP: Lonza, Basel, Switzerland) was used to determine transfection efficiency. Cells were imaged for GFP using a fluorescent microscope at 24 and 48 hrs, and harvested 48 hours post transfection. Cells were washed, scraped and pelleted in 1x PBS, pH 7.4. Cells were resuspended in SDS lysis buffer [(62.5 mM Tris pH 6.8, 5% glycerol, 2% SDS, 5% beta-mercaptoethanol, and 1x EDTA-free “cOmplete” protease inhibitor cocktail (Roche, Indianapolis, IN)] at a volume 5x the pellet weight and lysis was carried out by bath sonication for 7 min. total, high setting, 30s on/off (Bioruptor: Diagenode, Denville, NJ).

SDS-PAGE and Immunoblotting

Per lane on the gel, each sample contained 50 to 100 ug of whole cell lysate (WCL) or 0.001 ng to 10 µg of recombinant protein (see figure legends for details). All protein samples were mixed with an equal volume of 2x Laemmli sample buffer (Bio-Rad, Hercules, CA) and brought up to a final volume of 45 µL with SDS lysis buffer. Proteins were resolved on 4–15% gradient

SDS/PAGE gels (Mini-protean GTX: Bio-Rad, Hercules, CA) at 90 volts. For protein visualization, gels were stained with Coomassie brilliant blue overnight and destained with (v/v) 30% methanol, 10% glacial acetic acid in ultrapure water. For western blotting, resolved proteins were transferred to a 0.45 micron PVDF

Table 2-2: Antibody usage

Antibody	Manufacturer	Catalog Number	Species	Blocking Buffer	Primary Dilution	Secondary Dilution	Secondary Antibody	Size (kDa)
V5	Invitrogen	460705	mouse	StartingBlock T20	1:500	1:30,000	GαM	180
VDAC	Cell Signalling	46615	rabbit	StartingBlock T20	1:2500	1:3000	GαR	32
FLAG	Sigma-aldrich	F1804	mouse	StartingBlock T20	1:500	1:15,000	GαM	60
GST	Sigma-aldrich	71097	mouse	StartingBlock T20	1:10,000	1:5,000	GαM	60
H300 (NT PGC-1α)	Santa Cruz	SC-13067	rabbit	StartingBlock T20	1:100, 1:250, 1:500	1:10,000	GαR	91
K-15 (CT PGC-1α)	Santa Cruz	SC-5816	goat	StartingBlock T20	1:100, 1:250, 1:500, 1:1000	1:5000	DαG	91
PGC-1α-b specific	Genscript*	N/A	rabbit	5% NFDM in TBS-T	1:100	1:35,000	GαR	various
*first use in this thesis; not commercially available								

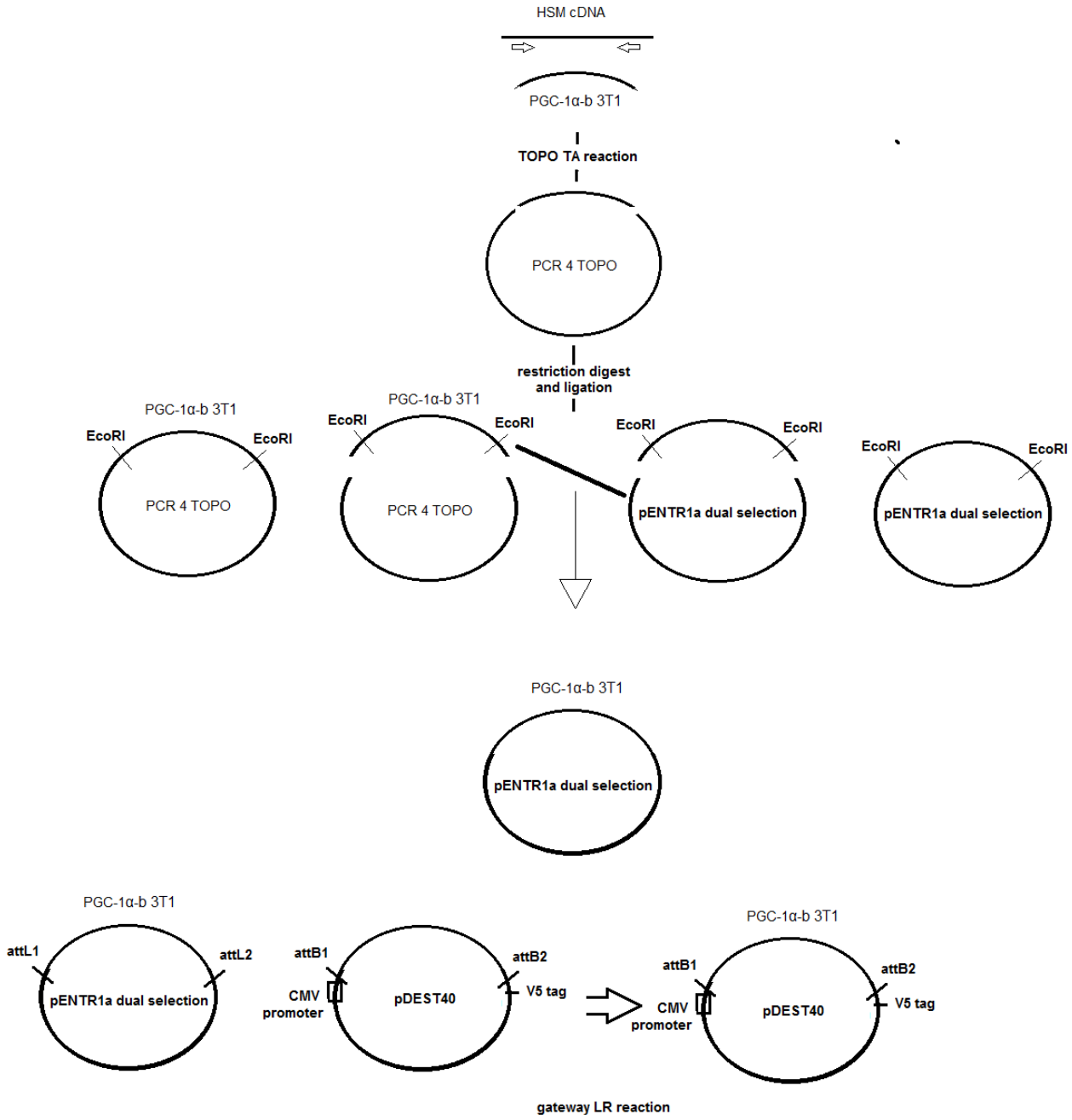

Fig. 2-2: Schematic of subcloning procedure of PGC-1a-b-3T1 into pDEST40.

membrane using a wet transfer apparatus for 1 hour at 100 volts in cold 1x transfer buffer (25 mM Tris, 192 mM glycine, 10% methanol, 0.1% SDS, pH 8.3). Membrane was then blocked in StartingBlock T20 (Thermo Scientific, Pittsburgh, PA) at 4°C, overnight with gentle rocking, followed by a 1 hr incubation at room temperature with primary antibody with gentle rocking, 3 x 10 minute washes with TBS-T at room temperature with vigorous shaking, 1 hr incubation at room temperature with an HRP-conjugated secondary antibody with gentle rocking, followed by another series of 3 x10 minute washes. The samples were then incubated for 5 min. with Supersignal West Dura extended duration chemiluminescent substrate (Pierce, Rockford, IL), exposed and developed on X-ray film. Where noted, 5% Nonfat dry milk (NFDM) in TBS-T was used as starting block with 1 hr RT incubation followed by overnight primary incubation (see figure legends). The primary and secondary antibodies used, their concentrations, % ECL reagent, and manufacturers are listed in table 2-2.

Trypsin digest and Mass Spectrometry

Gels were stained with Coomassie to visualize protein bands. The gel bands were subsequently cut from the gel and destained. The proteins were reduced, alkylated and digested with trypsin in the gel. The peptides formed in the digestion were extracted, concentrated, and characterized by LC-tandem mass spectrometry on a Thermo LCQ DECA-XP MAX ion trap (Thermo, San Jose, CA) upon elution from a reverse-phase phenyl resin (YMC, Kyoto, Japan) capillary column. The mass spectrometer was operated in the data dependent mode throughout the HPLC gradient with an acquisition duty cycle consisting of an initial MS^1 scan with a mass range of 300-1200 m/z followed by an MS^2 acquisition of the 5 most abundant ions. The MS^2 data was searched with SEQUEST as a tryptic digest against a composite database containing the PGC-1α construct. The carbamidomethylation of cysteine (+57 Da) and oxidation of methionine (+16 Da) were treated as variable modifications. The tryptic search results for each data file were filtered by xcoor for (+1, +2, +3) of (1.5,2.0,2.5).

Peptide Competition Assay

A peptide competition assay (PCA) was used to verify the binding specificity of the PGC-1α-b specific primary antibody, which was affinity purified and produced in rabbits by KLH-conjugation. The molar excess factor, or moles of blocking peptide per mole of antibody used, was determined via titration of 200-20,000 molar excess of peptide to antibody against 10 ng of recombinant GST/PGC-1α-b-3T1 fusion protein. Immunizing peptide for the isoform b specific antibody was prepared at 1 µg/µL in pH 5.5 PBS to prevent disulfide bond formation. Primary antibody was blocked by combining 0, 200, 2000, 5000, 10,000, or 20,000 molar excess of peptide to primary antibody aliquots followed and incubating them at RT with occasional mixing. The membrane was then probed as described in the western blotting procedure, using NFDM as block. PCA was then performed on 100 µg SY5Y WCL using 20,000 as the molar excess factor, but was not sufficient to block signal from WCL. This PCA experiment was repeated using 100,000 as the molar excess factor with successful blocking.

RNA isolation and purification

48 hours post transfection, cells were lysed directly in their 60 mM culture dishes in 1mL TRIzol (Invitrogen, Grand Island, NY). Homogenization was done via bath sonication for 7 min. total, high setting, 30s on/off (Bioruptor: Diagenode, Denville, NJ). Samples were frozen at -80°C. When thawed, the homogenized sample was incubated at RT for 5 minutes. Insoluble material was then pelleted at 12,000 x g for 10 minutes at 4°C. 250 ug / mL glycogen was then added to the supernatant and mixed prior to phase separation. Chloroform was then added at a ratio of 0.2 mL chloroform per 1 mL of Trizol, vigorously shaken for 15 seconds, and incubated at RT for 3 minutes. Samples were centrifuged at 12,000 x g for 15 minutes at 4°C. The aqueous phase was moved to a fresh tube and chloroform extracted once more. RNA was then precipitated with isopropanol at a ratio of 0.5 mL per 1 mL TRIzol initially used. This mixture was gently mixed and incubated at -20°C for 15 minutes. RNA was pelleted

from the samples by centrifugation at 12,000 x g for 10 minutes at 4°C. The supernatant was then removed and RNA pellet washed with 75% ethanol at a ratio of 1mL ethanol per 1mL TRIzol initially used. The sample was mixed with mild vortexing and centrifuged at 7500 x g for 5 min at 4°C. Once the supernatant was removed, the isolated RNA was air dried for 5 minutes and redissolved in sterile HPLC water at a ratio of 50 uL per 5 million cells initially used. 500 ng of RNA was run on a 1% agarose gel stained with EtBr at 100 V for 45 minutes and imaged with UV light to determine RNA quality.

RNA was then purified via 2-3 DNase treatments followed by phenol / chloroform / IAA extraction and ethanol precipitation. DNase treatments were performed by incubating isolated RNA with RNase-free DNase at a ratio of 1 unit per ug of RNA with 10x DNase reaction buffer (NEB, Ipswich, MA) at 37°C for 30 minutes. Phenol/chloroform/IAA (25:24:1) was mixed at an equal volume (at least 100 uL, brought up to volume with sterile HPLC water) to DNase treated RNA and spun down at 16,000 rpm for 5 minutes at 4°C. The aqueous layer was mixed with an equal volume of chloroform and spun down at 16,000 rpm for 5 minutes at 4°C. This chloroform extraction was repeated. The sample was then ethanol precipitated using 3x the reaction volume of 100% EtOH, incubated at -20°C for 20 minutes, and then centrifuged for 20 minutes at 16,000 rpm.. Supernatant was removed and the RNA pellet was washed with 1 volume of 75% EtOH, followed by centrifugation at 16,000 rpm for 5 minutes at 4°C. Supernatant was removed and the RNA containing pellet was air-dried for 5 minutes. RNA was resuspended in 30 µL HPLC water, checked for quality on an agarose gel as described, reverse transcribed, and amplified using human 12S rRNA primers to check for DNA contamination. This was repeated until no DNA contamination was seen in the no RT control on a 2% agarose EtBr gel after 30 cycles of PCR.

Site-directed Mutagenesis

Site-directed mutagenesis was carried out on the pDest constructs to delete all sequence between the 3' end of the CMV promoter to the coding sequence of the respective PGC-1α isoform. See table 2-1 for primer sequences and conditions. Site-directed mutagenesis was carried out using the Quikchange II kit (Agilent, Santa Clara, CA), following manufacturer's instructions. Colonies were PCR colony screened using a standard forward CMV primer (operon) and a reverse primer in exon 3 or 3a. Pure clones which contained the correct sized amplicons (382 bp for PGC-1α-b-3T1 ATG2 in pDEST40; 136 bp for PGC-1α-a in pDEST26 CT FLAG) visualized on an EtBr gel were CMVf standard primer (Operon) and a reverse primer set in either the V5 (for pDest40). A correct and high quality sequence clone was chosen and was midi-prepped for subsequent transfection.

CHAPTER 3
RESULTS

PGC-1α isoform b transcripts are expressed at much lower levels than that of isoform A transcripts in human brain

Our lab identified an upstream alternative exon 1b in human skeletal muscle mRNA via 5' RACE (Rapid Amplification of cDNA ends), and then verified the existence of this transcript in human brain for the first time (Lochmann, T. unpublished data). Considering previous findings of PGC-1α isoform a (canonical transcript) downregulation in Parkinson's disease human prefrontal cortex (PFC), we wanted to investigate the expression of this isoform in comparison to canonical in healthy vs. Parkinson's disease states (Thomas, Keeney, and Bennett, 2012). The expression levels of PGC-1α isoforms a and b were quantified via qRT-PCR from 6 human prefrontal cortex samples, 3 from Parkinson's disease patients and 3 from age-matched healthy patient samples. Locations of the primer sets that were used to distinguish isoform a versus isoform b transcripts, versus total PGC-1α is shown in Fig. 3-2A. Figure 3-2B shows that there is variability in relative RNA abundance between patient samples for each transcript, however there does not appear to be a disease specific difference in transcript levels for either PCG-1α-a or PGC-1α-b in these samples. More importantly, Fig. 3-2B shows that PGC-1α isoform b transcript levels are present at 15 to 20 fold lower than those of isoform b transcript, with isoform a levels on the same order of magnitude as total PGC-1α. Overall, this data shows that PGC-1α isoform b transcripts are expressed at much lower levels than that of canonical form of PGC-1α (isoform A), regardless of disease state in the case of Parkinson's disease.

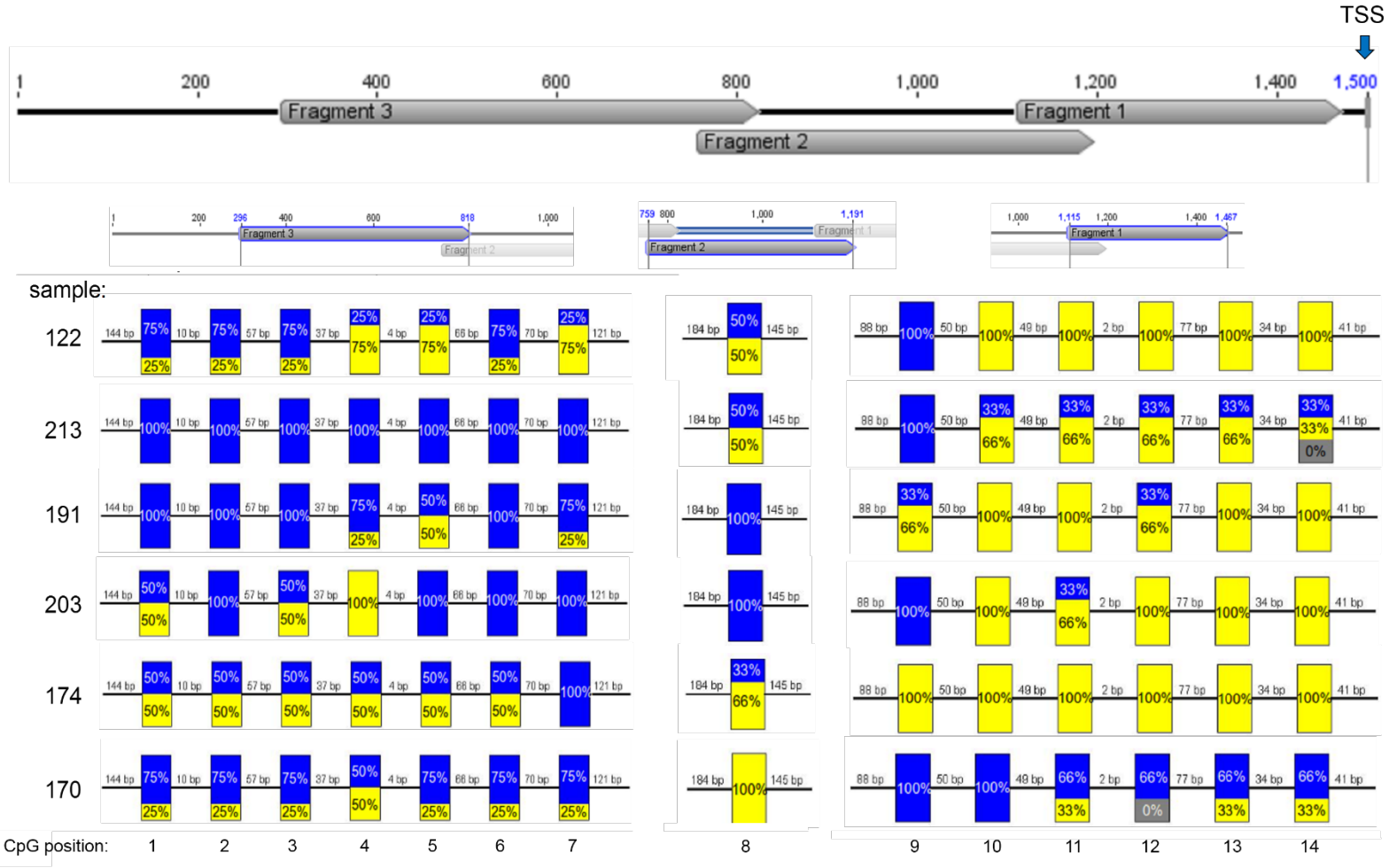

Cytosine methylation analysis of the 1500 bp upstream of promoter b in the PGC-1α gene. (TOP) Diagram of amplicon locations in the CpG sparse promoter region of PGC-1a. Three fragments (top panel) were amplified from bisulfite-treated DNA from 6 human brain samples, covering all 14 CpG sites. The fragments were cloned into PCR4-TOPO and sequenced. "fragment" represents each overlapping amplicon, NOTE: no overlapping CpG sites. TSS: Transcription start site. (BOTTOM) Each amplicon fragment of the promoter region is highlighted above the respective CpG sites (boxes) contained within it. Yellow represents methylation. Blue represents unmethylated sites. Percentages based on percent of total methylation or nonmethylation at that CpG position across bisulfite sequence analysis of n = 3-4 clones.

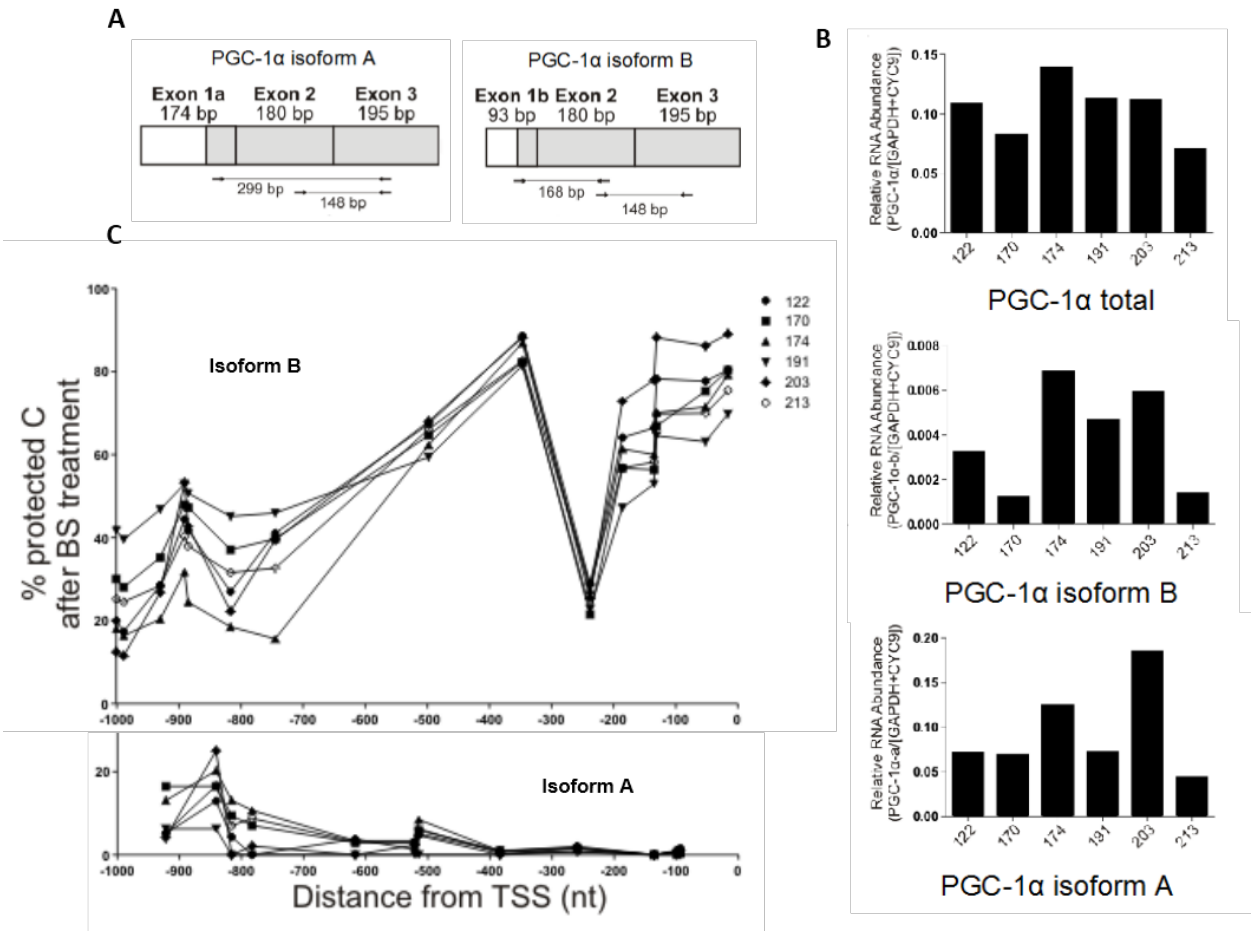

Fig. 3-2: DNA methylation correlates with isoform specific PGC1a expression levels in human brain. A total of 13 CpG sites located within 1000 bp of the TSS were analyzed. **(**A) Transcript map showing locations of isoform A specific (299 bp), isoform b specific (168 bp), and total PGC-1α (148 bp) primer sets used in qRT-PCR. Gray region indicates coding sequence. (B) Relative RNA abundance of total PGC-1α (upper panel), isoform b (middle), and isoform A (canonical PGC-1a, lower) normalized to control data (average of GAPDH and CYC9 mitochondrial reference genes, chosen for least degree of variance). n=3; mean of each normalized to control, depicted. (C) 454 high-throughput bisulfite sequencing of PGC1a isoform A and B promoter regions expressed as percent methylated cytosines over all reads (range n = 1200 to 200k reads per strand) at each CpG dinucleotide located within 1000bp of the transcription start site (TSS). Isoform b (upper) Isoform A (lower). Sample #s122, 170, 174 denote healthy patient PFC brain samples; 191, 203, 213 denote age-matched Parkinson's patient prefrontal cortex samples.

PGC-1α isoform b promoter region is highly methylated

To investigate whether this difference in isoform b transcript expression is regulated via epigenetic mechanisms, we applied first a bisulfite clone and sequence method with an n of 3-4 clones per amplified promoter region. The region amplified spanned 1.5 kb upstream of the TSS of the same samples utilized in the transcript expression studies. This preliminary study yielded interesting results, showing little to no methylation of all potential CpG dinucleotides 1.5 kb to 0.75 kb upstream of the TSS (<20% per CpG dinucleotide, Fig. 3-1) contrasted by a high degree of methylation closer to the transcription start site (TSS) (>75% per CpG dinucleotide, Fig. 3-1). To increase the statistical power of our data to obtain more definitive results, we utilized the method of 454 high-throughput pyrosequencing of bisulfite-treated DNA. Promoter regions were amplified on 7 separate amplicons for isoform a and 3 for isoform b spanning 1 kb prior to the TSS, and analyzed as pools using patient sample specific bar codes. Read depth for the different amplicons varied between ~1200 reads to ~200,000 reads per strand. This high-throughput method largely agreed with our low-power clone and sequence results (Fig. 3-1, 2C). After CpG #9 (positioned 350 bp upstream of the TSS), all but 1 CpG methylation site is methylated at levels >50% across all reads. At this single CpG dinucleotide, located ~250bp upstream of the TSS, there is a distinct drop in methylation evident across all reads and for all samples. In contrast, isoform a methylation levels remained below 20% across all possible CpG sites. Overall, Fig. 3-2C shows that the isoform b promoter region is methylated to a much higher degree than that of canonical PGC-1α (isoform A). Isoform b is highly methylated (>60%) across most potential methylation sites (CpG dinucleotides), with increases as the TSS is approached. Although no disease-specific correlations between transcript levels or DNA methylation were observed, we conclude that isoform b expression is controlled in part through epigenetic means, correlating with DNA methylation associated silencing, and that the low levels of transcript expression observed potentially are due to the distinct drop in methylation at 350 bp prior to the TSS.

PGC-1α isoform b transcript alternative splice variant found in human skeletal muscle and brain

From the 5' RACE on human skeletal muscle (HSM) conducted in our lab which identified human PGC-1α-b, one clone was identified which contained alternative splicing between exons 3 and 4 (Fig. 3-3A). Sequencing revealed that 82 bp of the intronic region between exons 3 and 4 were retained in the mature transcript, resulting in the formation of an early stop codon 21 bp into the 82 bp insertion. This variant transcript was named PGC-1α-b-3T1. We investigated whether this isoform variant also existed in other tissues, since it had not been reported previously in the literature. We conducted RT-PCR on our human brain RNA samples to determine the presence of this alternatively spliced isoform b variant. Using a sense primer in exon 1b and an antisense primer that spanned the insertion-3' UTR boundary (only extending into the insertion by 3 bases, we were able to ensure that the primer set should not amplify off immature transcript (Fig. 3-3A). A no RT control was used to validate that there was no genomic DNA present in the cDNA. This primer set was expected to produce a 571 bp amplicon. End-point RT-PCR revealed a band of the expected size, 571 bp, on an ethidium bromide UV-visualized agarose gel (Fig.3-3B). This confirmed the presence of PGC-1α-b-3T1 transcript not only in human skeletal muscle, but also in human brain. Due to the early stop codon introduced in this novel PGC-1α-b transcript variant, a severely truncated protein would be produced (Fig. 3-3C). If PGC-1α-b-3T1 is translated endogenously in humans, we should be able to detect a 147 amino acid protein (15.8 kDa) in brain or muscle cell lysates using the isoform b specific primary antibody that had been developed for us (Genscript).

Bacterial expression and purification of recombinant GST/PGC-1a-b-3T1 fusion protein

In order to optimize our PGC-1α isoform b specific primary antibody, we needed to produce pure, recombinant protein containing the epitope the antibody was raised against.

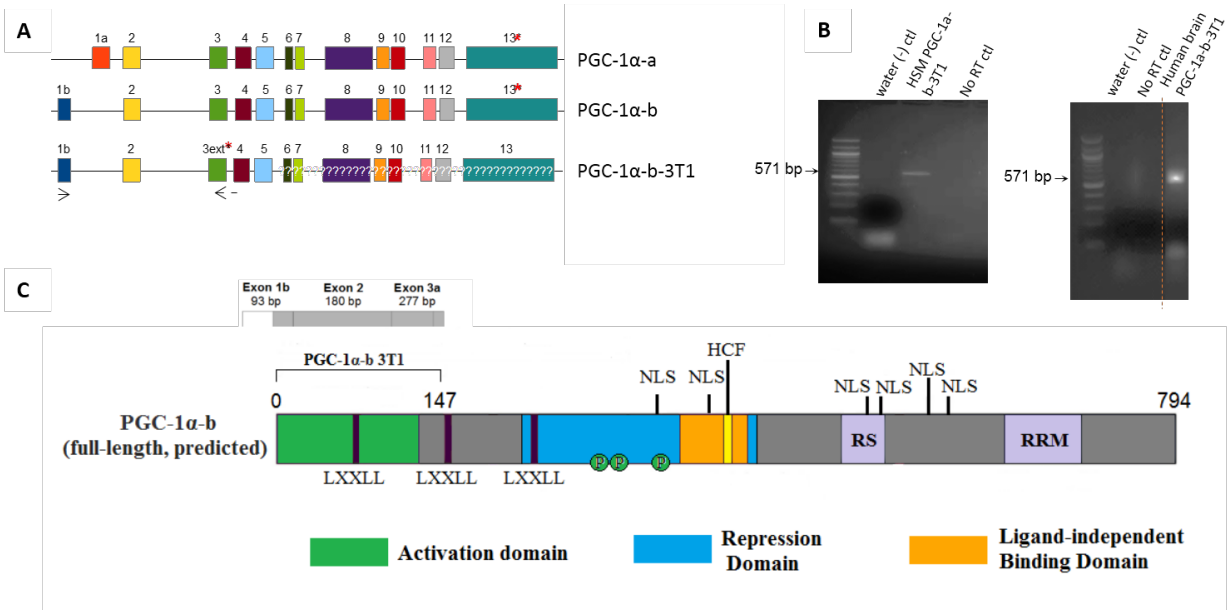

Figure 3-3: Identification of a new PGC1a isoform, PGC-1α-b 3T1 (exon 3 Truncated). (A) Schematic of PGC-1α-a (canonical isoform A) and PGC-1α-b (isoform b, isoform b 3T1) transcripts. Boxes indicate exons, lines indicate spliced introns, arrows indicate primer set location, red asterisks indicate stop codons in resultant CDS. (top) Isoform a (middle) Isoform b; transcript differs from isoform a only in the first exon. Isoform b has been found to extend to exon 13 in mice, with an unknown 3' end in human (Miura et al., 2008). (bottom) Isoform b variant 3T1 (PGC-1α-b-3T1), includes an 82 bp extension on exon 3 derived from intron 3, with an early stop codon located 21 bp after exon 3. (B) End-point RT-PCR of PGC-1α-b-3T1 transcript in HSM and human brain. 571 bp bands represent the identification of mature transcript in both HSM (left) and human brain (right No RT control indicates lack of genomic DNA contamination. (C) Schematic of predicted retained domains of PGC-1α-b-3T1 vs. PGC-1α-b. (HCF: host cell factor domain; NLS: nuclear localization signal; P = phosphorylation site; RS = arginine / serine rich domain; RRM = RNA binding motif - both RNA processing domains)

Considering that a transcript coding for a short version of PGC-1α isoform b had just been validated in a previous experiment (PGC-1α-b-3T1; see Fig. 3-3), we wanted to produce the predicted protein as a recombinant protein in bacteria. We originally chose this protein because it (1) contained our epitope, allowing us to optimize our antibody and determine its specificity and limit of detection; (2) had a low hydrophobicity index, indicating that it should be soluble and thus easily purified and potentially active to be able to probe its functions in vitro at a later time; and (3) it could be added to our whole cell lysates to determine the specificity of our antibody against a mammalian cell background; (4) it was a novel transcript, therefore we needed to know if it could produce viable protein and potential functions of that protein.

This protein was ultimately difficult to express in bacteria, however, and was therefore cloned as an N-terminal GST fusion protein instead of untagged, native PGC-1α-b-3T1. We used the pET41a vector, since it contained NT GST, which would aid in solubility, translation efficiency, and ease of purification of the target PGC-1α-b-3T1protein (Fig. 3-4A). pET41a also contained NT and CT 6xHis tags which provided us with the additional route of Ni-NTA affinity purification if the glutathione resin alone did not yield a pure enough fraction (Fig. 3-4A). We found that glutathione resin-based purification alone yielded protein of greater purity than Ni-NTA followed by glutathione resin purification (Fig. S2). BL21 DE3 competent cells with a 4 hour 1mM IPTG induction at 37˚C in LB were the conditions used to express the recombinant protein in bacteria, based on several small scale optimization experiments (Fig. S1).

The recombinant protein had a predicted size of 50 kDa. The protein we obtained from purification, however, migrated at ~60 kDa on SDS-PAGE gel, with several less abundant lower molecular weight bands occurring at ~40 kDa, ~30kDa, and ~26 kDa (Fig. 3-4B).

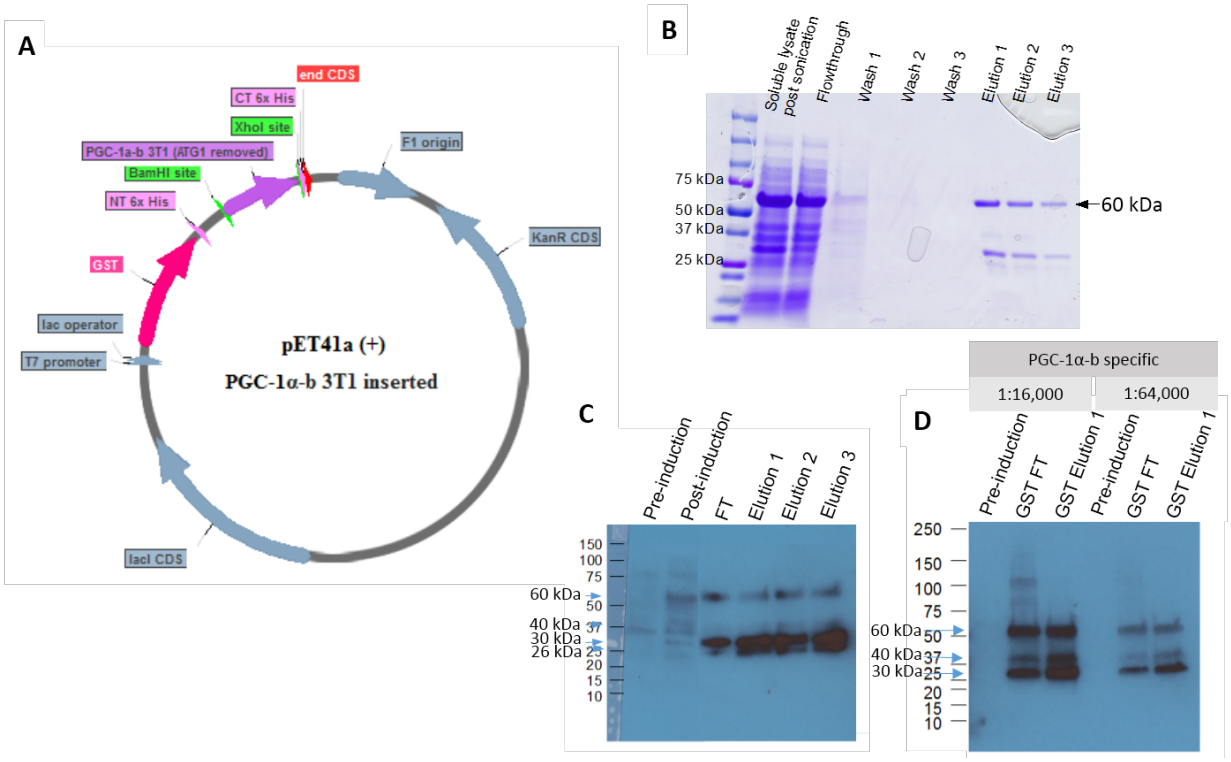

Fig. 3-4: Bacterial expression and purification of recombinant GST / PGC-1α-b-3T1 (A) vector map of pET41a after subcloning of PGC-1a. This vector produced an N-terminal fusion protein of approximately 50 kDa. (B) Coomassie-stained SDS-PAGE of recombinant PGC-1α-b-3T1 production and purification, using glutathione agarose resin. Target protein ran at ~60 kDa. Fractions of purifications steps were loaded with material from equal numbers of cells based on OD_{600}. (C) Immunoblot of GST-PGC-1a-b-3T1 recombinant protein using GST monoclonal antibody. 60 µg total protein was loaded for WCL and 10 µg total protein was loaded for the flow through and elution lanes. Chemiluminescent detection with full-strength dura ECL substrate, 4s exposure. (D) Immunoblot of purified recombinant GST-PGC-1a-b-3T1 fusion protein with PGC-1α isoform b specific primary antibody. Protein loaded was as in C above. A 1:5,000 dilution of secondary antibody was used. Exposed with full-strength dura ECL substrate for 4s.

In order to determine if the 60 kDa band was indeed full-length recombinant protein, the purification fractions were probed with both GST and our PGC-1α isoform b specific primary antibodies. From these western blots, it was evident that all four bands visible on the Coomassie stained gel contained GST (Fig. 3-4C), while only 3 contained PGC-1α-b-3T1 (Fig. 3-4D). The three bands detected by the isoform b antibody included all but the lowest (~26 kDa) band detected via Coomassie staining (Fig. 3-4D). These results showed that the protein was being degraded in some way prior to purification, since these bands are visible in lysate at 4 hours post-induction (Fig. 3-4C-D).

Since the specificity of our PGC-1α isoform b antibody had yet to be validated, another method was necessary to confirm that each band was truly a degradation product and not a contaminating bacterial protein. Mass-spectrometry of the bands in the Coomassie-stained gel was employed to confirm that our epitope was present, and also to confirm that the final purified product contained only our recombinant PGC-1α-b-3T1 protein. This verification was necessary for the intended use of PGC-1α-b-3T1 to optimize our PGC-1α isoform b specific primary antibody.

Mass spectroscopy validation of recombinant protein identity and antibody specificity via epitope peptide MS identification

Since there were multiple protein bands visualized from our purification that were not of the expected size, mass spectrometry was necessary to verify the identity of the recombinant protein. From immunoblots, it was determined that the upper band (~60 kDa) is most likely the full-length pure recombinant protein that was expected to run at 50 kDa on SDS-PAGE (see Fig. 3B-D). The remaining bands were presumed to be degradation products of the expressed construct. Mass spectrometry analysis was also necessary because although our PGC-1α isoform b specific primary antibody was able to detect protein in our elution fractions, the

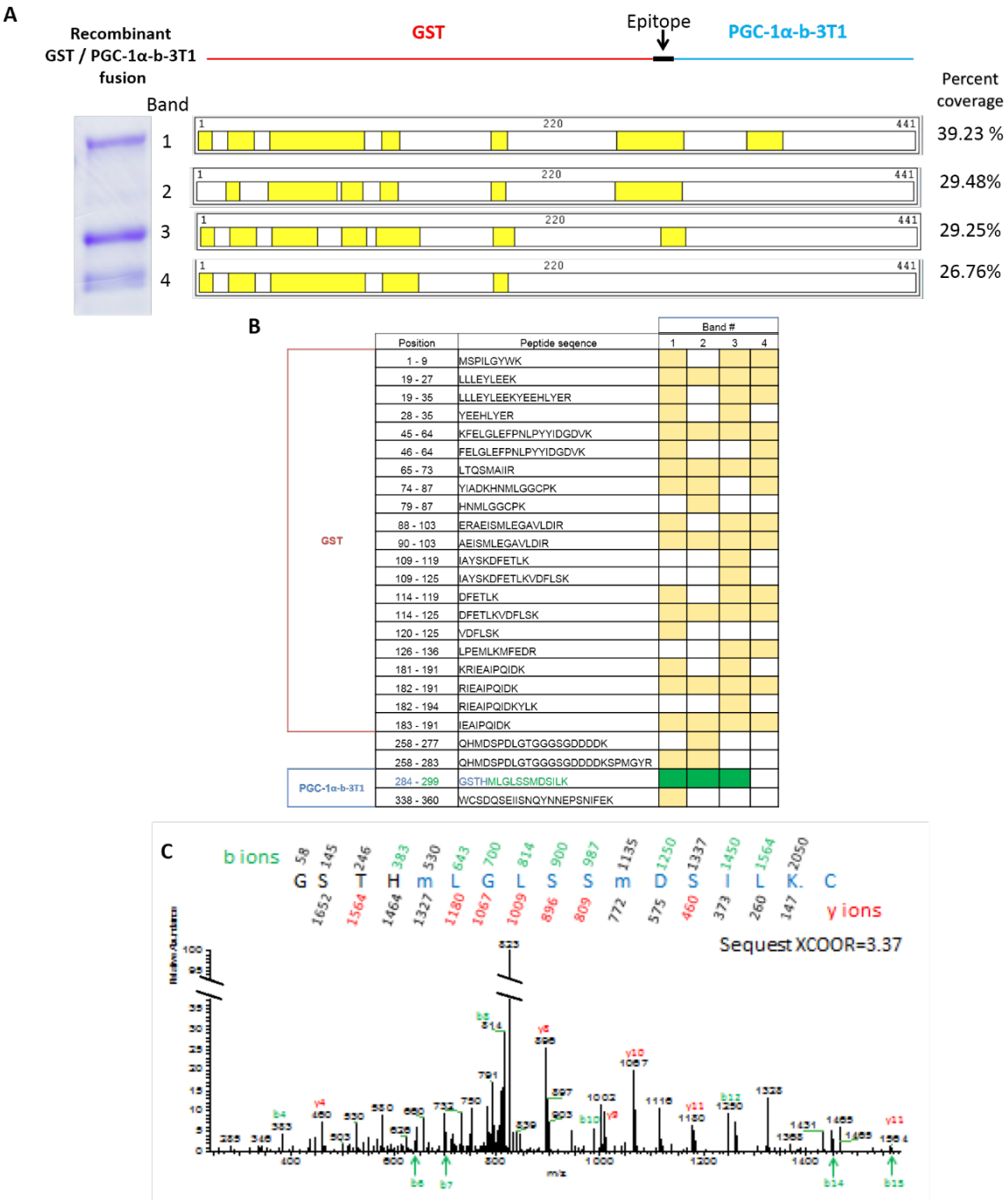

Fig. 3-5: Mass spectroscopy validation of recombinant protein identity and antibody specificity using peptide MS identification. (A) SDS-PAGE gel of purified recombinant GST/PGC-1a-b-3T1 fusion protein used for mass spec analysis (left). Bands 1-4 are ordered according to size (~60, 40, 30, and 26 kDa). Bands were excised, subjected to cleavage by trypsin, followed by MS/MS analysis. Tryptic peptides mapped to recombinant protein sequence as confirmed by SEQUEST (right). (B) Identified tryptic peptides across all samples. Bands refer to (A). The green region denotes the epitope location. Percent coverage is percent of amino acids identified from GST/ PGC-1α-b-3T1 fusion construct. (C) Representative spectrum of MS/MS acquisition for peptide containing the epitope for our PGC-1α isoform b specific primary antibody. B ions are peptides which increase in size from the NT. Y ions are peptides which increase in size from the CT. Xcoor cut- offs were 1.5 for a plus 1 charge state, 2.0 for a plus 2 charge state, and 2.5 for a plus 3 charge state.

antibody had not yet been validated nor evaluated for specificity. The recombinant protein would actually be the tool required to optimize our primary antibody. Mass spectrometry data would enable us to determine which bands contain the epitope of our antibody. If those epitope-containing bands were the same which were identified by our antibody in immunoblots, mass spectrometry analysis would thus provide support for validation of our antibody.

In the GST portion of the fusion construct, there were several excellent candidate tryptic peptides, however, we expected that trypsin cleavage would not yield many peptides in the PGC-1α-b-3T1 portion of our fusion protein that could be efficiently fingerprinted for this method. Most potential tryptic peptides formed from PGC-1α-b-3T1 were not of the optimal size or charge state for detection. One predicted optimal tryptic peptide within the PGC-1α-b-3T1 portion of our fusion protein contained the epitope to our PGC-1α isoform b specific antibody: MLGLSSDSILKC. Considering verification of this peptide in our sample was the objective of our analysis, and no other proteases or combination thereof would give us coverage of this epitope as well as good coverage of GST, we decided to use trypsin to accomplish cleavage of the proteins in our gel for MS/MS analysis. Each band visible on the Coomassie stained SDS-PAGE gel was excised, and the protein contained within it was then cleaved by trypsin (Fig. 3-5A). The resultant peptides were extracted and analyzed via MS/MS.

Upon mass spectrometry spectra analysis by SEQUEST, the upper band (band 1, ~60 kDa) was verified as our fusion construct with 39.23% coverage (Fig. 3-5A). Percent coverage is defined here as the percent of total amino acids identified from GST/ PGC-1α-b-3T1 fusion construct. The peptides identified from the remaining three lower molecular weight bands aligned with the recombinant protein sequence with 29.48, 29.23, and 26.76 percent coverage, respectively (fig. 4A- B). Bands 1-3 (~60, ~40, and ~ 30 kDa) all contained the tryptic peptide representing the epitope to our PGC-1α isoform b specific primary antibody (Fig. 3-5A-C). This peptide is positioned at amino acids 284-299 of the 441 aa fusion construct, with sequence

GSTHMLGLSSMDSILK. The epitope is located at position 288-300 (MLGLSSMDSILKC), therefore only the last amino acid was not represented in the peptide containing the epitope. In band 4 (~26 kDa), no peptides associated with the PGC-1α-b-3T1 portion of the fusion construct were identified. Therefore the percent coverage score only represents the GST portion of the fusion construct.

The results therefore showed that 3 out of the 4 bands visible on the Coomassie stained SDS-PAGE gel contained the epitope of interest, with the 4th band containing only GST. This result, along with >20% coverage of each of the bands for the fusion construct, gave concrete evidence that the GST PGC-1α-b-3T1 fusion construct was in fact the identity of our recombinant protein. This recombinant protein would now be the tool to validate and optimize our PGC-1α isoform b specific antibody. Considering the first immunoblot using this antibody selectively identified the 3 out of 4 bands which contained the epitope, the ability of the antibody to detect its target protein with some degree of specificity was apparent. This specificity of detection was observed on a minimal protein background, however, and alone could not completely reveal the degree of specificity of this antibody. This validated recombinant protein would serve as a means to optimize the western blotting conditions for this antibody to ultimately establish its limit of detection and specificity.

PGC-1α isoform b specific antibody: optimization, limit of detection, and specificity

In order to probe for endogenous human isoform b proteins and variants, it was necessary to develop an antibody specific to all possible forms of PGC-1α isoform b. The only location for such an antibody to be directed against was within the coding sequence resulting from exon 1b. This epitope was the only known distinction between isoform a and isoform b that would positively identify isoform b (Fig. 3-6A). Now that several isoform b variant transcripts have been

discovered, antibody directed against this epitope location should be able to detect any protein translated using exon 1b.

The optimization of this antibody will allow probing for all of the possible PGC-1α-b variants. Based on predicted size of these variants from mature transcript sequences (see Fig. 3-6 and table 1-2), these variants can be identified in cell lines and tissues. Based on our studies and current literature (see table 1-2) we predict 4 isoform b variants of molecular mass 90, 50, 40, and 17 kDa produced from various isoform b specific transcripts (Fig. 1-5, table 1-2). However, there is currently no information about endogenous protein production from any of these transcripts. If proteins of a predicted size were specifically detected by the isoform b antibody, the protein could be considered to be an endogenous functioning entity in that tissue type. With this antibody tool optimized and validated, we can then begin to further characterize endogenous protein-producing PGC-1α-b variant isoforms both in vivo and in vitro to better understand their function. More importantly, with this optimized antibody, we can eventually determine how PGC-1α isoform b and its variants are different from each other and PGC-1α-a in terms of function, regulation, and localization. Knowledge of the characteristics which are unique to each isoform could allow PGC-1α functions to be pharmacologically targetable in a spatio-temporal manner. Thus diseases which have a pathology attributed to misregulation of PGC-1α can have novel, specific treatment options.

The antigenicity within exon 1b was low based on Genscript analysis, however the antibody raised to this region (Fig. 3-6A) had a high titer in initial ELISA experiments (1:512,000). We therefore expected our antibody to effectively be able to detect PGC-1α-b and any of its possible variants. We also expected it to be specific, as a BLAST search did not reveal any similar human sequences. It is difficult to predict nonspecific binding, however. We aimed to determine the optimal western blotting conditions in order to obtain the highest degree of signal and lowest background, while retaining specificity.

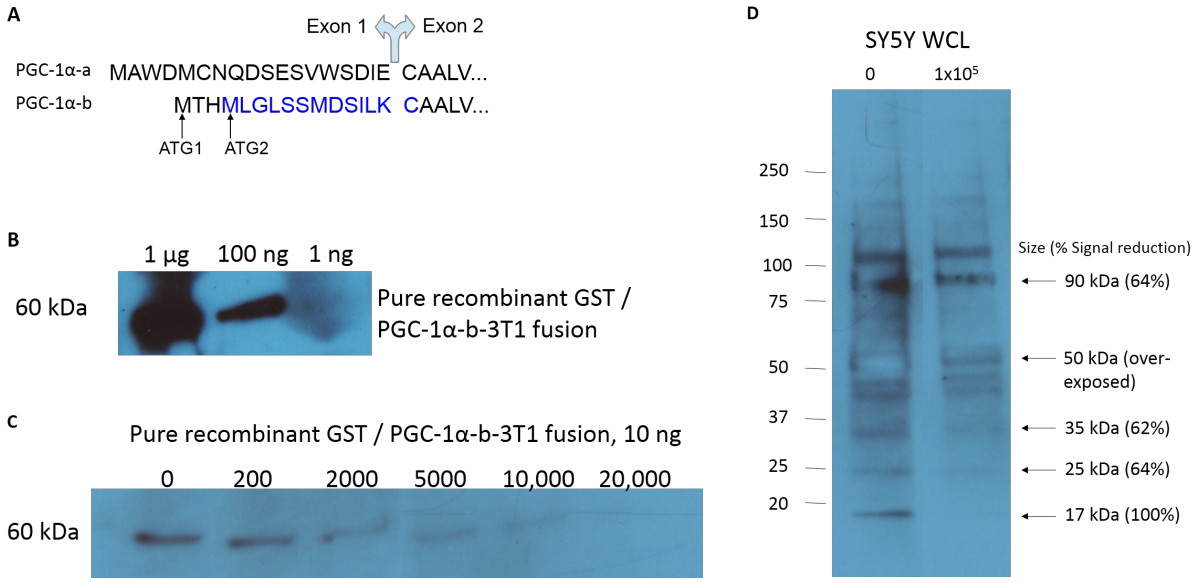

Fig. 3-6: PGC-1α-b specific antibody: optimization, limit of detection, and specificity (A) Epitope location of PGC-1a-b isoform specific antibody: Amino acid sequence of PGC-1α-a vs. PGC-1α-b. Epitope location (blue) is unique to PGC-1a-b. (B) Antibody sensitivity using recombinant GST / PGC-1a-b-3T1 fusion protein. Optimized 1:100 dilution of primary PGC-1a-b isoform specific Ab, 1:30,000 dilution of secondary Ab with T20 Starting Block (Thermo). Exposed in full dura ECL substrate for 2 minutes. (C) Peptide competition assay (PCA) optimization. 0-20,000: range of molar excess of peptide to PGC-1α-b antibody used. Exposed in full dura for 4s. Peptide used shown in blue in part A. (D) Degree of specificity of PGC-1α-b specific primary Ab by PCA. 0-100,000: molar excess of peptide to PGC-1α-b antibody used. Each lane contained 100 ug of SY5Y WCL per lane. Arrows indicate bands in which decreased signal is observed upon peptide competition, indicating specific binding. Blot was exposed with 1/8 dura for 4s. 5% non-fat dry milk in TBS-T was used as the blocking buffer in parts B-D.

We assumed that levels of protein would be minimal for PGC-1α-b and its variants under normal conditions. This prediction was based upon qPCR data showing that all possible isoform b variant transcripts combined are present at 1/10th the levels of PGC-1α-a containing transcripts in human brain (see figure 1B) and several other tissues, including kidney (Ruas et al., 2012). We make the assumption that transcript levels would reflect levels of protein; however, this is not always true. Based on tissue specific expression levels, we chose SH-SY5Ys (human neuroblastoma) and HEK293 (human embryonic kidney) for initial antibody tests. Endogenous PGC-1α-a was difficult to detect even with commercially available antibodies, based on previous experience in our lab. We assumed that isoform b would be present in the nanogram range at best, and titrated from 1 µg down to 1 pg of 60 kDa recombinant protein. Probing with a previously tested 1:16,000 dilution via western blot revealed that this optimized dilution could only detect down to between 1 µg and 100 ng of PGC-1α-b protein (Fig. S4). Therefore, several primary antibody concentrations were assessed, and a 1:100 dilution of the primary antibody yielded detection down to 1 ng (Fig. 3-6B). Although we could detect 1 ng, conditions needed to be further optimized to reduce background. By switching to blocking with 5% milk in TBS-T versus starting block (Thermo), a dramatic change in background levels were observed, eliminating all background even with a 2 minute exposure using full strength dura ECL substrate (Fig. S5). Combining information gained from these optimization experiments, the final optimized conditions were 5% milk in TBS-T blocking buffer, a 1:100 dilution of PGC-1α isoform b specific primary antibody, and a 1:35,000 dilution of goat anti-rabbit (GαR) HRP-conjµgated secondary antibody, probed in full to ½ dura with a 2min exposure (recombinant and WCL, respectively).

With the optimized conditions and limit of detection determined, the specificity of our PGC-1α- b specific primary antibody was assessed. Although our antibody already showed no non-specific signal on a bacterial lysate background (Fig. 3-4D), specificity on a mammalian

whole cell lysate background had not yet been determined. The gold standard to determine antibody specificity is the Peptide Competition Assay (PCA), in which primary antibody is incubated with its matching immunizing peptide prior to immunoblotting; this way, only nonspecific binding should be detected. The recombinant PGC-1α-b-3T1 protein was used to optimize peptide competition conditions. We determined the molar excess factor of peptide to antibody needed to block detection of recombinant protein, as well as peptide-antibody incubation conditions. After several tries, the molar excess factor which resulted in 100% blocking of 10 ng of recombinant protein was 20,000 (Fig. 3-6C). The optimal incubation conditions were determined to be 2 hours at room temperature with occasional mixing (Agrisera PCA protocol incubation conditions). Most importantly, peptide needed to be dissolved in pH 5.5 buffer in order to prevent disulfide bond formation prior to being incubated with primary antibody. Since this peptide was KLH-conjµgated, there is a Cys at the NT of the peptide in addition to the internal Cys at the CT of the peptide; if a disulfide bond formed, peptide would be bound to itself and would not be able to bind primary antibody, minimizing any blocking effect.

Once peptide blocking conditions were determined, the peptide competition experiments were conducted on WCLs. SH-SY5Y cells were chosen because they are a human neuronal cell line and several new PGC-1α isoforms had been reported in brain, including a mitochondrial isoform with unknown parent transcript. We had also found isoform b transcripts in human brain tissue (Fig. 3-2A-B, Fig. 3-3B). Blocking with 20,000 molar excess of peptide was not enough to fully block any signal using 100 µg SY5Y WCL (Fig. S6). The molar excess factor was then increased to 100,000, which was enough to cause a visual reduction in signal after exposure in 1/8 dura ECL substrate for 4s from 5 bands: ~90, 50, 35, 25, and 17 kDa. Of these 5 bands, the 17 kDa band was completely competed by the peptide. Signal for the ~90 kDa band was reduced by 64%. For the ~50 kDa band, signal was reduced by 62%. For the ~35 kDa band, the degree of signal reduction could not be determined because the band was overexposed. Even

at 1/16 dura ECL substrate, this band was overexposed. This experiment needs to be repeated to determine the exact percent reduction in signal for this 50 kDa band. For the 25 kDa band, signal was reduced by 64%. All percent reductions in signal from competing peptide were determined by ImageJ analysis (Rasband, W.S.; NIH).

Expected protein sizes were between 90 and 114 kDa for PGC-1α-b, and ~ 15 kDa representing PGC-1α-b-3T1. Other potential expected sizes include the remaining isoform b variants: PGC-1α-2 (41kDa) and PGC-1α-4 (29 kDa) (Ruas et al, 2012). There could also potentially be isoform b versions of NT-PGC-1α (38 kDa, Zhang et al., 2009) or PGC-1α ex1-8a (33 kDa, Soyal et al., 2012). The parent transcript of the mitochondrial isoform of PGC-1α is unknown, although this isoform was identified as a 35 kDa protein in SY5Ys by immunoblot. This mitochondrial isoform could potentially be an isoform b variant as well. Based on these predicted sizes, it is likely that the 90 kDa isoform b specific protein detected is full-length PGC-1α-b (resultant CDS ending in exon 13). PGC-1α-2 was shown to migrate closer to 50 kDa, and could therefore be represented in the 50 kDa isoform b specific protein which was detected. The 35 kDa protein detected is a likely candidate for mitochondrial PGC-1α, both observed to migrate at 35 kDa in SH-SY5Y cells. It is also a possibility that this 35 kDa protein detected represents an isoform b version of PGC-1αex1-8a, migrating a few kDa higher than predicted. It is possible that the identity of the mitochondrial isoform is the isoform b version of PGC-1α ex1-8a. No predicted size protein matches well with the 25 kDa protein detected. There is a possibility that this represents PGC-1α-b-3T1, but it would be migrating 10 kDa higher than expected. The other possibility is that this 25 kDa species represents a novel isoform b variant. The 17 kDa band detected to be specific for the isoform b specific primary antibody most likely represents PGC-1α-b-3T1, migrating slightly higher than expected.

Overall these results show that our PGC-1α-b specific antibody can detect PGC-1α-b protein and that this detection is specific, however, there are several nonspecific binding events

observed on immunoblots. There is potential confirmation of human versions of several predicted mouse isoform b variants. There is also potential confirmation of isoform b versions of several isoform a variants. Most intriguingly, the identity of the 35 kDa mitochondrial PGC-1α isoform may be solved. It migrates at the same size as an isoform b specific detected protein. An isoform a variant could also migrate at this size, and thus the true identity of the mitochondrial isoform could potentially be PGC-1α-b-ex8a. This is the first step in further characterizing these isoforms and understanding their function.

PGC-1α isoform b 3T1 overexpression in HEK293 cells

I generated CMV driven overexpression constructs containing PGC-1α-b-3T1 for determination of its functions in vitro. PGC-1α-a was also cloned in the same manner as PGC-1α-b-3T1 for side-by-side comparison to canonical PGC-1α. The final constructs contained a CT V5 or FLAG tag for immunodetection of PGC-1α-b-3T1 and PGC-1α-a, respectively (Fig. 3-7A). Inclusion of epitope tags in these constructs was necessary because the antibodies we had used to detect PGC-1α-a (including NT ones that could also theoretically detect PGC-1α-b and its variants) had several nonspecific bands and did not detect endogenous PGC-1α-a even in recommended positive controls (Fig. S3). The PGC-1α-b-3T1 construct was made because it was the only known human isoform b variant to date in which the entire CDS could be accounted for by the transcript. Mouse isoform b transcripts had not yet been fully identified in human tissues, including PGC-1α-b. Only transcript through exon 5 had been validated for human PGC-1α-b (Lochmann, T. unpublished data). Thus, the entire coding sequences for the possible isoform b transcripts in humans have yet to be determined. Although it was not known whether this protein was endogenously translated in humans, it was the only validated human version of isoform b for which its entire coding sequence was accounted for in the parent transcript (see Fig. 3-3).

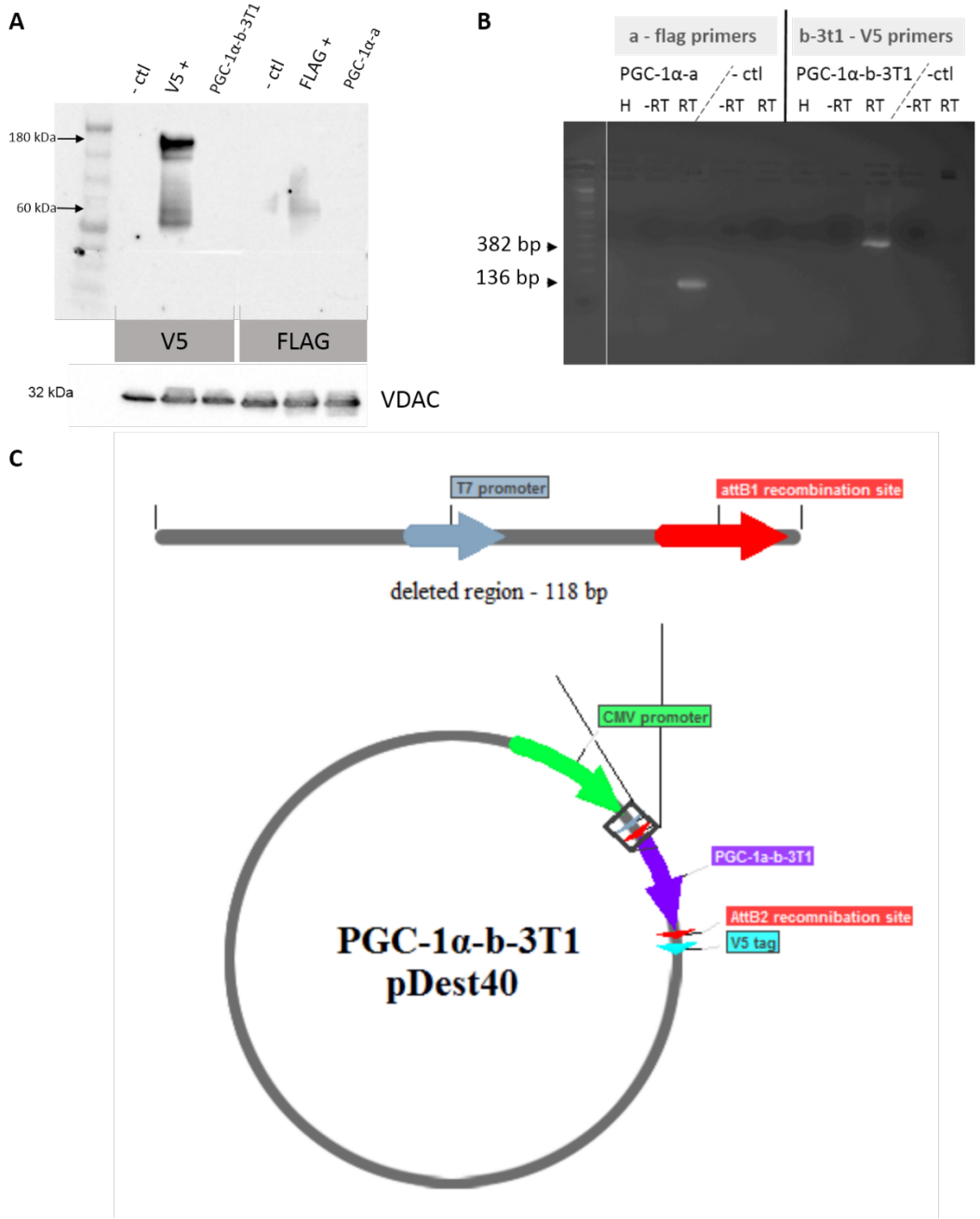

Fig. 3-7: PGC-1a-a and PGC-1a-b-3T1 overexpression in HEK293 cells (A) Lack of translation of PGC-1α pDEST constructs in immunoblots of HEK293 WCL. PGC-1a-a and PGC-1a-b-3T1 were cloned into pDest26-CT-FLAG and pDEST40, respectively (see Methods, figure 1), and transfected into HEK293 cells. Positive control for V5 (lane 2: hDNMT1 in pDEST40) and FLAG (lane 5: wt IDH2 in pDEST26-CT-FLAG) transfected at the same time served as controls for epitopes, transfection, as well as vectors. Expected sizes: 180 kDa, V5+; 60 kDa, FLAG+; 101 kDa, PGC-1a-a; 19 kDa, PGC-1a-b-3T1. Mock transfected HEK293 WCL was used as the negative control and VDAC as loading control. Blots were exposed for 10 min following detection with full dura ECL substrate and chemiluminescence visualized via LI-COR. (B) End-point RT-PCR of RNA extracted from HEK293 transfected with PGC-1α pDEST constructs. Sense primers were located near the 3' end of PGC-1α transcripts with antisense in the fusion tags. (H: water negative control; -RT: no reverse transcriptase negative control; RT: reverse transcribed sample. – ctl: empty vector negative control; M: 1 kb + marker). (C) Site-directed mutagenesis deletion of sequence between CMV promoter and PGC-1α CDS: schematic of deleted region.

We therefore sought to overexpress PGC-1α-b-3T1. This overexpression would initially allow us to determine the phenotypic effects of overexpression of PGC-1α-b-3T1 on cells. In comparison to endogenous levels (nontransfected) as well as overexpressed PGC-1α-a, this could provide initial information on conserved functional roles as well as any unique effects. Once overexpressed successfully, this manipulation of the amount of PGC-1α would allow us to see extreme effects on cells, which could eventually be contrasted by siRNA-mediated knockdown studies to further elucidate functional differences. We would also be able to look at changes in rates of mitochondrial respiration, binding interactions, and changes in levels of target genes. This would enable us to tease apart the specific functions of PGC-1α-b-3T1 which could contribute to those already attributed to PGC-1α-a.

We chose to transfect HEK cells with these PGC-1α constructs for their characteristic high transient transfection efficiencies. Also, in our lab PGC-1α-a had been previously transiently overexpressed in cell culture and were still viable (Shock, et al., 2011). Due to these results, we expected that these constructs would be easy to express in HEK293 cells. Upon transfection, no expression of these constructs was ever seen in western blot (Fig. 3-7B). Since CT fusion tags were being used to indirectly assess expression of PGC-1α, we sequenced the plasmids used in our transfections to determine that the sequence had not rearranged during large scale endotoxin-free preparation. DNA sequencing validated that PGC-1α was in frame with the tags used for immunodetection, and had not rearranged. In our lab, murine mtDNMT1 had been cloned into gateway vectors with no success in translation, although RT-PCR studies showed that they were being transcribed (Burton, E., unpublished observations). The problems expressing this protein were resolved upon removal of the Gateway *attB* sites and additional nucleotides between the end of the CMV promoter and the CDS. We therefore asked whether transcripts could be detected in transient transfection with the PGC1a expression vectors. Cells from transient transfections of these PGC-1α constructs were harvested and RNA extracted.

Primer sets to detect transcript expression were designed with sense primers specific to PGC-1α-a or PGC-1α-b and antisense primers specific to its respective tag in the gateway vector (FLAG or V5). If transcription was taking place, an amplicon of 136 bp for PGC-1α-a and 382 bp for PGC-1α-b-3T1 was expected (Fig. 3-7B)

Upon RT-PCR, bands of the expected size were visualized with no genomic DNA contamination shown from the lack of bands in the no reverse transcriptase control. From these results, it was determined that these constructs were indeed being transcribed. I used site-directed mutagenesis to remove the sequence between the CMV promoter and the CDS. This was successful for the PGC-1α-b-3T1 construct only. However, considering a new PGC-1α NT antibody had been made commercially available with success in detecting PGC-1α-a, it was decided that the construct made by Lisa Shock mentioned previously would be used to transfect PGC-1α-a for direct comparison to PGC-1α-b-3T1 (Shock et al., 2011). This experiment will be conducted in the near future.

CHAPTER 4

DISCUSSION

Transcriptional regulation of PGC1a: insights from mRNA expression and genomic DNA methylation studies

Our results suggest that DNA methylation may play a key role in the differential transcriptional regulation of PGC-1α-b versus canonical PGC-1α-a. PGC-1α-b is expressed 15 to 20 fold lower than PGC-1α-a, based upon normalized qRT-PCR data of human brain samples (see Fig. 3-2B). A high degree of methylation, known to correlate with gene silencing in many genes, was observed at each CpG 1 kb upstream of the transcription start site within the promoter region of PGC-1α-b (see Fig. 3-1,2C). Little to no methylation was observed in the promoter region of PGC-1α-a (see Fig. 3-2C). This difference in gene silencing methylation status could explain the difference in transcript expression between the two isoforms. It is of importance to note that PGC-1α does not contain CpG islands even 20 kb upstream of the TSS, and therefore is considered to be a CpG sparse promoter. Tissue-specific gene-silencing is frequently found in CpG sparse promoter regions, however (Nagae et al., 2011; Racanelli et al., 2008; Rishi et al., 2010).

The literature has recently reported several PGC-1α-a and PGC-1α-b variants, as described in this thesis (5 PGC-1α-a variants: Soyal et al., 2012; Spiegelman et al., 1998; Zhang et al., 2009; 3 PGC-1α-b variants: Miura et al., 2008; Ruas et al., 2012). Although we have not yet verified the 3' end of the mature transcripts in human brain (transcripts have been verified through to exon 5), our transcription data would apply to all currently established isoform a and

b variants of PGC-1α because all transcripts thus far reported contain exon 1a or exon 1b and exons 2 and 3, which is where our qPCR primers were located (see Fig. 3-2A). Most of these isoforms have been found in rodents, and we are currently conducting 3' RACE experiments to verify the existence of any of these isoforms, or potential new alternative splice variants, in human tissues, specifically human skeletal muscle and brain. The lab is also currently conducting 5' RACE of human brain to determine whether any additional alternative spliced transcripts upstream of isoform b exist. From our previous 5' RACE experiments, however, we know that exon 1a and exon 1b are two primary exons with unique promoter regions, which are transcribed in human skeletal muscle. For the studies reported here, cDNA was made from human prefrontal cortex. Other published 5' RACE studies using RNA from whole human brain samples found transcripts with TSS much farther upstream of exon 1b (Soyal et al., 2012), but failed to identify any isoform b promoter based transcripts. One potential explanation for this is that the isoforms we found are region-specific to the prefrontal cortex. Since we found that these isoforms are very low in abundance, they would be enriched in our samples compared to whole brain homogenates if regional specificity was a factor.

The first instance of PGC-1α-b identification was from studies using mouse skeletal muscle RNA (Miura et al, 2008). Similar to our findings, Miura and colleagues showed that transcript levels of PGC-1α-b were lower than that of PGC-1α-a at basal transcription levels. After mice were exercised, however, they found that levels of PGC-1α-b rose 100% higher than basal or exercised levels of PGC-1α-a 3 hours post exercise, becoming the predominant isoform. This effect was time-dependent and transient, with maximal PGC1a-b levels 30 min post exercise (700% increase relative to PGC-1α-a levels), and returning to basal levels between 6 and 24 hr post exercise (Tadaishi et al., 2011). Thus, it appears that, in skeletal muscle the isoform b promoter is poised for rapid activation. If a similar phenomenon were also occurring during periods of metabolic stress due to energy consumption in brain, then we would expect that the

methylation levels we have measured in this promoter might also include substantial levels of hydroxymethylation, which cannot be distinguished from methylation by bisulfite sequencing. Hydroxymethylation has been shown to occur in the nucleus as an intermediate on the path to demethylation, and therefore could offer this rapid switching mechanism under periods of metabolic stress (Tahiliani et al., 2009). Dr. Timothy Lochmann in our lab is currently conducting ChIP studies on the PGC-1α-a vs. b promoters. Thus far, he has shown that there are low levels of activating histone marks, but relatively low levels as well of repressive marks, suggesting a poised promoter in brain. The distinct drop in methylation levels that is seen 250 bp upstream of the TSS occurs at the proximal promoter, which is generally where polymerase II binds to begin transcription (see Fig. 3-2C). There could potentially be an area of heavy hydroxymethylation in the methylated promoter surrounding this region, which could lead to the rapid increase in transcript levels seen upon exercise. Future studies will look into locus-specific levels of hydroxymethylation to see if the proposed rapid switch demethylation regulation mechanism is occurring.

A novel PGC-1α-b variant transcript allowed validation and optimization of PGC-1α-b specific antibody.

The results from our 5' RACE and RT-PCR experiments revealed that PGC-1α-b-3T1 transcript is expressed in human skeletal muscle and brain (see Fig. 3-3B). The resultant protein of the PGC-1α-b-3T1 transcript would be truncated – in comparison to full length PGC-1α-b – due to the introduction of an early stop codon via alternative splicing between exons 3 and 4 (See Fig. 3-3A). Due to this truncation, only the first 147 amino acids of PGC-1α-b would be retained (see Fig. 3-3C). It was expected that this transcript may not be found in our human brain prefrontal cortex samples, even though its parent transcript, PGC-1α-b, is transcribed there (Lochmann, T. unpublished findings). This uncertainty stemmed from the studies in

whole brain (Soyal et al., 2012) in which they failed to find this variant, suggesting that the PGC-1α variants exhibit a tissue-specific or even tissue region-specific pattern of expression.

We now have some evidence that PGC-1α-b-3T1 is translated endogenously (see fig. 3-6D), although a functional assay is necessary to prove functionality. One such experiment could be cotransfection of this construct with a plasmid containing a reporter gene fused to the coding sequence for a nuclear hormone receptor. This experiment could show whether transcriptional coactivator activity intrinsic to canonical PGC-1α function is occurring, If these constructs are functional, this would be a reasonable function to test considering the activation domain containing the nuclear hormone receptor binding motif (LXXLL) is retained in all of these constructs. An alternative approach would be immunoprecipitation of this protein followed by mass spectrometry, which could allow for detection of endogenous binding partners. If the protein is bound to PPAR or other transcription factors, we would expect endogenous functionality. We predicted, however, that even if the protein was capable of being translated in vitro, there was a chance it may have a different function from canonical PGC-1α. The 147 amino acids of PGC-1α-b that are retained contain the activation domain only, which includes one LXXLL binding motif and sites which interact with SRC-1 and CBP (see Fig. 3-3C). Traditionally, the second LXXLL motif interacts with hormone nuclear receptors (PPARs, RXRs, TRs, GRs) necessary for its function as a transcriptional coactivator. It is possible that the one LXXLL site retained could compensate for the two missing LXXLL sites, lending it transcriptional coactivator function. However, it would still be missing nuclear localization signals, which may or may not be necessary for PGC-1α to localize to the nucleus. For example, NT-PGC-1α is similarly truncated compared to PGC-1α-a, and like PGC-1a-b-3T1, is missing all NLSs. Despite this, a small proportion of NT-PGC-1α (~10%) is localized to the nucleus and is active there (Zheng et al., 2009). There is no explicit reason to suggest that PGC-1α-b-3T1 would carry out any different functions from PGC-1α-b, because there is no new sequence to encode for

additional binding sites, however, there is no longer a repression domain, which could create a "gain of function" compared to canonical PGC-1a. This could occur since the retained activation domain could no longer be regulated by other proteins through the repression domain, such as p160 myb. This repression domain is also a region in which several post-translational modifications occur, which have either inhibitory or excitatory effects on PGC-1α activity (see Table 1-1). Since PGC-1α-b-3T1 would be missing almost all of these post-translational modification sites, retaining only 2 excitatory or inhibitory acetylation / deacetylation sites, it could change the rate of activation. Also, it is not known how many sites need to be acetylated or deacetylated to cause activation or inhibition of PGC-1α activity. One could argue that a smaller protein may be more specialized to a particular function, since only one functional domain would be retained. There is another possibility that this protein would only be active under certain conditions. This has already been evident in upregulation of PGC-1α-b transcript in exercised skeletal muscle and heart (Miura et al., 2008; Tadaishi et al., 2011; Thomas, R. and Lochmann, T., unpublished observations). Reasons for this upregulation are unknown, and also may not necessarily translate into changes in protein levels, as no studies have been done to determine whether this is the case. Perhaps this isoform b variant would provide a redundancy for the role of nuclear hormone receptor transcriptional coactivator under extreme conditions (such as where PGC-1α-b could no longer be expressed). Since PGC-1α-b regulation is still not completely understood, it is difficult to presume functions for its alternatively spliced variants. However, identification of endogenous protein isoforms using an isoform specific antibody, in this case isoform b, would allow the study of functionality. We have generated such an antibody using a N-terminal peptide unique to isoform b.

By using the predicted CDS of this truncated PGC-1α-b transcript, we were able to create recombinant protein. This protein was created because there were no definitive positive controls with which to optimize our PGC-1α-b specific primary antibody, as endogenous PGC-

1α-b protein had not yet been identified in human tissues. This construct was chosen because it contains CDS from a verified mature transcript in human skeletal muscle and human brain tissue (see Fig. 3-3B), and could thus represent a true small PGC-1α-b protein – optimal for verifying the quality of our antibody.

This recombinant GST/PGC-1α-b-3T1 fusion protein was successfully expressed and purified from bacteria (see Fig. 3-4B). Using antibodies to both the GST and PGC-1α-b portions of the protein, immunoblots confirmed that the major protein species produced was in fact the recombinant PGC-1α-b-3T1 GST fusion protein (see fig. 3-4C-D). However, due to the series of lower molecular weight bands also detected by the antibodies, further support was necessary to determine whether these were degradation products or contaminating bacterial proteins co-purified with our recombinant protein (see Fig. 3-4C-D).

Upon mass spectrometry analysis to determine the identity of the bands representing proteins in the final elution fraction, it was determined that all bands contained GST and that 3 out of the 4 bands visualized contained the epitope for the PGC-1α-b specific antibody (see Fig. 3-5). This data not only allowed for optimization of the PGC-1α-b specific primary antibody to proceed, but it also showed that the antibody could positively detect the protein intended for detection (see Fig. 3-4B, D). Also, these results showed that the antibody could detect its target protein with some degree of specificity. This was evident because signal was detected in only 3 out of the 4 bands visualized in the western blot utilizing this antibody; these were the same bands shown in mass spectrometry analysis to contain the epitope (see Fig. 3-4D, Fig. 3-5). The fourth band (-26 kDa), was most likely a CT degradation product in which the entirety of PGC-1α-b-3T1 had been cleaved from GST. This was evident in the MS results and was also intuitively determined prior, considering GST alone is 25 kDa. Also, anti-GST detected this band while the isoform b antibody did not.

The reasons for degradation in the GST/PGC-1α-b-3T1 fusion protein are unknown. Degradation appeared to have occurred during expression of the construct in bacteria, since lower molecular weight bands were seen prior to purification steps (see Fig. 3-4B). It was possible that degradation occurred upon cell lysis; however, great care was taken to include an excess of all protease inhibitors, with lysate treated gently and kept on ice at all times. The product data sheet which came with the antibody reported that GST fusion proteins generally appear on stained gels with a series of lower molecular weight bands, but did not give a reason for this detail (Pierce, cat. #16100). Perhaps the bacteria were trying to eliminate the foreign protein while it was being expressed, but only partial degradation of some of the overexpressed product was achieved. There is also potential that translation stalled once it reached PGC-1α-b-3T1 regions due to the bacteria's lower abundance of correct tRNAs to produce human codons such as those for Leucine or Proline, which were abundant in PGC-1α-b-3T1. If this is the reason for degradation, codon optimization via site-directed mutagenesis could minimize this problem, without affecting the antigen sequence.

Despite the degradation, the mass spectrometry data ultimately provided us with confirmation of the identity of our recombinant protein, GST/ PGC-1α-b-3T1 fusion, and showed that our antibody was able to detect PGC-1α-b protein. Western blotting conditions for the PGC-1α-b specific antibody were then optimized. Optimized immunoblot conditions were determined to be a 1:100 dilution of PGC-1α-b specific primary antibody, incubated at 4°C overnight, and 1:35,000 dilution of goat-anti-rabbit HRP-conjugated secondary antibody incubated for 1 hour at room temperature, both diluted in 5% nonfat dry milk in TBS-T. Using the recombinant GST/PGC-1α-b which was developed in order to validate this antibody, the limit of detection was determined to be 10 ng (see Fig. 3-6B). This antibody is the key to identifying endogenous PGC-1α-b isoforms, ultimately enabling us to characterize their functions.

Peptide competition assay of PGC-1α-b specific primary antibody enabled identification of putative isoform b protein variants

After peptide-antibody incubation conditions were determined utilizing recombinant GST/PGC-1α-b-3T1 fusion protein (see Fig. 3-6C), several specific bands were identified in SY5Y WCL upon immunoblot (see Fig. 3-6D). All of the bands successfully competed by peptide immunogen (60-100% reduction in signal) matched the predicted size of proteins produced from previously identified mouse PGC-1α-b or human PGC-1α-a isoform transcripts, with one exception. The isoform b specific protein which migrated at 25 kDa does not match well to the predicted size of any PGC-1α isoform reported. This could mean that this protein is a novel PGC-1α-b variant isoform, or a CT-degradation product from the larger PGC-1α-b specific proteins detected.

The remaining isoform b specific proteins identified migrated at ~90, 50, 35, and 17 kDa (see Fig. 3-6D). The 90 kDa band most likely represents PGC-1α-b. This is the 794 aa version of this protein. The full transcript was identified in mice (Miura et al., 2008), however, full transcript has not yet been sequenced from human sources. Also, endogenous 794 aa PGC-1α-b protein had not yet been reported in the literature, most likely because there was no way of differentiating between PGC-1α-a (798 aa) and PGC-1α-b (794 aa) prior to development of our isoform-specific antibody. Therefore, this study provides the first identification of endogenous PGC-1α-b protein. This is a milestone for studies of PGC-1α isoforms and would allow for in vitro as well as in vivo studies of verified correct full length human sequence for PGC-1α-b. I had begun to subclone 794 aa PGC-1α CDS into pDEST40 to use in mammalian overexpression experiments, but experienced difficulty in obtaining stable clones. Since full-length (exon 1b to exon 13) human PGC-1α-b transcript had not been fully sequenced either in our lab (our 5' RACE had only revealed exon 1b – exon 5), or in published studies from other labs, these cloning efforts were halted until protein of the expected size could be detected. Now

that data supports the existence of endogenous 794 aa PGC-1α-b, cloning experiments will resume. The 794 aa CDS construct is also ready to clone into a lentiviral vector expressing fluorescent fusion protein, namely pLVX-PA-mCherry-N1 (Clontech). This way, PGC-1α-b and its variants can be transfected into SY5Y cells, where they have been detected, and localization can be determined via the fluorescent tags in immunocytochemistry experiments utilizing confocal microscopy. Stable clones can also be developed in order to create high, medium, and low level expressing PGC-1α-b isoforms. This would be optimal since highly overexpressing levels of PGC-1α-b may be toxic. This could be especially true in SY5Y cells since neurons overexpressing PGC-1α in the nigrostriatal tract became more susceptible to ROS toxicity as well as neurodegeneration (Ciron et al., 2012). Considering these neurons were dopaminergic and that SY5Y cells are dopaminergic as well, a similar effect could be observed when overexpressing PGC-1α-b isoforms. Therefore, having low level expressers may be essential to studying the effects of PGC-1α-b isoforms in cell lines.

The 50 kDa band most likely represents PGC-1α-2 (Ruas et al., 2012), originally identified as an isoform b variant present in mouse, with a predicted size of 41 kDa. In their PGC-1α-2 transgenic mice, however, this isoform migrated nearer to 50 kDa (Ruas et al., 2012). This was believed to occur due to post-translational modifications increasing the molecular weight. The conserved domains retained include portions of the activation and repression domains. The repression domain contains several sites for potential post-translational modifications, including acetylation by GCN5 and phosphorylation by p38 MAPK or AMPK. No functional studies have been conducted on this isoform to date. Due to several alternative splicing events differentiating PGC-1α-2 from PGC-1α-b, including the exclusion of all but portions of exons 3, 7, and 8 and ending in a novel exon 14, it will be interesting to see what functions are retained for this isoform.

The 35 kDa band most likely represents the isoform b version of PGC-1α-a-ex8a. PGC-1α-a-ex8a is an isoform a variant with an alternatively spliced exon 8 (Soyal et al., 2012). This 204 bp exon 8 includes a 9 amino acid extension from the intron between exons 7 and 8, resulting in the formation of an in frame stop codon, and thus a 301 aa protein. Although this protein is predicted to be 32 kDa, post-translational modifications could increase the molecular weight and therefore have a higher migration on an SDS-PAGE gel. Due to the minimal change in size that would occur between PGC-1α-a-ex8a and an isoform b version of this protein, the 35 kDa band could represent a novel PGC-1α-b-ex8a. Interestingly, a 35 kDa protein of unknown parent transcript was identified in the mitochondrial of human brain samples as well as the SY5Y human neuroblastoma cell line (Choi et al., 2013). Due to similarity in size this 35 kDa band could represent PGC-1α-b-ex8a and thus the true identity of the mitochondrial PGC-1α isoform may be known. Additional experiments would be necessary in order to support this theory. This would include obtaining pure mitochondrial fractions from SY5Y cells and probing those lysates with PGC-1α-b once more. A negative control to show that this isoform is present only in the mitochondrion would be necessary, thus the mitochondria-extracted cytosolic fraction would be probed as well. If this isoform were present in the mitochondria, qRT-PCR experiments which observe an increase in any PGC-1α-b transcript levels upon exercise in mitochondrially abundant tissues (skeletal muscle, Tadaishi et al., 2012; heart, Thomas, R. and Lochmann, T. unpublished data) could be easily connected since an isoform b variant of PGC-1α would be localized directly to the mitochondrion. Lastly, the 17 kDa band most likely represents PGC-1α-b-3T1. This isoform was identified by our lab in clones from 5' RACE experiments. PGC-1α-b-3T1 encodes a 147 aa protein with a predicted molecular mass of 15.3 kDa. It could migrate higher on SDS-PAGE gels due to post-translational modifications. Acetylation via GCN5 is one such modification which can take place in the activation domain, a region retained in this truncated PGC-1α-b variant. Considering our lab previously identified this isoform and it was used to optimize our PGC-1α-b specific primary antibody, we already have

this construct in several different vectors, and the cDNA can be subcloned to lentiviral vectors very easily either from the TOPO vector or through gateway cloning (see Fig. 2-1).

Since the peptide competition assay was only conducted once using SY5Y lysates, this experiment would need to be repeated, perhaps under conditions where 100% blocking of signal from specific bands could be achieved, in order to support our conclusions.100% signal reduction could be reached by increasing the molar excess factor by at least 40%, from 100,000 to >140,000, determined from the percentage of no peptide control signal remaining in the competed sample. Also in order to provide further support for all these conclusions, I would like to probe SY5Y WCL side-by-side with a pan PGC-1α N-terminal antibody (EMD Millipore ST1202) and PGC-1α-b specific primary antibodies. This PGC-1α N-terminal antibody should be able to detect all b isoforms that contain part of amino acids 1-120 of canonical PGC-1α. Considering any predicted PGC-1α- b isoform variant would contain all but the first 12 amino acids of this epitope, this could serve as positive control for PGC-1α. This would show that each band detected as being specific for the amino acids of exon 1b also contains additional PGC-1α common sequence from exon 2. These blots would be complicated by the detection of isoform a variants as well, which could co-migrate. Alternatively, one could immunoprecipitate these proteins from SY5Y WCL using the PGC-1α-b specific antibody and verify their identity via immunoblot with the pan PGC-1α N-terminal antibody followed by mass spectrometry analysis (see Fig. 3-5).

Creation of tools for overexpression of PGC-1α isoforms in mammalian cells for future functional experiments

While PGC-1α-a and PGC-1α-b-3T1 mammalian overexpression constructs were created and sequence verified (see Fig. 2-1), it was found that the target CDS was able to be transcribed but not translated in RT-PCR experiments of transiently transfected HEK293 cells

(see Fig. 3-7B-C). It was not clear as to why these constructs were not being expressed. It was possible that the sequence was not in frame with the epitope fusion tag used to indirectly detect the constructs via WB. Sequencing of the exact vector aliquots used for transfection showed that the tags were in frame, however. Previous constructs utilizing gateway vectors displayed a similar phenomenon in our laboratory; removal of the vector sequence between the CMV promoter and the translation start lifted the block to translation. The region removed includes the AttB1 recombination site and the T7 promoter. Reasons as to why this may work could be that spacing between the promoter and the CDS may not be optimal for efficient translation. Another possibility is that the Kozak consensus sequence may not be strong enough to initiate translation. With this deletion, however, a new Kozak consensus sequence is formed, which may serve to enhance translation initiation. Most likely, however, the sequence between the CDS and the CMV promoter contains mRNA secondary structure upstream or over the ribosome binding site/start ATG.

This region between the CMV promoter and CDS was deleted in the PGC-1α-b-3T1 pDEST40 construct via site-directed mutagenesis (see Fig. 3-7C). Due to time constraints, transfections of these constructs were not completed prior to publication of this thesis, but will be conducted in the near future. Site-directed mutagenesis was attempted on the PGC-1α-a pDEST26 CT FLAG constructs, however, no colonies were produced which contained the deletion. Several different conditions were tried, including loading a range of 5-50 ng of template for the site-directed mutagenesis reaction, using 1-5 µL of this reaction in the transformation with XL1-Blue competent cells, and growing colonies at RT, 30°C, as well as 37°C. The only other option would be to redesign the primers used in the site-directed mutagenesis reaction. However, since we have recently obtained an antibody which can accurately detect endogenous PGC-1α (Teresa Leone, personal communication: PGC-1α-a NT aa1-120; ST1202 EMD Millipore), we will use this instead to detect PGC-1α-a. There is a construct used in Shock et al.,

2011 from our lab which overexpresses PGC-1α, but does not contain a FLAG tag for immunodetection. Therefore, prior to the recommendation of this antibody, we were not able to consider using this construct in our transfections to compare to PGC-1α-b-3T1.

It is of importance to note that all PGC-1α-a and PGC-1α-b mammalian expression plasmids were extremely difficult to grow in bacteria, due to the instability of the constructs. Growing conditions had to be altered even for the TOPO vector to grow without rearranging. After failure at several temperatures with TOP10 competent cells, Stbl3 cells (Invitrogen) were used in order to obtain stable plasmids with PGC-1α isoforms in PCR 4 TOPO (Invitrogen), pDONR201 (Invitrogen), and pENTR1a (Invitrogen) with growing conditions at 30°C. However, when glycerol stocks from the mini-prepped bacteria were used to scale up to plasmid midi-prep, endotoxin free preparations, all clones were found to have rearranged, by DNA sequences analysis. Retransformation into SURE2 cells (Stratagene) prior to the gateway reaction to form destination vectors, with growth temperature adjusted to 37°C increased stability of these constructs, and no rearrangement was detected upon sequencing of the midi-preps. However, for unknown reasons, the distributions of fragments upon restriction digest were not as expected; less signal was observed from the larger fragments than the smaller ones. Although this is indicative of rearrangement, none was seen in sequencing. This also affected the apparent concentration read via nanodrop, which was much higher than the true concentration determined via LI-COR densitometry by a factor of 100. After making glycerol stocks at OD 0.5 from mini-prepped bacterial cultures and using freshly streaked colonies from these glycerol stocks for midi-preps, as well as only harvesting cells when OD reached between 1.0 and 1.5, I was able to finally obtain stable plasmid to use in transfections.

It is also of importance to note that all PGC-1α-b human isoform variants have 2 possible translation start sites, ATG1 and ATG2, separated by 2 amino acids: **M**TH**M**... It is unknown which start site is preferred, but considering that only ATG2 is present in murine PGC-1α-b, this

is most likely the correct translation start site (Miura et al., 2008). Due to increased difficulty in obtaining stable clones for ATG1 versus ATG2 constructs, some support for ATG2 as the preferred translation start site is evident as well. Now that we were able to detect endogenous PGC-1α-b, our antibody can be used to immunoprecipitate these proteins, and Edman sequencing can be conducted to determine which translation start site is preferred for human PGC-1α-b.

Ultimately, now that methods to produce stable clones containing these isoforms in various vectors exist, it should be considerably easier to create new constructs for the isoform b variants believed to be detected endogenously in this project for future functional studies in vitro.

Perspectives

In conclusion, this thesis was able to accomplish the goal of expanding our knowledge of PGC-1α and its isoforms in addition to developing necessary tools to study PGC-1α-b variants more extensively in the future. Epigenetics in the form of DNA methylation was found to correlate to the difference seen in transcript expression of PGC-1α-b versus PGC-1α-a. A novel isoform variant of PGC-1α-b, deemed PGC-1α-b-3T1, was identified in two different human tissues, and putative endogenous protein of this variant was found to be expressed in a human neuronal cell line. Recombinant protein of this isoform was successfully expressed, fused to GST for ease of purification and validation. This recombinant GST / PGC-1α-b-3T1 fusion protein was then used to validate our PGC-1α-b specific primary antibody, aided by mass spectrometry analysis and immunoblotting. This recombinant protein was also used to determine optimal immunoblotting conditions, limit of detection, and degree of specificity of our novel antibody. The antibody was then used to identify 5 putative endogenous PGC-1α-b isoform variant proteins in a peptide competition assay. Mammalian expression vectors containing PGC-1α-a and PGC-1α-b-3T1 have been developed and isoform overexpression in

mammalian cells will be tested using these constructs in the near future. In addition, PGC-1α-a, PGC-1α-b, and PGC-1α-b-3T1 are all cloned into vectors which would enable them to be moved easily into lentiviral vectors or fluorescently tagged vectors for siRNA knockdown and localization studies. Now that protocols have been optimized and tools are available to study these isoforms, obtaining insight into their functions is within reach. This will allow us to gain a more complete picture of the varied roles of PGC-1α in mitochondrial biogenesis, metabolism, and disease providing the field with the required information to develop novel PGC-1α based therapeutics.

APPENDIX I

Supplemental Figures

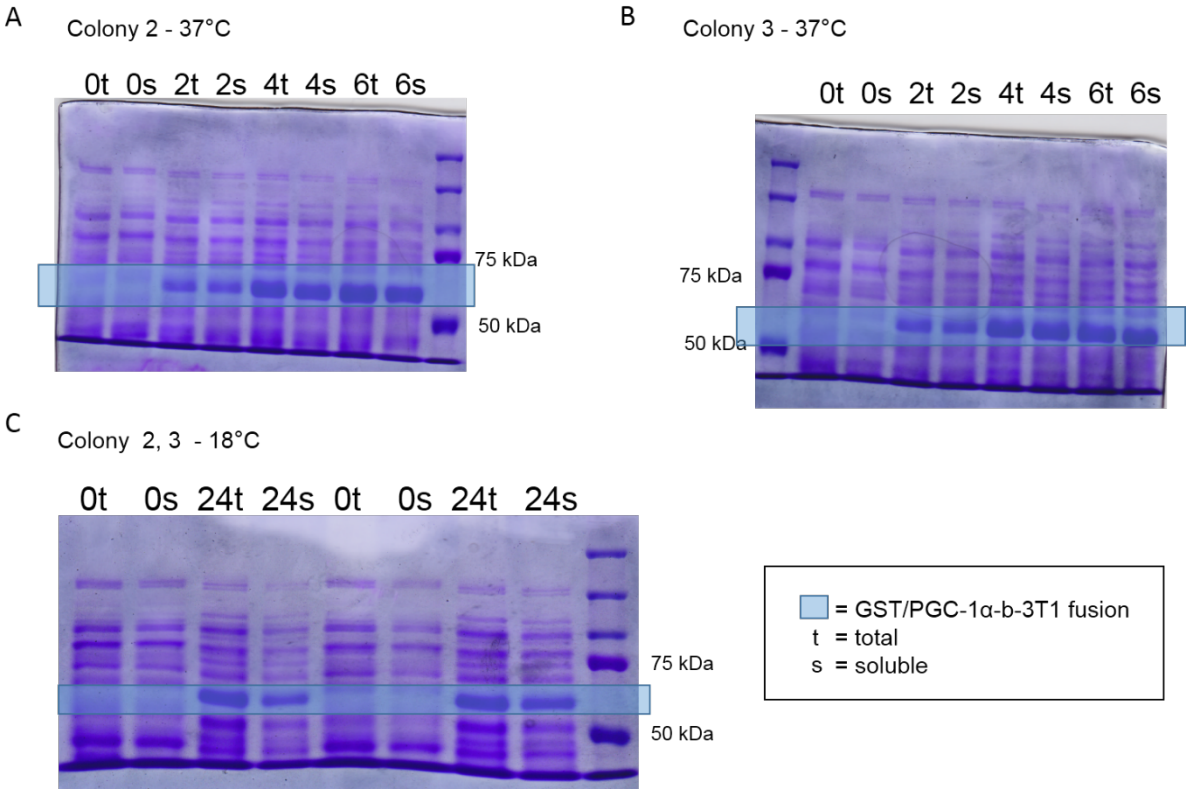

Fig. S1: Small scale induction for optimization of recombinant protein expression conditions. Two freshly streaked colonies of PGC-1α-b-3T1 subcloned into pET41a with BamHI, XhoI (c2: part A; c3: part B) were chosen to look at colony-specific changes in target protein expression. Each colony was grown in 6mL of LB broth in a 50mL conical for 8hrs in presence of 50ug/mL Kanamycin (Kan) at 37 C with 225rpm shaking until OD_{600} reached 0.5. The cultures were then incubated at 4°C overnight. 3 mL of each culture was then spun down for 30s at 18K x g and resuspended in fresh LB and Kan to seed 100mL of LB + Kan. Cultures were grown to OD_{600} of 0.6, then induced with 1mM IPTG. This culture was split into 2-50mL cultures, one to induce for 24 hours at 18°C, and the other to induce a total of 6 hr at 37°C. 1mL aliquot timepoints were collected prior to induction (0 hr) as well as 2, 4, and 6 hr post induction (parts A and B) and 24 hr post induction for the 18°C culture only (part C). The OD_{600} of each of these aliquots were taken, then the cells were harvested at 8K rpm for 5 min, freeze thawed and lysed in 100 µL lysis buffer containing 500ug/mL lysozyme and benzonase with 20min rt incubation, followed by 15 min bath sonication at 4°C. Soluble fraction was collected after half the sample was spun for 10 min at 10K x g. Equivalent sample amounts were then loaded onto 7.5% acrylamide gels based on cell density (OD_{600}). Optimal conditions (containing the most soluble induced target protein) were chosen as 4 hr induction at 37°C.

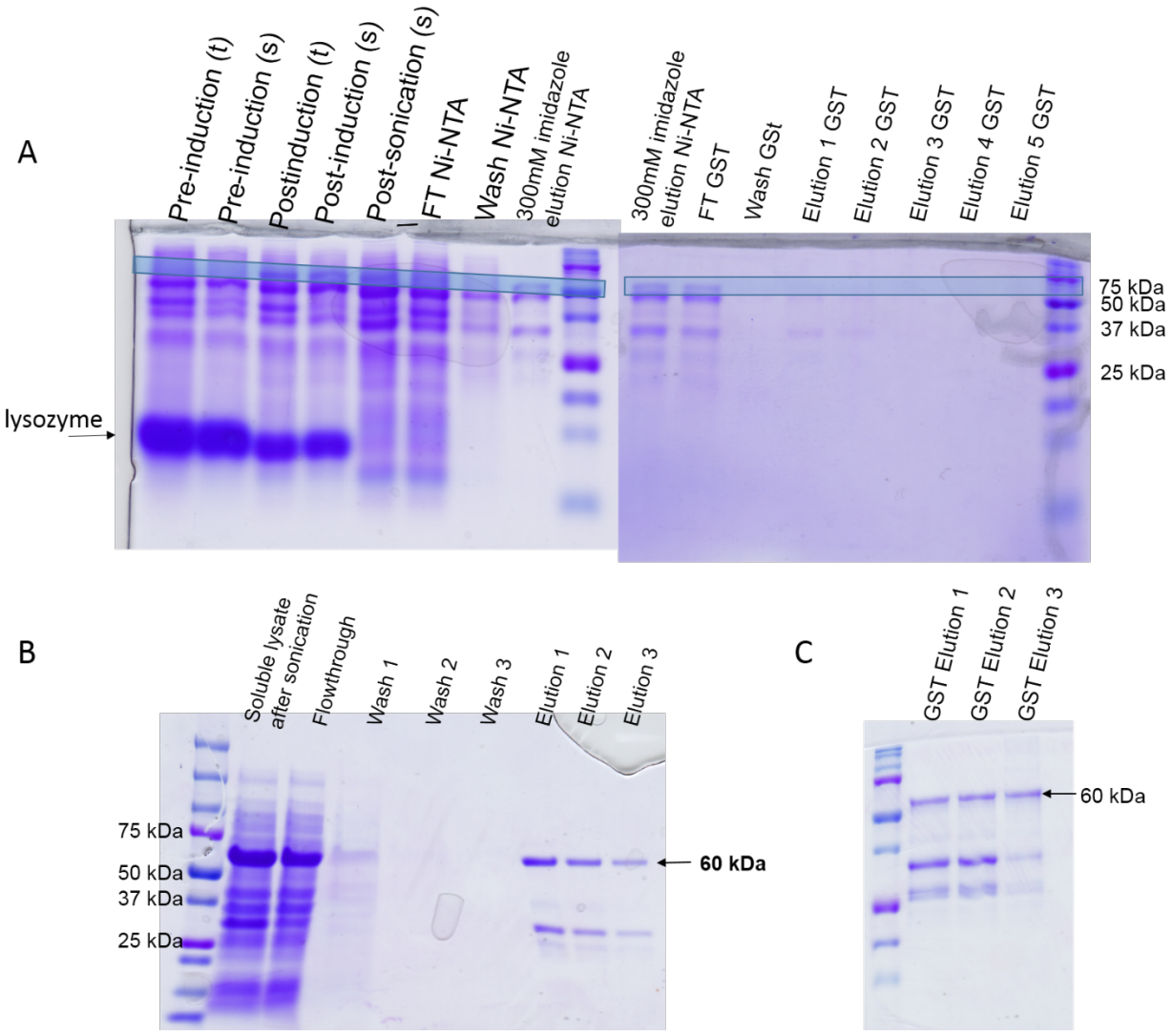

Fig. S2: Comparison of purification procedures for recombinant GST/PGC-1α-b-3T1 fusion. (A) Cultures were grown exactly as in Fig. S1, with the addition that 33 mL of the 100 mL culture was used to seed the 1L final culture volume. Protein was induced at OD_{600} of 0.6 with 1mM final concentration of IPTG for 4 hr. Cells were then harvested at 4000 rpm for 30 min. Cell pellets were freeze thawed and lysed with lysis buffer followed by sonication using the large probe tip program 9, 3x. The lysate was spun for 1hr 15min at 12k x g for 1 hr, followed by 13.5k x g for 15 min. Soluble lysate was loaded onto Ni-NTA agarose resin, eluted in 300 mM imidazole, and then diluted 2 fold in equilibration buffer (same as Ni-NTA lysis buffer) in order to reduce imidazole concentration to a compatible 150mM for second glutathione agarose (GST) column. Protein was eluted in presence of 10 mM free glutathione adjusted to pH 8.0 in a total of 10mL, taken in 2 mL fractions. The first 4 lanes of part A were lysed as in Fig. S1. Each lane was loaded with extract from an equivalent number of cells, based upon OD and resolved on a 15% acrylamide gel. s = soluble lysate fraction, t = total lysate fraction, box indicates GST / PGC-1α-b-3T1 fusion target recombinant protein. (B) Glutathione agarose (GST) alone batch purification of 50 mL total culture resolved on a 4-15% gradient acrylamide gel (Bio-Rad). Cells were lysed in 2 mL total volume BugBuster (EMD Millipore) via 15 min bath sonication. (C) 10 ug (determined via Bradford assay) of elutions 1-3 from purification in part A were resolved on a 12.5% acrylamide gel. Cleaner elutions with more concentrated protein was obtained from purification procedure used in part B.

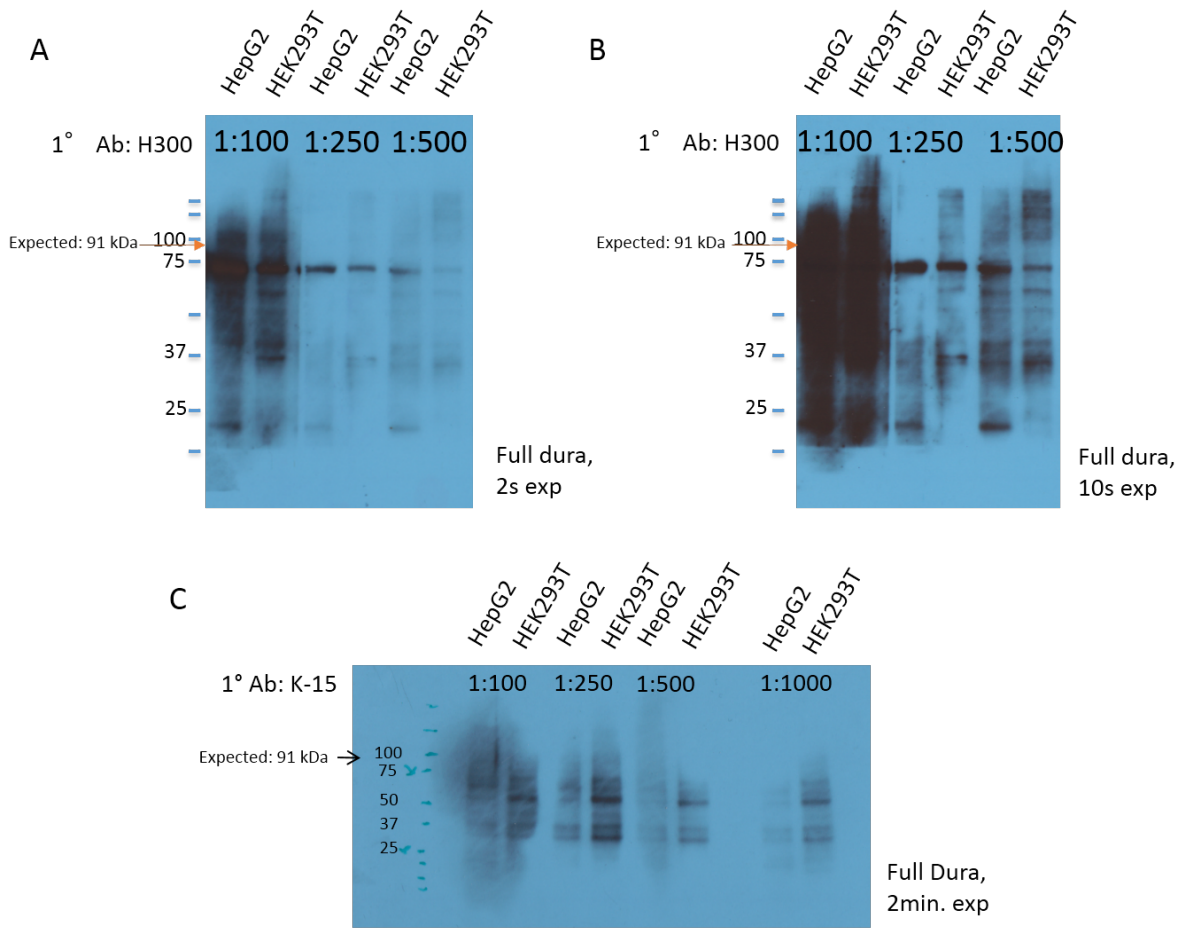

Fig. S3: **Attempted detection of PGC-1α-a with commercially available PGC-1α antibodies.** The expected size of PGC-1a-a was 91 kDa (arrow). HEPG2 WCL was used as a positive control and HEK293 is the cell line which would be probed in WB post-transient transfection. In each blot, each lane contained 50 ug of WCL. (A) Blot of WCL probed with several concentrations of H300 N-terminal PGC-1α Ab (Santa cruz). Secondary Ab: GαR, 1:5000. (B) Longer exposure of part A. (C) Blot of WCL probed with several concentrations of K-15 Ab (Santa cruz). Secondary Ab: DαG, 1:10,000. There was no band visualized at the expected size of canonical PGC-1α with K-15 antibody (Santa Cruz). A faint band higher than the predicted size of canonical PGC-1α was seen with H300, although there was nonspecific binding observed, especially at 75 kDa.

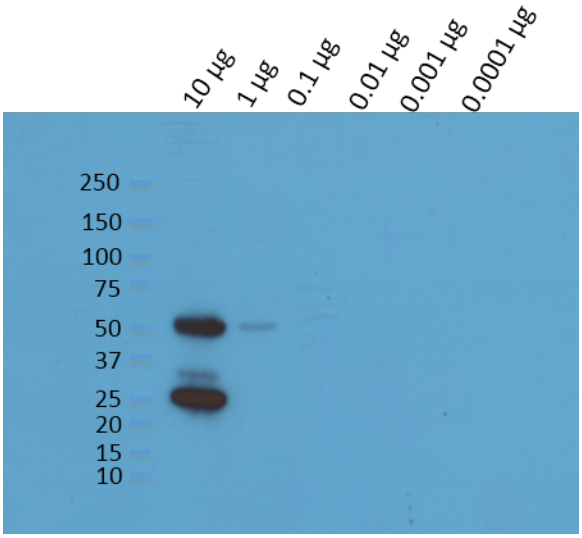

Fig. S4: Titration of purified recombinant GST/PGC-1a-b-3T1 fusion to determine PGC-1a-b specific Ab sensitivity. The blot contains a titration of decreasing amounts of purified recombinant GST/PGC-1α fusion protein. The blot was probed with a 1:16,000 dilution of PGC-1a-b specific primary Ab followed by GαR secondary Ab at a 1:5000 dilution. The blot was exposed with full strength dura chemiluminescent substrate (Thermo) for 2 s. Sensitivity at this concentration of primary was determined to be between 0.1 and 1 µg. The blot was exposed for up to 20 min with no change in the result shown here.

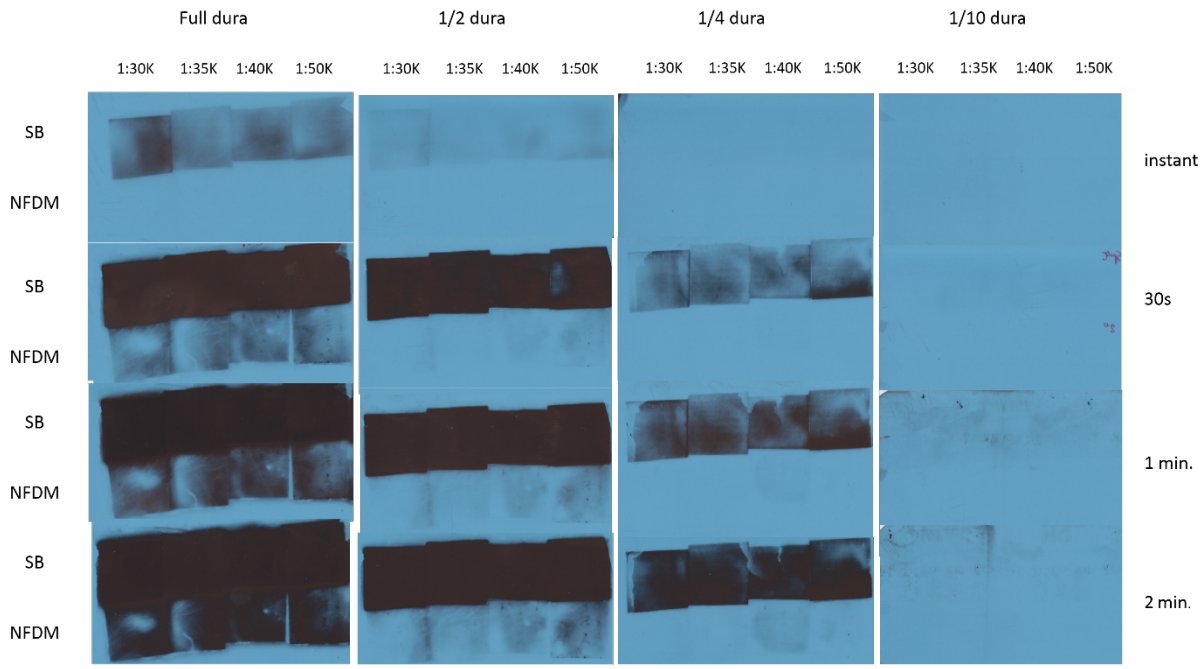

Fig. S5: Optimization of blocking conditions. Two different blocking buffers were utilized: T20 Starting Block (SB) (Thermo) and 5% Nonfat dry milk in TBS-T (NFDM). Pieces of PVDF membrane containing no transferred samples were blocked for 1 hr with moderate shaking at RT. Membrane was incubated overnight with several concentrations of PGC-1α-b specific primary Ab prepared in the respective blocking buffer (1:100, 1:500, 1:1000, 1:2000; only 1:100 shown here as a representation). Membrane was then washed and incubated for 1 hour in several concentrations of GαR secondary Ab (varied for each primary concentration used, based on previous optimization experiments at those concentrations; 1:30K, 1:35K, 1:40K, 1:50K represented here). All combinations of primary and secondary were each exposed in 1/10th, ¼, ½, and full strength dura substrate for 0s (instant), 30s, 1min, and 2min. The optimal blocking buffer was NFDM and optimal probing conditions based on blot background were chosen as a 1:100 dilution of primary Ab blocked in NFDM with 1:35,000 dilution of secondary Ab, exposed in <1/2 dura.

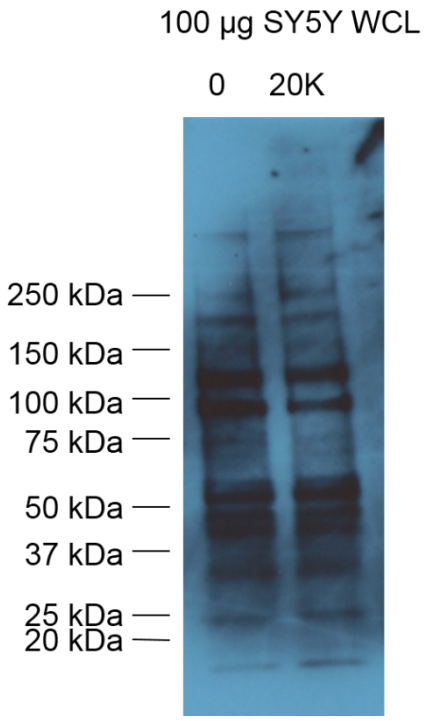

Fig. S6: Peptide competition assay optimization against WCL. Undifferentiated SH-SY5Y WCL was probed with pre-incubated primary antibody and a molar excess of its immunizing peptide to observe peptide competition and thus specificity. Molar excess factors of peptide to PGC-1α-b specific Ab of 0 (no peptide, control lane) and 20,000 (20K lane) were used in this assay. A 1:100 dilution of primary and 1:35,000 dilution of secondary (GαR) in 5% NFDM TBS-T was used. Blots were exposed in 1/8 dura ECL substrate for 8s. Although 20.000 molar excess of peptide to antibody was enough to completely block 10 ng of recombinant protein (Fig. 5), it was not able to block in a WCL setting.

REFERENCES

Akimoto, T., Sorg, B.S., and Yan, Z. (2004a). Real-time imaging of peroxisome proliferator-activated receptor-gamma coactivator-1alpha promoter activity in skeletal muscles of living mice. Am. J. Physiol. Cell Physiol. *287*, C790–6.

Akimoto, T., Ribar, T.J., Williams, R.S., and Yan, Z. (2004b). Skeletal muscle adaptation in response to voluntary running in Ca 2 ε / calmodulin-dependent protein kinase IV-deficient mice. *27704*, 1311–1319.

Andersson, U., and Scarpulla, R.C. (2001). PGC-1-Related Coactivator , a Novel , Serum-Inducible Coactivator of Nuclear Respiratory Factor 1-Dependent Transcription in Mammalian Cells. *21*, 3738–3749.

Aquilano, K., Vigilanza, P., Baldelli, S., Pagliei, B., Rotilio, G., and Ciriolo, M.R. (2010). Peroxisome proliferator-activated receptor gamma co-activator 1alpha (PGC-1alpha) and sirtuin 1 (SIRT1) reside in mitochondria: possible direct function in mitochondrial biogenesis. J. Biol. Chem. *285*, 21590–21599.

Arany, Z., He, H., Lin, J., Hoyer, K., Handschin, C., Toka, O., Ahmad, F., Matsui, T., Chin, S., Wu, P.-H., et al. (2005). Transcriptional coactivator PGC-1 alpha controls the energy state and contractile function of cardiac muscle. Cell Metab. *1*, 259–271.

Austin, S., Klimcakova, E., and St-Pierre, J. (2011). Impact of PGC-1α on the topology and rate of superoxide production by the mitochondrial electron transport chain. Free Radic. Biol. Med. *51*, 2243–2248.

Bagattin, A., Hugendubler, L., and Mueller, E. (2010). Transcriptional coactivator PGC-1alpha promotes peroxisomal remodeling and biogenesis. Proc. Natl. Acad. Sci. U. S. A. *107*, 20376–20381.

Barger, P.M., Brandt, J.M., Leone, T.C., Weinheimer, C.J., and Kelly, D.P. (2000). Deactivation of peroxisome proliferator-activated receptor-alpha during cardiac hypertrophic growth. J. Clin. Invest. *105*, 1723–1730.

Barrès, R., Osler, M.E., Yan, J., Rune, A., Fritz, T., Caidahl, K., Krook, A., and Zierath, J.R. (2009). Non-CpG methylation of the PGC-1alpha promoter through DNMT3B controls mitochondrial density. Cell Metab. *10*, 189–198.

Birnbaum, M.J. (2005). Activating AMP-activated protein kinase without AMP. Mol. Cell *19*, 289–290.

Cantó, C., and Auwerx, J. (2009). Europe PMC Funders Group PGC-1alpha , SIRT1 and AMPK , an energy sensing network that controls energy expenditure. *20*, 98–105.

Cao, J., Semenova, M.M., Solovyan, V.T., Han, J., Coffey, E.T., and Courtney, M.J. (2004). Distinct requirements for p38alpha and c-Jun N-terminal kinase stress-activated protein kinases in different forms of apoptotic neuronal death. J. Biol. Chem. *279*, 35903–35913.

Chabi, B., Adhihetty, P.J., Ljubicic, V., and Hood, D. a. (2005). How is Mitochondrial Biogenesis Affected in Mitochondrial Disease? Med. Sci. Sport. Exerc. *37*, 2102–2110.

Chang, J.S., Huypens, P., Zhang, Y., Black, C., Kralli, A., and Gettys, T.W. (2010). Regulation of NT-PGC-1alpha subcellular localization and function by protein kinase A-dependent modulation of nuclear export by CRM1. J. Biol. Chem. *285*, 18039–18050.

Chen, H., Detmer, S. a, Ewald, A.J., Griffin, E.E., Fraser, S.E., and Chan, D.C. (2003). Mitofusins Mfn1 and Mfn2 coordinately regulate mitochondrial fusion and are essential for embryonic development. J. Cell Biol. *160*, 189–200.

Chinsomboon, J., Ruas, J., Gupta, R.K., Thom, R., Shoag, J., Rowe, G.C., Sawada, N., Raghuram, S., and Arany, Z. (2009). The transcriptional coactivator PGC-1alpha mediates exercise-induced angiogenesis in skeletal muscle. Proc. Natl. Acad. Sci. U. S. A. *106*, 21401–21406.

Choi, J., Batchu, V.V.K., Schubert, M., Castellani, R.J., and Russell, J.W. (2013). A novel PGC-1α isoform in brain localizes to mitochondria and associates with PINK1 and VDAC. Biochem. Biophys. Res. Commun. *435*, 671–677.

Ciron, C., Lengacher, S., Dusonchet, J., Aebischer, P., and Schneider, B.L. (2012). Sustained expression of PGC-1α in the rat nigrostriatal system selectively impairs dopaminergic function. Hum. Mol. Genet. *21*, 1861–1876.

Da Cruz, S., Parone, P. a, Lopes, V.S., Lillo, C., McAlonis-Downes, M., Lee, S.K., Vetto, A.P., Petrosyan, S., Marsala, M., Murphy, A.N., et al. (2012). Elevated PGC-1α activity sustains mitochondrial biogenesis and muscle function without extending survival in a mouse model of inherited ALS. Cell Metab. *15*, 778–786.

Cui, L., Jeong, H., Borovecki, F., Parkhurst, C.N., Tanese, N., and Krainc, D. (2006). Transcriptional repression of PGC-1alpha by mutant huntingtin leads to mitochondrial dysfunction and neurodegeneration. Cell *127*, 59–69.

Cunningham, J.T., Rodgers, J.T., Arlow, D.H., Vazquez, F., Mootha, V.K., and Puigserver, P. (2007). mTOR controls mitochondrial oxidative function through a YY1-PGC-1alpha transcriptional complex. Nature *450*, 736–740.

Daitoku, H., Yamagata, K., Matsuzaki, H., Hatta, M., and Fukamizu, A. (2003). Regulation of PGC-1 promoter activity by protein kinase B and the forkhead transcription factor FKHR. Diabetes *52*, 642–649.

Delerive, P., Wu, Y., Burris, T.P., Chin, W.W., and Suen, C.S. (2002). PGC-1 functions as a transcriptional coactivator for the retinoid X receptors. J. Biol. Chem. *277*, 3913–3917.

Dillon, L.M., Williams, S.L., Hida, A., Peacock, J.D., Prolla, T. a, Lincoln, J., and Moraes, C.T. (2012). Increased mitochondrial biogenesis in muscle improves aging phenotypes in the mtDNA mutator mouse. Hum. Mol. Genet. *21*, 2288–2297.

Dufour, C.R., Wilson, B.J., Huss, J.M., Kelly, D.P., Alaynick, W. a, Downes, M., Evans, R.M., Blanchette, M., and Giguère, V. (2007). Genome-wide orchestration of cardiac functions by the orphan nuclear receptors ERRalpha and gamma. Cell Metab. *5*, 345–356.

Evans, M.J., and Scarpulla, R.C. (1990). NRF-1: a trans-activator of nuclear-encoded respiratory genes in animal cells. Genes Dev. *4*, 1023–1034.

Fan, M., Rhee, J., St-pierre, J., Handschin, C., Puigserver, P., Lin, J., Jäeger, S., Erdjument-bromage, H., Tempst, P., and Spiegelman, B.M. (2004). Suppression of mitochondrial respiration through recruitment of p160 myb binding protein to PGC-1 ⎵ : modulation by p38 MAPK. 278–289.

Felder, T.K., Soyal, S.M., Oberkofler, H., Hahne, P., Auer, S., Weiss, R., Gadermaier, G., Miller, K., Krempler, F., Esterbauer, H., et al. (2011). Characterization of novel peroxisome proliferator-activated receptor γ coactivator-1α (PGC-1α) isoform in human liver. J. Biol. Chem. *286*, 42923–42936.

Feng, H., Kang, C., Dickman, J.R., Koenig, R., Awoyinka, I., Zhang, Y., and Ji, L.L. (2013). Training-induced mitochondrial adaptation: role of peroxisome proliferator-activated receptor γ coactivator-1α, nuclear factor-κB and β-blockade. Exp. Physiol. *98*, 784–795.

Foretz, M., Pacot, C., Dugail, I., Lemarchand, P., Guichard, C., Le Lièpvre, X., Berthelier-Lubrano, C., Spiegelman, B., Kim, J.B., Ferré, P., et al. (1999). ADD1/SREBP-1c is required in the activation of hepatic lipogenic gene expression by glucose. Mol. Cell. Biol. *19*, 3760–3768.

Frescas, D., Valenti, L., and Accili, D. (2005). Nuclear trapping of the forkhead transcription factor FoxO1 via Sirt-dependent deacetylation promotes expression of glucogenetic genes. J. Biol. Chem. *280*, 20589–20595.

Garstka, H.L. (2003). Import of mitochondrial transcription factor A (TFAM) into rat liver mitochondria stimulates transcription of mitochondrial DNA. Nucleic Acids Res. *31*, 5039–5047.

Geng, T., Li, P., Okutsu, M., Yin, X., Kwek, J., Zhang, M., and Yan, Z. (2010). PGC-1 ⎵ plays a functional role in exercise-induced mitochondrial biogenesis and angiogenesis but not fiber-type transformation in mouse skeletal muscle. 572–579.

Gerhart-Hines, Z., Rodgers, J.T., Bare, O., Lerin, C., Kim, S.-H., Mostoslavsky, R., Alt, F.W., Wu, Z., and Puigserver, P. (2007). Metabolic control of muscle mitochondrial function and fatty acid oxidation through SIRT1/PGC-1alpha. EMBO J. *26*, 1913–1923.

Gervois, P., Torra, I.P., Fruchart, J.C., and Staels, B. (2000). Regulation of lipid and lipoprotein metabolism by PPAR activators. Clin. Chem. Lab. Med. *38*, 3–11.

Gomez-Cabrera, M.-C., Domenech, E., Romagnoli, M., Arduini, A., Borras, C., Pallardo, F. V, Sastre, J., and Viña, J. (2008). Oral administration of vitamin C decreases muscle mitochondrial biogenesis and hampers training-induced adaptations in endurance performance. Am. J. Clin. Nutr. *87*, 142–149.

Gutsaeva, D.R., Carraway, M.S., Suliman, H.B., Demchenko, I.T., Shitara, H., Yonekawa, H., and Piantadosi, C. a (2008). Transient hypoxia stimulates mitochondrial biogenesis in brain subcortex by a neuronal nitric oxide synthase-dependent mechanism. J. Neurosci. *28*, 2015–2024.

Hallberg, M., Morganstein, D.L., Kiskinis, E., Shah, K., Kralli, A., Dilworth, S.M., White, R., Parker, M.G., and Christian, M. (2008). A functional interaction between RIP140 and PGC-1alpha regulates the expression of the lipid droplet protein CIDEA. Mol. Cell. Biol. *28*, 6785–6795.

Hanai, J., Cao, P., Tanksale, P., Imamura, S., Koshimizu, E., Zhao, J., Kishi, S., Yamashita, M., Phillips, P.S., Sukhatme, V.P., et al. (2007). The muscle-specific ubiquitin ligase atrogin-1 / MAFbx mediates statin-induced muscle toxicity. *117*.

Handschin, C., and Spiegelman, B.M. (2008). The role of exercise and PGC1alpha in inflammation and chronic disease. Nature *454*, 463–469.

Handschin, C., Rhee, J., Lin, J., Tarr, P.T., and Spiegelman, B.M. (2003). An autoregulatory loop controls peroxisome expression in muscle. *100*.

Handschin, C., Kobayashi, Y.M., Chin, S., Seale, P., Campbell, K.P., and Spiegelman, B.M. (2007a). PGC-1 ␣ regulates the neuromuscular junction program and ameliorates Duchenne muscular dystrophy. 770–783.

Handschin, C., Kobayashi, Y.M., Chin, S., Seale, P., Campbell, K.P., and Spiegelman, B.M. (2007b). PGC-1alpha regulates the neuromuscular junction program and ameliorates Duchenne muscular dystrophy. Genes Dev. *21*, 770–783.

Handschin, C., Chin, S., Li, P., Liu, F., Maratos-Flier, E., Lebrasseur, N.K., Yan, Z., and Spiegelman, B.M. (2007c). Skeletal muscle fiber-type switching, exercise intolerance, and myopathy in PGC-1alpha muscle-specific knock-out animals. J. Biol. Chem. *282*, 30014–30021.

Hervouet, E., Demont, J., Pecina, P., Vojtísková, A., Houstek, J., Simonnet, H., and Godinot, C. (2005). A new role for the von Hippel-Lindau tumor suppressor protein: stimulation of mitochondrial oxidative phosphorylation complex biogenesis. Carcinogenesis *26*, 531–539.

Herzig, S., Long, F., Jhala, U.S., Hedrick, S., Quinn, R., Bauer, a, Rudolph, D., Schutz, G., Yoon, C., Puigserver, P., et al. (2001). CREB regulates hepatic gluconeogenesis through the coactivator PGC-1. Nature *413*, 179–183.

Hoeks, J., Arany, Z., Phielix, E., Moonen-Kornips, E., Hesselink, M.K.C., and Schrauwen, P. (2012). Enhanced lipid-but not carbohydrate-supported mitochondrial respiration in skeletal muscle of PGC-1α overexpressing mice. J. Cell. Physiol. *227*, 1026–1033.

Jäger, S., Handschin, C., St-Pierre, J., and Spiegelman, B.M. (2007). AMP-activated protein kinase (AMPK) action in skeletal muscle via direct phosphorylation of PGC-1alpha. Proc. Natl. Acad. Sci. U. S. A. *104*, 12017–12022.

Kaddour-djebbar, I., Choudhary, V., Brooks, C., Ghazaly, T., Lakshmikanthan, V., Dong, Z., and Kumar, M.V. (2010). Specific mitochondrial calcium overload induces mitochondrial fission in prostate cancer cells. 1437–1444.

Kang, C., and Ji, L.L. (2013). Role of PGC-1a in muscle function and aging. *2*, 81–86.

KAY, B.K., WILLIAMSON, M.P., and SUDOL, M. (2000). The importance of being proline: the interaction of proline-rich motifs in signaling proteins with their cognate domains. FASEB J *14*, 231–241.

Kim, D., Nguyen, M.D., Dobbin, M.M., Fischer, A., Sananbenesi, F., Rodgers, J.T., Delalle, I., Baur, J. a, Sui, G., Armour, S.M., et al. (2007). SIRT1 deacetylase protects against neurodegeneration in models for Alzheimer's disease and amyotrophic lateral sclerosis. EMBO J. *26*, 3169–3179.

Knutti, D., Kaul, A., and Kralli, A. (2000). A Tissue-Specific Coactivator of Steroid Receptors, Identified in a Functional Genetic Screen. Mol. Cell. Biol. *20*, 2411–2422.

Knutti, D., Kressler, D., and Kralli, a (2001). Regulation of the transcriptional coactivator PGC-1 via MAPK-sensitive interaction with a repressor. Proc. Natl. Acad. Sci. U. S. A. *98*, 9713–9718.

Kong, X., Wang, R., Xue, Y., Liu, X., Zhang, H., Chen, Y., Fang, F., and Chang, Y. (2010). Sirtuin 3, a new target of PGC-1alpha, plays an important role in the suppression of ROS and mitochondrial biogenesis. PLoS One *5*, e11707.

Koo, S.-H., Satoh, H., Herzig, S., Lee, C.-H., Hedrick, S., Kulkarni, R., Evans, R.M., Olefsky, J., and Montminy, M. (2004). PGC-1 promotes insulin resistance in liver through PPAR-alpha-dependent induction of TRB-3. Nat. Med. *10*, 530–534.

Kutik, S., Guiard, B., Meyer, H.E., Wiedemann, N., and Pfanner, N. (2007). Cooperation of translocase complexes in mitochondrial protein import. J. Cell Biol. *179*, 585–591.

Lagouge, M., Argmann, C., Gerhart-Hines, Z., Meziane, H., Lerin, C., Daussin, F., Messadeq, N., Milne, J., Lambert, P., Elliott, P., et al. (2006). Resveratrol improves mitochondrial function and protects against metabolic disease by activating SIRT1 and PGC-1alpha. Cell *127*, 1109–1122.

Leick, L., Lyngby, S.S., Wojtaszewski, J.F.P., Wojtasewski, J.F.P., and Pilegaard, H. (2010). PGC-1alpha is required for training-induced prevention of age-associated decline in mitochondrial enzymes in mouse skeletal muscle. Exp. Gerontol. *45*, 336–342.

Lemasters, J.J. (2005). John j. lemasters. *8*, 3–5.

Leone, T.C., Lehman, J.J., Finck, B.N., Schaeffer, P.J., Wende, A.R., Boudina, S., Courtois, M., Wozniak, D.F., Sambandam, N., Bernal-Mizrachi, C., et al. (2005). PGC-1alpha deficiency causes multi-system

energy metabolic derangements: muscle dysfunction, abnormal weight control and hepatic steatosis. PLoS Biol. *3*, e101.

Liang, H., Ward, W.F., Jang, Y.C., Bhattacharya, A., Bokov, A.F., Li, Y., Jernigan, A., Richardson, A., and Van Remmen, H. (2011). PGC-1α protects neurons and alters disease progression in an amyotrophic lateral sclerosis mouse model. Muscle Nerve *44*, 947–956.

Lin, J., Puigserver, P., Donovan, J., Tarr, P., and Spiegelman, B.M. (2002a). Peroxisome proliferator-activated receptor gamma coactivator 1beta (PGC-1beta), a novel PGC-1-related transcription coactivator associated with host cell factor. J. Biol. Chem. *277*, 1645–1648.

Lin, J., Wu, H., Tarr, P.T., Zhang, C., and Wu, Z. (2002b). Transcriptional co-activator PGC-1 a drives the formation of slow-twitch muscle fibres. *418*, 797–801.

Lin, J., Wu, P.-H., Tarr, P.T., Lindenberg, K.S., St-Pierre, J., Zhang, C.-Y., Mootha, V.K., Jäger, S., Vianna, C.R., Reznick, R.M., et al. (2004). Defects in adaptive energy metabolism with CNS-linked hyperactivity in PGC-1alpha null mice. Cell *119*, 121–135.

Ling, C., Del Guerra, S., Lupi, R., Rönn, T., Granhall, C., Luthman, H., Masiello, P., Marchetti, P., Groop, L., and Del Prato, S. (2008). Epigenetic regulation of PPARGC1A in human type 2 diabetic islets and effect on insulin secretion. Diabetologia *51*, 615–622.

López-Lluch, G., Hunt, N., Jones, B., Zhu, M., Jamieson, H., Hilmer, S., Cascajo, M. V, Allard, J., Ingram, D.K., Navas, P., et al. (2006). Calorie restriction induces mitochondrial biogenesis and bioenergetic efficiency. Proc. Natl. Acad. Sci. U. S. A. *103*, 1768–1773.

Ma, D., Li, S., Lucas, E.K., Cowell, R.M., and Lin, J.D. (2010). Neuronal inactivation of peroxisome proliferator-activated receptor γ coactivator 1α (PGC-1α) protects mice from diet-induced obesity and leads to degenerative lesions. J. Biol. Chem. *285*, 39087–39095.

Mangiarini, L., Sathasivam, K., Seller, M., Cozens, B., Harper, a, Hetherington, C., Lawton, M., Trottier, Y., Lehrach, H., Davies, S.W., et al. (1996). Exon 1 of the HD gene with an expanded CAG repeat is sufficient to cause a progressive neurological phenotype in transgenic mice. Cell *87*, 493–506.

Mason, S.D., Rundqvist, H., Papandreou, I., Duh, R., Mcnulty, W.J., Howlett, R.A., Olfert, I.M., Sundberg, C.J., Denko, N.C., Poellinger, L., et al. (2007). HIF-1 ⎵ in endurance training : suppression of oxidative metabolism. *0377*, 2059–2069.

Matiello, R., Fukui, R.T., Silva, M.E., Rocha, D.M., Wajchenberg, B.L., Azhar, S., and Santos, R.F. (2010). Differential regulation of PGC-1alpha expression in rat liver and skeletal muscle in response to voluntary running. Nutr. Metab. (Lond). *7*, 36.

McInerney, E.M., Rose, D.W., Flynn, S.E., Westin, S., Mullen, T.M., Krones, a, Inostroza, J., Torchia, J., Nolte, R.T., Assa-Munt, N., et al. (1998). Determinants of coactivator LXXLL motif specificity in nuclear receptor transcriptional activation. Genes Dev. *12*, 3357–3368.

Meeusen, S., DeVay, R., Block, J., Cassidy-Stone, A., Wayson, S., McCaffery, J.M., and Nunnari, J. (2006). Mitochondrial inner-membrane fusion and crista maintenance requires the dynamin-related GTPase Mgm1. Cell *127*, 383–395.

Meirhaeghe, A., Crowley, V., Lenaghan, C., Lelliott, C., Green, K., Stewart, A., Hart, K., Schinner, S., Sethi, J.K., Yeo, G., et al. (2003). Characterization of the human, mouse and rat PGC1 beta (peroxisome-proliferator-activated receptor-gamma co-activator 1 beta) gene in vitro and in vivo. Biochem. J. *373*, 155–165.

Michael, L.F., Wu, Z., Cheatham, R.B., Puigserver, P., Adelmant, G., Lehman, J.J., Kelly, D.P., and Spiegelman, B.M. (2001). Restoration of insulin-sensitive glucose transporter (GLUT4) gene expression in muscle cells by the transcriptional coactivator PGC-1. Proc. Natl. Acad. Sci. U. S. A. *98*, 3820–3825.

Miura, S., Kai, Y., Kamei, Y., and Ezaki, O. (2008). Isoform-specific increases in murine skeletal muscle peroxisome proliferator-activated receptor-gamma coactivator-1alpha (PGC-1alpha) mRNA in response to beta2-adrenergic receptor activation and exercise. Endocrinology *149*, 4527–4533.

Monsalve, M., Wu, Z., Adelmant, G., Puigserver, P., Fan, M., and Spiegelman, B.M. (2000). Direct coupling of transcription and mRNA processing through the thermogenic coactivator PGC-1. Mol. Cell *6*, 307–316.

Mootha, V.K., Handschin, C., Arlow, D., Xie, X., St Pierre, J., Sihag, S., Yang, W., Altshuler, D., Puigserver, P., Patterson, N., et al. (2004). Erralpha and Gabpa/b specify PGC-1alpha-dependent oxidative phosphorylation gene expression that is altered in diabetic muscle. Proc. Natl. Acad. Sci. U. S. A. *101*, 6570–6575.

Moreadith, R.W. (1995). Structural Characterization and Regulatory Element Analysis of the Heart Isoform of Cytochrome c Oxidase VIa. J. Biol. Chem. *270*, 26433–26440.

Mounier, C., and Posner, B.I. (2006). ` SE REVIEW / SYNTHE Transcriptional regulation by insulin : from the receptor to the gene 1. *724*, 713–724.

Mozdy, A.D., and Shaw, J.M. (2003). A fuzzy mitochondrial fusion apparatus comes into focus. Nat. Rev. Mol. Cell Biol. *4*, 468–478.

Mozdy, A.D., McCaffery, J.M., and Shaw, J.M. (2000). Dnm1p Gtpase-Mediated Mitochondrial Fission Is a Multi-Step Process Requiring the Novel Integral Membrane Component Fis1p. J. Cell Biol. *151*, 367–380.

Mudò, G., Mäkelä, J., Di Liberto, V., Tselykh, T. V, Olivieri, M., Piepponen, P., Eriksson, O., Mälkiä, A., Bonomo, A., Kairisalo, M., et al. (2012). Transgenic expression and activation of PGC-1α protect dopaminergic neurons in the MPTP mouse model of Parkinson's disease. Cell. Mol. Life Sci. *69*, 1153–1165.

Nagae, G., Isagawa, T., Shiraki, N., Fujita, T., Yamamoto, S., Tsutsumi, S., Nonaka, A., Yoshiba, S., Matsusaka, K., Midorikawa, Y., et al. (2011). Tissue-specific demethylation in CpG-poor promoters during cellular differentiation. Hum. Mol. Genet. *20*, 2710–2721.

Nemoto, S., Fergusson, M.M., and Finkel, T. (2004). Nutrient availability regulates SIRT1 through a forkhead-dependent pathway. Science *306*, 2105–2108.

Nichol, D., Christian, M., Steel, J.H., White, R., and Parker, M.G. (2006). RIP140 expression is stimulated by estrogen-related receptor alpha during adipogenesis. J. Biol. Chem. *281*, 32140–32147.

Nisoli, E., Tonello, C., Cardile, A., Cozzi, V., Bracale, R., Tedesco, L., Falcone, S., Valerio, A., Cantoni, O., Clementi, E., et al. (2005). Calorie restriction promotes mitochondrial biogenesis by inducing the expression of eNOS. Science *310*, 314–317.

Nolte, R.T., Wisely, G.B., Westin, S., Cobb, J.E., Lambert, M.H., Kurokawa, R., Rosenfeld, M.G., Willson, T.M., Glass, C.K., and Milburn, M. V (1998). Ligand binding and co-activator assembly of the peroxisome. 137–143.

Norrbom, J., Sällstedt, E.K., Fischer, H., Sundberg, C.J., Rundqvist, H., and Gustafsson, T. (2011). Alternative splice variant PGC-1α-b is strongly induced by exercise in human skeletal muscle. Am. J. Physiol. Endocrinol. Metab. *301*, E1092–8.

O'Hagan, K.A., Cocchiglia, S., Zhdanov, A. V, Tambuwala, M.M., Tambawala, M.M., Cummins, E.P., Monfared, M., Agbor, T.A., Garvey, J.F., Papkovsky, D.B., et al. (2009). PGC-1alpha is coupled to HIF-1alpha-dependent gene expression by increasing mitochondrial oxygen consumption in skeletal muscle cells. Proc. Natl. Acad. Sci. U. S. A. *106*, 2188–2193.

Olmos, Y., Valle, I., Borniquel, S., Tierrez, A., Soria, E., Lamas, S., and Monsalve, M. (2009). Mutual dependence of Foxo3a and PGC-1alpha in the induction of oxidative stress genes. J. Biol. Chem. *284*, 14476–14484.

Otsuga, D. (1998). The Dynamin-related GTPase, Dnm1p, Controls Mitochondrial Morphology in Yeast. J. Cell Biol. *143*, 333–349.

Patti, M.E., Butte, A.J., Crunkhorn, S., Cusi, K., Berria, R., Kashyap, S., Miyazaki, Y., Kohane, I., Costello, M., Saccone, R., et al. (2003). Coordinated reduction of genes of oxidative metabolism in humans with insulin resistance and diabetes: Potential role of PGC1 and NRF1. Proc. Natl. Acad. Sci. U. S. A. *100*, 8466–8471.

Pino, E., Wang, H., McDonald, M.E., Qiang, L., and Farmer, S.R. (2012). Roles for peroxisome proliferator-activated receptor γ (PPARγ) and PPARγ coactivators 1α and 1β in regulating response of white and brown adipocytes to hypoxia. J. Biol. Chem. *287*, 18351–18358.

Puigserver, P. (1999). Activation of PPAR Coactivator-1 Through Transcription Factor Docking. Science (80-.). *286*, 1368–1371.

Puigserver, P. (2003). Peroxisome Proliferator-Activated Receptor-gamma Coactivator 1alpha (PGC-1alpha): Transcriptional Coactivator and Metabolic Regulator. Endocr. Rev. *24*, 78–90.

Puigserver, P., Wu, Z., Park, C.W., Graves, R., Wright, M., and Spiegelman, B.M. (1998). A cold-inducible coactivator of nuclear receptors linked to adaptive thermogenesis. Cell *92*, 829–839.

Puigserver, P., Rhee, J., Lin, J., Wu, Z., Yoon, J.C., Zhang, C., Krauss, S., Mootha, V.K., Lowell, B.B., and Spiegelman, B.M. (2001). Cytokine Stimulation of Energy Expenditure through p38 MAP Kinase Activation of PPAR Coactivator-1. *8*, 971–982.

Qin, W., Haroutunian, V., Katsel, P., Cardozo, C.P., Ho, L., Buxbaum, J.D., and Pasinetti, G.M. (2009). PGC-1alpha expression decreases in the Alzheimer disease brain as a function of dementia. Arch. Neurol. *66*, 352–361.

Racanelli, A.C., Turner, F.B., Xie, L.-Y., Taylor, S.M., and Moran, R.G. (2008). A mouse gene that coordinates epigenetic controls and transcriptional interference to achieve tissue-specific expression. Mol. Cell. Biol. *28*, 836–848.

Rishi, V., Bhattacharya, P., Chatterjee, R., Rozenberg, J., Zhao, J., Glass, K., Fitzgerald, P., and Vinson, C. (2010). CpG methylation of half-CRE sequences creates C/EBPalpha binding sites that activate some tissue-specific genes. Proc. Natl. Acad. Sci. U. S. A. *107*, 20311–20316.

Rodgers, J.T., Lerin, C., Haas, W., Gygi, S.P., Spiegelman, B.M., and Puigserver, P. (2005). Nutrient control of glucose homeostasis through a complex of PGC-1 a and SIRT1. *434*, 3–8.

Ruas, J.L., White, J.P., Rao, R.R., Kleiner, S., Brannan, K.T., Harrison, B.C., Greene, N.P., Wu, J., Estall, J.L., Irving, B.A., et al. (2012). A PGC-1α Isoform Induced by Resistance Training Regulates Skeletal Muscle Hypertrophy. Cell *151*, 1319–1331.

Safdar, A., Little, J.P., Stokl, A.J., Hettinga, B.P., Akhtar, M., and Tarnopolsky, M. a (2011). Exercise increases mitochondrial PGC-1alpha content and promotes nuclear-mitochondrial cross-talk to coordinate mitochondrial biogenesis. J. Biol. Chem. *286*, 10605–10617.

Sahin, E., Colla, S., Liesa, M., Moslehi, J., Müller, F.L., Cooper, M., Kotton, D., Fabian, A.J., Walkey, C., Richard, S., et al. (2013). NIH Public Access. *470*, 359–365.

Sandri, M., Lin, J., Handschin, C., Yang, W., Arany, Z.P., Lecker, S.H., Goldberg, A.L., and Spiegelman, B.M. (2006). PGC-1 protects skeletal muscle from atrophy by suppressing FoxO3 action and atrophy-specific gene transcription.

Savkur, R.S., Bramlett, K.S., Stayrook, K.R., Nagpal, S., and Burris, T.P. (2005). Coactivation of the Human Vitamin D Receptor by the Peroxisome Proliferator-Activated Receptor Coactivator-1 . *68*, 511–517.

Schieke, S.M., Phillips, D., McCoy, J.P., Aponte, A.M., Shen, R.-F., Balaban, R.S., and Finkel, T. (2006). The mammalian target of rapamycin (mTOR) pathway regulates mitochondrial oxygen consumption and oxidative capacity. J. Biol. Chem. *281*, 27643–27652.

Schreiber, S.N., Knutti, D., Brogli, K., Uhlmann, T., and Kralli, A. (2003). The transcriptional coactivator PGC-1 regulates the expression and activity of the orphan nuclear receptor estrogen-related receptor alpha (ERRalpha). J. Biol. Chem. *278*, 9013–9018.

Schreiber, S.N., Emter, R., Hock, M.B., Knutti, D., Cardenas, J., Podvinec, M., Oakeley, E.J., and Kralli, A. (2004). The estrogen-related receptor (ERR) functions mitochondrial biogenesis. *101*.

Seelan, R.S.., and Grossman, L.I. (1997). Structural Organization and Promoter Analysis of the Bovine Cytochrome c Oxidase Subunit VIIc Gene. A FUNCTIONAL ROLE FOR YY1. J. Biol. Chem. *272*, 10175–10181.

Semple, R.K., Crowley, V.C., Sewter, C.P., Laudes, M., Christodoulides, C., Considine, R. V, Vidal-Puig, a, and O'Rahilly, S. (2004). Expression of the thermogenic nuclear hormone receptor coactivator PGC-1alpha is reduced in the adipose tissue of morbidly obese subjects. Int. J. Obes. Relat. Metab. Disord. *28*, 176–179.

Shang, Y., Hu, X., DiRenzo, J., Lazar, M. a, and Brown, M. (2000). Cofactor dynamics and sufficiency in estrogen receptor-regulated transcription. Cell *103*, 843–852.

Shen, T., Liu, Y., and Schneider, M.F. (2012). Localization and regulation of the N terminal splice variant of PGC-1α in adult skeletal muscle fibers. J. Biomed. Biotechnol. *2012*, 989263.

Sheng, B., Wang, X., Su, B., Lee, H., Casadesus, G., Perry, G., and Zhu, X. (2012). Impaired mitochondrial biogenesis contributes to mitochondrial dysfunction in Alzheimer's disease. J. Neurochem. *120*, 419–429.

Shin, J., Ko, H.S., Kang, H., Lee, Y., Lee, Y., Troconso, J.C., Dawson, V.L., and Dawson, T.M. (2012). NIH Public Access. *144*, 689–702.

Shock, L.S., Thakkar, P. V, Peterson, E.J., Moran, R.G., and Taylor, S.M. (2011). DNA methyltransferase 1, cytosine methylation, and cytosine hydroxymethylation in mammalian mitochondria. Proc. Natl. Acad. Sci. U. S. A. *108*, 3630–3635.

Soyal, S.M., Felder, T.K., Auer, S., Hahne, P., Oberkofler, H., Witting, A., Paulmichl, M., Landwehrmeyer, G.B., Weydt, P., and Patsch, W. (2012). A greatly extended PPARGC1A genomic locus encodes several new brain-specific isoforms and influences Huntington disease age of onset. Hum. Mol. Genet. *21*, 3461–3473.

St-Pierre, J., Lin, J., Krauss, S., Tarr, P.T., Yang, R., Newgard, C.B., and Spiegelman, B.M. (2003). Bioenergetic analysis of peroxisome proliferator-activated receptor gamma coactivators 1alpha and 1beta (PGC-1alpha and PGC-1beta) in muscle cells. J. Biol. Chem. *278*, 26597–26603.

St-Pierre, J., Drori, S., Uldry, M., Silvaggi, J.M., Rhee, J., Jäger, S., Handschin, C., Zheng, K., Lin, J., Yang, W., et al. (2006). Suppression of reactive oxygen species and neurodegeneration by the PGC-1 transcriptional coactivators. Cell *127*, 397–408.

Suwa, M., Nakano, H., Radak, Z., and Kumagai, S. (2008). Endurance exercise increases the SIRT1 and peroxisome proliferator-activated receptor gamma coactivator-1alpha protein expressions in rat skeletal muscle. Metabolism. *57*, 986–998.

Tadaishi, M., Miura, S., Kai, Y., Kano, Y., Oishi, Y., and Ezaki, O. (2011). Skeletal muscle-specific expression of PGC-1α-b, an exercise-responsive isoform, increases exercise capacity and peak oxygen uptake. PLoS One *6*, e28290.

Taherzadeh-Fard, E., Saft, C., Andrich, J., Wieczorek, S., and Arning, L. (2009). PGC-1alpha as modifier of onset age in Huntington disease. Mol. Neurodegener. *4*, 10.

Tahiliani, M., Koh, K.P., Shen, Y., Pastor, W.A., Brudno, Y., Agarwal, S., Iyer, L.M., David, R., Aravind, L., and Rao, A. (2009). NIH Public Access. *324*, 930–935.

Tcherepanova, I., Puigserver, P., Norris, J.D., Spiegelman, B.M., and McDonnell, D.P. (2000). Modulation of estrogen receptor-alpha transcriptional activity by the coactivator PGC-1. J. Biol. Chem. *275*, 16302–16308.

Teyssier, C., Ma, H., Emter, R., Kralli, A., and Stallcup, M.R. (2005). Activation of nuclear receptor coactivator PGC-1 ⌴ by arginine methylation. 1466–1473.

Tontonoz, P., Kim, J.A.E.B.U.M., Graves, R.A., and Spiegelman, B.M. (1993). and differentiation . ADDi : a Novel Helix-Loop-Helix Transcription Factor Associated with Adipocyte Determination and Differentiation. *13*.

Valle, I., Alvarez-Barrientos, A., Arza, E., Lamas, S., and Monsalve, M. (2005). PGC-1alpha regulates the mitochondrial antioxidant defense system in vascular endothelial cells. Cardiovasc. Res. *66*, 562–573.

Vega, R.B., Huss, J.M., and Kelly, D.P. (2000). The Coactivator PGC-1 Cooperates with Peroxisome Proliferator-Activated Receptor α in Transcriptional Control of Nuclear Genes Encoding Mitochondrial Fatty Acid Oxidation Enzymes The Coactivator PGC-1 Cooperates with Peroxisome Proliferator-Activated Rece.

Ventura-Clapier, R., Garnier, A., and Veksler, V. (2008). Transcriptional control of mitochondrial biogenesis: the central role of PGC-1alpha. Cardiovasc. Res. *79*, 208–217.

Verdin, E., Hirschey, M.D., Finley, L.W.S., and Haigis, M.C. (2010). Sirtuin regulation of mitochondria: energy production, apoptosis, and signaling. Trends Biochem. Sci. *35*, 669–675.

Virbasius, J. V, Virbasius, C. a, and Scarpulla, R.C. (1993). Identity of GABP with NRF-2, a multisubunit activator of cytochrome oxidase expression, reveals a cellular role for an ETS domain activator of viral promoters. Genes Dev. *7*, 380–392.

Vogel, J.L., and Kristie, T.M. (2000). The novel coactivator C1 (HCF) coordinates multiprotein enhancer formation and mediates transcription activation by GABP. EMBO J. *19*, 683–690.

Wang, X., Su, B., Lee, H., Li, X., Perry, G., Smith, M. a, and Zhu, X. (2009). Impaired balance of mitochondrial fission and fusion in Alzheimer's disease. J. Neurosci. *29*, 9090–9103.

Wareski, P., Vaarmann, A., Choubey, V., Safiulina, D., Liiv, J., Kuum, M., and Kaasik, A. (2009). PGC-1{alpha} and PGC-1{beta} regulate mitochondrial density in neurons. J. Biol. Chem. *284*, 21379–21385.

Weitzel, J.M., and Iwen, K.A. (2011). Coordination of mitochondrial biogenesis by thyroid hormone. Mol. Cell. Endocrinol. *342*, 1–7.

Wenz, T. (2013). Regulation of mitochondrial biogenesis and PGC-1α under cellular stress. Mitochondrion *13*, 134–142.

Wenz, T., Rossi, S.G., Rotundo, R.L., Spiegelman, B.M., and Moraes, C.T. (2009). Increased muscle PGC-1alpha expression protects from sarcopenia and metabolic disease during aging. Proc. Natl. Acad. Sci. U. S. A. *106*, 20405–20410.

Westin, S., Kurokawa, R., Nolte, R.T., Wisely, G.B., McInerney, E.M., Rose, D.W., Milburn, M. V, Rosenfeld, M.G., and Glass, C.K. (1998). Interactions controlling the assembly of nuclear-receptor heterodimers and co-activators. Nature *395*, 199–202.

Weydt, P., Pineda, V. V, Torrence, A.E., Libby, R.T., Satterfield, T.F., Lazarowski, E.R., Gilbert, M.L., Morton, G.J., Bammler, T.K., Strand, A.D., et al. (2006). Thermoregulatory and metabolic defects in Huntington's disease transgenic mice implicate PGC-1alpha in Huntington's disease neurodegeneration. Cell Metab. *4*, 349–362.

Wilson-fritch, L., Nicoloro, S., Chouinard, M., Lazar, M.A., Chui, P.C., Leszyk, J., Straubhaar, J., Czech, M.P., and Corvera, S. (2004). Mitochondrial remodeling in adipose tissue associated with obesity and treatment with rosiglitazone. *114*, 1281–1289.

Wu, Z., Puigserver, P., Andersson, U., Zhang, C., Adelmant, G., Mootha, V., Troy, a, Cinti, S., Lowell, B., Scarpulla, R.C., et al. (1999). Mechanisms controlling mitochondrial biogenesis and respiration through the thermogenic coactivator PGC-1. Cell *98*, 115–124.

Wu, Z., Huang, X., Feng, Y., Handschin, C., Feng, Y., Gullicksen, P.S., Bare, O., Labow, M., Spiegelman, B., and Stevenson, S.C. (2006). Transducer of regulated CREB-binding proteins (TORCs) induce PGC-1alpha transcription and mitochondrial biogenesis in muscle cells. Proc. Natl. Acad. Sci. U. S. A. *103*, 14379–14384.

Yang, X., Enerbäck, S., and Smith, U. (2003). Reduced expression of FOXC2 and brown adipogenic genes in human subjects with insulin resistance. Obes. Res. *11*, 1182–1191.

Yoon, J.C., Puigserver, P., Chen, G., Donovan, J., Wu, Z., Rhee, J., Adelmant, G., Stafford, J., Kahn, C.R., Granner, D.K., et al. (2001). Control of hepatic gluconeogenesis through the transcriptional coactivator PGC-1. Nature *413*, 131–138.

Yoshioka, T., Inagaki, K., Noguchi, T., Sakai, M., Ogawa, W., Hosooka, T., Iguchi, H., Watanabe, E., Matsuki, Y., Hiramatsu, R., et al. (2009). Identification and characterization of an alternative promoter of the human PGC-1alpha gene. Biochem. Biophys. Res. Commun. *381*, 537–543.

Yuryev, a, Patturajan, M., Litingtung, Y., Joshi, R. V, Gentile, C., Gebara, M., and Corden, J.L. (1996). The C-terminal domain of the largest subunit of RNA polymerase II interacts with a novel set of serine/arginine-rich proteins. Proc. Natl. Acad. Sci. U. S. A. *93*, 6975–6980.

Zechner, C., Lai, L., Zechner, J.F., Geng, T., Yan, Z., Rumsey, J.W., Collia, D., Chen, Z., Wozniak, D.F., Leone, T.C., et al. (2010). Total skeletal muscle PGC-1 deficiency uncouples mitochondrial derangements from fiber type determination and insulin sensitivity. Cell Metab. *12*, 633–642.

Zhang, Y., Huypens, P., Adamson, A.W., Chang, J.S., Henagan, T.M., Boudreau, A., Lenard, N.R., Burk, D., Klein, J., Perwitz, N., et al. (2009). Alternative mRNA splicing produces a novel biologically active short isoform of PGC-1alpha. J. Biol. Chem. *284*, 32813–32826.

Zhao, J., Li, L., Pei, Z., Li, C., Wei, H., Zhang, B., Peng, Y., Wang, Y., Tao, Y., and Huang, R. (2012). Peroxisome proliferator activated receptor (PPAR)-γ co-activator 1-α and hypoxia induced factor-1α mediate neuro- and vascular protection by hypoxic preconditioning in vitro. Brain Res. *1447*, 1–8.

Zheng, B., Liao, Z., Locascio, J.J., Lesniak, K. a, Roderick, S.S., Watt, M.L., Eklund, A.C., Zhang-James, Y., Kim, P.D., Hauser, M. a, et al. (2010). PGC-1α, a potential therapeutic target for early intervention in Parkinson's disease. Sci. Transl. Med. *2*, 52ra73.

Zheng, B., Liao, Z., Locascio, J.J., Lesniak, K.A., Roderick, S.S., Watt, M.L., Eklund, A.C., Zhang-james, Y., Kim, P.D., Hauser, M.A., et al. (2011). NIH Public Access. *2*.

Zirngibl, R. a, Chan, J.S.M., and Aubin, J.E. (2008). Estrogen receptor-related receptor alpha (ERRalpha) regulates osteopontin expression through a non-canonical ERRalpha response element in a cell context-dependent manner. J. Mol. Endocrinol. *40*, 61–73.

VITA

Shannon Hedrick was born and raised in New Orleans, LA. She attended elementary school at Our Lady of Prompt Succor in Chalmette, LA and graduated as valedictorian of her 8th grade class. She then attended high school at Mount Carmel Academy, graduating in 2007 with honors and hundreds of service hours from volunteer work. Shannon then decided to attend University of Richmond for her undergraduate studies. There, she worked under the guidance of Dr. Ellis Bell for independent research, and was chosen to present her work at the annual Protein Society conference in 2010. At U of R, Shannon was also involved in several volunteer organizations and was chairwoman of the Relay for Life committee. She graduated in 2011 with a Bachelor of Science in Biochemistry and Molecular Biology and a minor in Russian Studies. That year, Shannon was accepted into Virginia Commonwealth University's School of Medicine in the Molecular Biology and Genetics program. She completed her Master's Degree under the guidance of Dr. James Bennett and Dr. Shirley Taylor.